Untersuchungen zur Biokompatibilität von Magnesium Scaffolds aus der Legierung LAE442 mit verschiedenen Beschichtungen und Porengrößen

von Laura Marie Witting

Inaugural-Dissertation zur Erlangung der Doktorwürde
der Tierärztlichen Fakultät der Ludwig-Maximilians-Universität
München

Untersuchungen zur Biokompatibilität von Magnesium Scaffolds aus der Legierung LAE442 mit verschiedenen Beschichtungen und Porengrößen

von Laura Marie Witting

aus Frankfurt am Main

München 2021

Aus dem Zentrum für Klinische Tiermedizin der Tierärztlichen Fakultät

der Ludwig-Maximilians-Universität München

Lehrstuhl für Chirurgie der Kleintiere

Arbeit angefertigt unter der Leitung von:

Univ.-Prof. Dr. Andrea Meyer-Lindenberg

Mitbetreuung durch:

Franziska Feichtner, Ph.D.

Dr. Anja-Christina Waselau

Gedruckt mit Genehmigung der Tierärztlichen Fakultät

der Ludwig-Maximilians-Universität München

Dekan: Univ.-Prof. Dr. Reinhard K. Straubinger, Ph.D.

Berichterstatter: Univ.-Prof. Dr. Andrea Meyer-Lindenberg

Korreferent/en: Univ.-Prof. Dr. Ellen Kienzle

Tag der Promotion: 17. Juli 2021

Meinen Eltern, meinem Bruder, meiner Oma

und Oskar

INHALTSVERZEICHNIS

ABKÜRZUNGSVERZEICHNIS

3D	Dreidimensional
AE42	Mg-Basislegierung (4 wt.% Aluminium, 2 wt.% SE)
Al	Aluminium
AX30	Mg-Legierung (3 wt.% Aluminium, ≤ 1 wt.% Kalzium)
AZ31	Mg-Legierung (3 wt.% Aluminium, 1 wt.% Zink)
AZ91	Mg-Legierung (9 wt.% Aluminium, 1 wt.% Zink)
BV/TV	Bone Volume/Total Volume
CaP	Kalziumphosphat
Ce	Cerium
Conn.D	Konnektivitätsdichte
CSD	Critical size defect
CT	Computertomographie
FBGC	Fremdkörperriesenzellen
H_2	Wasserstoff
H_2O	Wasser
HCL	Salzsäure
La	Lanthanum
LAE442	Legierung aus Lithium, Aluminium und Seltenen Erden (4 wt.% Li, 4 wt.% Al, 2 wt.% SE)
LANd442	Legierung aus Lithium, Aluminium und Seltenen Erden (4 wt.% Li, 4 wt.% Al, 2 wt.% Nd)
Li	Lithium
Mg	Magnesium
Mg-La^2	Mg-Legierung (2 wt.% La)
$Mg(OH)_2$	Magnesiumhydroxid
MgCa0.8	Mg-Legierung (99,2 wt.% Mg, 0,8 wt.% Ca)
MgF_2	Magnesiumfluorid
Mn	Mangan
n	Größe der Grundgesamtheit
Nd	Neodymium
OcS/BS	Osteocalst surface per bone surface
OS/BS	Osteoid surface per bone surface
p	Signifikanzwert
P1	Porengröße von 400 µm
P2	Porengröße von 500 µm
PLA	Polymilchsäure
r	Korrelationskoeffizient
ROI	Region of Interest
SE	Seltene Erden
SMI	Structure Model Index
ß-TCP	ß-Tricalciumphosphat
Tb.N	Trabecular Number
Tb.Sp	Trabecular Separation
Tb.Th	Trabecular Thickness
TiAl6V4	Titanlegierung mit 6 wt.% Aluminium, 4 wt.% Vanadium
WE43	Mg-Legierung (4 wt.% Yttrium, 3 wt.% SE)
wt.%	weight percent (Massenanteil)
ZEK100	Mg-Legierung (0,96 wt.% Zink, 0,21 wt.% Zirconium, 0,3 wt.% SE)
Zn	Zink
µCT	Mikrocomputertomographie
µm	Mikrometer

I. EINLEITUNG

Wenn große Knochendefekte nicht von selbst heilen, werden sie häufig mit autologen oder allogenen Transplantaten behandelt (Sutherland und Bostrom 2005, Nandi et al. 2010). Diese sind jedoch nicht immer verfügbar und oft mit operativen Risiken verbunden (Staiger et al. 2006, Lalk et al. 2010). Seit einigen Jahren wird daher an resorbierbaren und nicht resorbierbaren Biomaterialien geforscht (Staiger et al. 2006, Hampp et al. 2013, Lalk et al. 2013). Nicht resorbierbare Materialien wie Titan müssen oft bei einem zweiten Eingriff aus dem Körper entfernt werden (Pohler 2000), während resorbierbare Materialien wie Polymere und Keramiken im Körper verbleiben und degradieren (Von Der Höh et al. 2009, Meyer-Lindenberg et al. 2010, Nandi et al. 2010, Reifenrath et al. 2013). Biomaterialien sollten adäquate Eigenschaften hinsichtlich der Degradation, Biokompatibilität und besonders der Osseointegration aufweisen (Waizy et al. 2013, Veronesi et al. 2015, Shahrezaee et al. 2018). Resorbierbare Materialien werden bei Degradation optimaler Weise zeitgleich von neuem Knochengewebe ersetzt (Staiger et al. 2006, Thomann et al. 2009, Lalk et al. 2013, Liu et al. 2014). Doch obwohl resorbierbare Keramiken und Polymere eine gute Osseointegration und Degradation gewährleisten, sind sie für den krafttragenden Knochen nicht stabil genug (Sutherland und Bostrom 2005, Shahrezaee et al. 2018, Yang et al. 2020). Metallische Biomaterialien, besonders Magnesiumlegierungen, sind aufgrund ihrer guten mechanischen Eigenschaften in den Vordergrund der Forschung gerückt (Witte et al. 2007, Walker et al. 2014, Kleer et al. 2019). Sie weisen eine sehr gute Biokompatibilität auf und eignen sich besonders für den krafttragenden Knochen, da das Elastizitätsmodul (Young's modulus) dem des natürlichen Knochens ähnelt (Staiger et al. 2006, Reifenrath et al. 2013, Waizy et al. 2013, Xu et al. 2018). Reines Magnesium degradiert im Körper jedoch sehr schnell, wobei Wasserstoff entsteht (Gray und Luan 2002, Witte et al. 2006, Yang et al. 2020). Um die Degradationsrate von Magnesium zu reduzieren, werden oft Elemente wie Aluminium oder Lithium hinzulegiert (Haferkamp et al. 2000, Waizy et al. 2013, Weizbauer et al. 2014). Seltene Erden können außerdem die Festigkeit dieser Legierungen erhöhen (Angrisani et al. 2012, Willbold et al. 2015). Als besonders vielversprechend hat sich die Magnesiumlegierung LAE442 (4 wt.% Li, 4 wt.% Al, 2 wt.% SE) erwiesen (Witte et al. 2006, Reifenrath et al. 2011, Angrisani et al. 2016), die in vivo bereits

in fester Form als auch porös getestet wurde (Thomann et al. 2009, Witte et al. 2010, Bobe et al. 2013, Kleer et al. 2019). Auch Beschichtungen können die Degradation und die Gasbildung beeinflussen, indem sie eine Schutzschicht um das Implantat bilden (Gray und Luan 2002, Lalk et al. 2013, Julmi et al. 2019). Das Beschichten von Magnesiumlegierungen mit Magnesiumfluorid (MgF_2) wurde dabei als vorteilhaft beschrieben (Lalk et al. 2013, Julmi et al. 2019, Kleer et al. 2019). Auch Calciumphosphat (CaP)- und Polymilchsäure (PLA)-Beschichtungen wurden in einigen Studien als gut biokompatibel eingestuft (Xu et al. 2009, Lalk et al. 2013, Zeng et al. 2014, Julmi et al. 2019). Noch mehr Vorteile hinsichtlich Degradation und Gasbildung zeigten Beschichtungskombinationen von MgF_2 und PLA/CaP; sie wurden jedoch erst in vitro erforscht (Hort et al. 2010, Julmi et al. 2019, Maier et al. 2020). Poröse Knochenersatzstoffe, sogenannte ‚Scaffolds' sind für den Einsatz im spongiösen Knochen gut geeignet, da ihre Architektur den feinen Knochentrabekeln der Spongiosa ähnelt (Cheng et al. 2016, Julmi et al. 2017, Kleer et al. 2019, Yang et al. 2020). Um das Einwachsen von neuen Knochenzellen in die Scaffolds zu erleichtern, wurde in einigen Studien ein Porendurchmesser von > 300 µm empfohlen (Bobe et al. 2013, Cheng et al. 2016, Yang et al. 2020). Für die Beurteilung der Degradation und Biokompatibilität der Scaffolds sind bildgebende Verfahren wie Röntgenaufnahmen und µCT-Scans sowie histologische Analysen hilfreich (von Doernberg et al. 2006, Thomann et al. 2009, Lalk et al. 2010, Reifenrath et al. 2013). In dieser Studie sollte erstmalig der Einfluss zweier Kombinationsbeschichtungen (MgF_2/PLA; MgF_2/CaP) auf das Degradationsverhalten und die Biokompatibilität von porösen Magnesium Scaffolds der Legierung LAE442 in vivo untersucht werden.

II. LITERATURÜBERSICHT

1. Knochenanatomie

1.1 Trabekuläre Knochenarchitektur und Knochengewebe

Lange Röhrenknochen lassen sich unterteilen in ein Mittelstück (Diaphyse), das von einem Knochenmantel (Substantia compacta) umgeben ist und innen eine Markhöhle (Cavum medullare) einschließt, und zwei End- beziehungsweise Halsstücken, der Epiphysis proximalis beziehungsweise Metaphysis proximalis und Epiphysis distalis, beziehungsweise Metaphysis distalis. Diese sind von einer dünnen Knochenrinde (Substantia corticalis) überzogen (Platzer 2009, König und Liebich 2012). Im Inneren der Epiphysen befindet sich die Substantia spongiosa, ein schwammartiges Netzwerk aus Knochentrabekeln. Die Trabekel sind gefäßlos (König und Liebich 2012). Somit werden die Osteozyten aus den Gefäßen des Knochenmarks durch Diffusion versorgt. Die Knochentrabekel ordnen sich entlang von Trajektorien (Kraftlinien) an, welche aus Druck- und Zugspannungen resultieren. Durch den trajektoriellen Aufbau hält der Knochen den ständigen Druck- und Zugbelastungen der Sehnen und Bänder stand (Nickel et al. 1992, Platzer 2009). Die Knochengrundsubstanz besteht zum Großteil aus Mineralien (60-70%) sowie aus organischen Verbindungen und Wasser (Nickel et al. 1992). Den größten Teil der organischen Substanzen nimmt Kollagen (90-95%) ein. Der restliche Teil setzt sich aus Proteoglykanen und Glykosaminoglykanen zusammen (Nickel et al. 1992). Die anorganische Substanz besteht vorwiegend aus Calciumcarbonat (10%) und Calciumphosphat (85%). Das restliche anorganische Material verteilt sich auf Magnesium, Nitrat, Natrium, Fluor und Spurenelemente (Nickel et al. 1992). Der Knochen spielt nicht nur für die Stützfunktion, sondern auch für den Mineralstoffhaushalt eine wichtige Rolle. Hierfür bildet Knochen den größten Speicher für Calcium und Phosphat (Dahme und Reinacher 1988).

1.2 Knochenentwicklung

Bei der Knochenentwicklung unterscheidet man die direkte desmale Ossifikation und die indirekte chondrale Ossifikation, welche in eine enchondrale und eine perichondrale Ossifikation aufgeteilt werden kann (Platzer 2009). Im Gegensatz zur desmalen Ossifikation basiert die chondrale Ossifikation auf der Bildung von

hyalinem Knorpel als Ausgangsmaterial für das Längenwachstum. Danach wird der vorläufige Knorpel schrittweise wieder abgebaut und durch permanentes Knochengewebe ersetzt (König und Liebich 2012). Osteoklasten sind für diese Knochenbildung die Voraussetzung. Sie bauen die Knorpelsubstanz ab und geben den Osteoblasten die Möglichkeit zur Knochenneubildung (Platzer 2009). Unter desmaler Ossifikation versteht man eine direkte Umwandlung von undifferenzierten Mesenchymzellen in Präosteoblasten, die dann wiederum in Osteoblasten umgewandelt werden. Die Osteoblasten produzieren während der Ossifikation eine unverkalkte Knochenmatrix, das sogenannte Osteoid, welches überwiegend (etwa 90%) Kollagen Typ I und Spuren von Kollagen Typ V enthält (König und Liebich 2012). Zu etwa 10% besteht Osteoid aus nichtkollagenen Proteinen, welche ebenfalls von den Osteoblasten gebildet werden und die zur Mineralisation beitragen (McCarthy und Frassica 2014). Hierzu gehören unter anderem die Glykoproteine Osteocalcin, Osteonectin und Osteopontin (McCarthy und Frassica 2014). Während die Osteoblasten die Bestandteile des Osteoids synthetisieren, bilden sie untereinander Gap junctions zur Kommunikation aus (Platzer 2009). Schließlich werden einige der Osteoblasten durch Apoptose beseitigt, andere werden zurück in den inaktiven Zustand versetzt und etwa 5 – 20 % betten sich in das Osteoid ein und differenzieren sich zu Osteozyten (Lüllmann-Rauch 2015). Damit erfolgt die Mineralisierung der Knochengrundsubstanz (Ossein) (König und Liebich 2012). Die desmale Ossifikation ist mit einer Einsprossung von Blutgefäßen stark verbunden; somit übernimmt der Knochen auch eine stoffwechselartige Funktion (König und Liebich 2012).

1.3 Knochenheilung

Große Knochendefekte können oft nicht von selbst heilen (Nandi et al. 2010). Die Defekte können mit autologen oder allogenen Transplantaten behandelt werden (Sutherland und Bostrom 2005, Nandi et al. 2010), die jedoch nicht immer verfügbar und mit Risiken verbunden sind (Staiger et al. 2006, Lalk et al. 2010). Seit einigen Jahren sind somit resorbierbare und nicht resorbierbare Implantate und Knochenersatzstoffe in den Vordergrund der Forschung gerückt (Staiger et al. 2006, Lalk et al. 2013, Pawelec und Planell 2018). Implantate und Knochenersatzstoffe gelten für den Körper als Fremdkörper und rufen deshalb immer eine Fremdkörper-, beziehungsweise Entzündungsreaktion hervor, die wenige Sekunden nach Gewebekontakt beginnt. Diese Entzündungsreaktion ähnelt

dem physiologischen Wund- und Frakturheilungsprozess (Nuss und von Rechenberg 2008, Anderson 2015). Die Reaktion des Körpers startet mit einer akuten Entzündungsreaktion und der Ausschüttung von Immunglobulinen und Leukozyten (Anderson 2015). Es folgt eine chronische Entzündungsreaktion, bei der Entzündungszellen wie Lymphozyten und Monozyten, die sich zu Makrophagen differenzieren, angezogen werden (Horbett 2004, Anderson 2015). Es entsteht Granulationsgewebe und Fibroblasten wandern ein. Dann folgt eine fibroblastische Proliferation und Kapillarbildung. Fibroblasten bilden Kollagen, welches sich zu einer bindegewebigen Kapsel formiert (Anderson 1988, Nuss und von Rechenberg 2008). Um den Fremdkörper beziehungsweise das Implantat bildet sich somit eine innere Schicht aus Makrophagen, die sich teilweise zu Fremdkörperriesenzellen zusammenschließen, sowie eine zweite äußere Schicht aus Fibroblasten und Bindegewebe (Anderson 2015). Ist die Blutzirkulation im Bereich des Implantats ausreichend und sind keine Infektionen vorhanden, kann die Osseointegration beginnen. Diese wird als direkte funktionelle und strukturelle Verbindung zwischen Implantatoberfläche und vitalem Knochen definiert (Le Guéhennec et al. 2007). Die Verbindung gewährleistet eine gute biomechanische Fixierung des Implantats. Neues Knochengewebe, das am Implantat anhaftet, kann durch die Einwanderung von aktiven Osteoblasten gebildet werden (Von Der Höh et al. 2009, Yang et al. 2020).

2. Knochenimplantate

Knochenimplantate werden in der Medizin zur chirurgischen Versorgung von Knochendefekten oder Frakturen in Form von Pins, Schrauben, Nägeln oder Platten eingesetzt (Staiger et al. 2006, Witte et al. 2010, Walker et al. 2014, Yang et al. 2020). Dabei kann man zwischen nicht resorbierbaren und resorbierbaren Implantaten unterscheiden.

2.1 Nicht resorbierbare Implantate

Nicht resorbierbare metallische Materialien wie Titan, Kobalt-Chrom, Zirkonium oder Stahl sind biologisch inert und haben sich in der Osteosynthese jahrelang aufgrund ihrer guten Biokompatibilität und ihrer Korrosionsresistenz bewährt (Pohler 2000, Grün et al. 2018). Sie müssen jedoch oft bei einem erneuten operativen Eingriff aus dem Körper entfernt werden, was mit weiteren Risiken für den Patienten verbunden ist (Joeris et al. 2017). Bei Stahllegierungen kann es

außerdem zu Immunreaktionen auf toxische Bestandteile wie Nickel oder Kobalt kommen (Erdmann et al. 2010, Joeris et al. 2017). Außerdem ist bei diesen Materialien eine fibröse Kapselbildung möglich, was die Einbettung und Fixation der Implantate ins Knochengewebe erschwert (Le Guéhennec et al. 2007, Joeris et al. 2017). Ein weiterer Nachteil ist die Belastungsabschirmung (stress shielding), die aufgrund der höheren Steifigkeit von Implantaten gegenüber Knochen entstehen kann (Nagels et al. 2003, Staiger et al. 2006, Ullmann et al. 2011). Bei diesem Phänomen erfolgt eine Verringerung der Knochendichte als Folge von Belastungsänderungen des Knochens oder bei Wegnahme der Belastung durch das Implantat (Nagels et al. 2003, Staiger et al. 2006). Nach dem Wolff'schen Gesetz baut sich dann der gesunde Knochen als Reaktion auf die fehlende Belastung um (Pawelec und Planell 2018). Wenn die Belastung des Knochens abnimmt, gibt es keinen Stimulus für den Knochenumbau mehr und der Knochen wird weniger dicht und schwächer (Pawelec und Planell 2018).

2.2 Resorbierbare Implantate

In den letzten Jahren wurde häufig an resorbierbaren Knochenimplantaten geforscht. Diese haben den Vorteil, dass sie in physiologischer Umgebung degradieren und kein weiterer chirurgischer Eingriff notwendig ist (Bondarenko et al. 2014). Polymere sind häufig verwendete Biomaterialien aufgrund ihrer guten Biokompatibilität und Bearbeitbarkeit (Feng et al. 2019). In der Literatur werden vor allem Polycaprolacton (PCL), Polylactid (PLA) und Polylactid-Glycolid (PGA)- Derivate genannt (Grün et al. 2018, Feng et al. 2019). Die schlechte mechanische Festigkeit sowie die sauren Degradationsprodukte der Polymere schränken ihre Anwendung jedoch erheblich ein (Grün et al. 2018, Feng et al. 2019). Der Einsatz von Polymerimplantaten beschränkt sich demnach auf den nicht krafttragenden Knochen (Grün et al. 2018). Im Bereich der resorbierbaren Implantate sind vor allem metallische Biomaterialien in den Vordergrund der Forschung gerückt (Staiger et al. 2006, Dorozhkin 2014). Sie bilden aufgrund ihrer Festigkeit und Bruchzähigkeit eine erfolgsversprechende Voraussetzung für temporäre Implantate sowie für Anwendungen im krafttragenden Knochen (Staiger et al. 2006, Dorozhkin 2014). Implantate auf Eisen-Basis bringen oft Einschränkungen aufgrund der möglichen Freisetzung toxischer Metallionen durch Korrosionsprozesse mit sich (Staiger et al. 2006). Magnesiumlegierungen sind hingegen sehr gut biokompatibel und weisen mechanische Eigenschaften auf, die

denen von Knochen ähneln (Erdmann et al. 2010, Dorozhkin 2014, Grün et al. 2018). Durch die langsame Implantatkorrosion von Magnesiumimplantaten kann der ‚stress-shielding' Effekt verringert oder vermieden werden (Staiger et al. 2006, Ullmann et al. 2011, Wolters et al. 2015).

2.3 Einsatz von Legierungen bei Magnesiumimplantaten

Die Bruchzähigkeit und Stabilität von Magnesiumimplantaten sind höher als bei keramischen Biomaterialien oder Polymeren (Staiger et al. 2006, Erdmann et al. 2010). Die Nachteile von Magnesiumimplantaten sind jedoch je nach Zusammensetzung eine zu schnelle Degradation und die Entstehung von Wasserstoffgas bei Degradation (Witte et al. 2005, Staiger et al. 2006) ($Mg + 2H_2O \rightarrow Mg(OH)_2 + H_2$) (Pourbaix 1984). Um die Degradationsrate von Magnesiumimplantaten zu senken und damit die Gasbildung zu verringern, wurden verschiedene Elemente wie Aluminium, Zink oder Seltene Erden hinzulegiert (Haferkamp et al. 2000, Chia et al. 2009, Angrisani et al. 2016). In der Literatur führte das Hinzulegieren von Seltenen Erden (Nd, Ce, La) zu einer höheren Materialstabilität und einer erhöhten Korrosionsbeständigkeit von reinen Magnesiumimplantaten (Chia et al. 2009, Willbold et al. 2015). Magnesiumlegierungen, wie AZ91 (9 wt.% Aluminium, 1 wt.% Zink), WE43 (4 wt.% Yttrium, 3 wt.% SE), LAE442 (4 wt.% Lithium, 4 wt.% Aluminium, 2 wt.% Seltene Erden), MgCa0.8 (99,2 wt.% Mg, 0,8 wt.% Ca), ZEK100 (0,96 wt.% Zink, 0,21 wt.% Zirconium, 0,3 wt.% SE) und LANd442 (4 wt.% Li, 4 wt.% Al, 2 wt.% Nd) wurden bereits in vivo untersucht (Reifenrath et al. 2011, Reifenrath et al. 2013, Bondarenko et al. 2014). Dabei wurde in der Literatur die Magnesiumlegierung LAE442 als besonders vielversprechend eingestuft. Diese zeigte die geringste Degradationsrate im Vergleich zu den anderen Magnesiumlegierungen (Thomann et al. 2009, Reifenrath et al. 2011, Angrisani et al. 2016). LAE442 wurde in unterschiedlicher Form getestet. Thomann et al. (2009) verglichen in ihrer in vivo Studie im Kaninchenmodell die Degradation von stranggepressten intramedullären LAE442 Pins in der Tibia mit der Degradation von MgCa0.8 Implantaten und fanden heraus, dass LAE442 Implantate im Vergleich langsamer degradierten (Thomann et al. 2009). Krause et al. (2010) forschten ebenfalls mit LAE442 Pins. Sie setzten die Pins in Kaninchentibiae ein und evaluierten das Degradationsverhalten sowie die mechanischen Eigenschaften der Implantate (Krause et al. 2010). Dabei beschrieben sie die Legierung LAE442 als stabil,

langsam degradierend und vielversprechend für den Einsatz zur intramedullären Frakturversorgung im krafttragenden Knochen (Krause et al. 2010). Witte et al. (2005/2006) testeten die Magnesiumlegierung LAE442 in Form von Stäben in vitro und in vivo und fanden heraus, dass LAE442 korrosionsbeständiger war als die Magnesiumlegierungen AZ91, AZ31 und WE43. Auch Angrisani et al. (2016) führten in vivo Studien an LAE442 Magnesiumimplantaten durch und stuften sie als gut biokompatibel und langsam degradierend ein.

2.4 Einsatz von Beschichtungen bei Magnesiumimplantaten

Oberflächenbeschichtungen oder -behandlungen von Implantaten auf Magnesiumbasis ermöglichen einen höheren Korrosionswiderstand und damit eine geringere Implantatdegradation im Vergleich zu unbeschichteten Implantaten (Thomann et al. 2010, Yang et al. 2011). Durch Beschichtungen konnte außerdem der Implantat-Knochen-Kontakt verbessert werden (Rammelt et al. 2007). Dabei sollte die Beschichtung gut haftend, gleichmäßig und porenfrei sein (Gray und Luan 2002). Bei Magnesiumlegierungen wurden bereits verschiedene Beschichtungen aus reinem Titan, Polymeren, Natriumhydrogencarbonatlösungen, Fluoridbeschichtungen, sowie Oberflächenbehandlungen, wie zum Beispiel die Alkalin-Wärmebehandlung oder die ‚micro-arc oxidation' getestet (Song 2007, Thomann et al. 2010, Witte et al. 2010, Dorozhkin 2014). Thomann et al. zeigten, dass eine Beschichtung von Magnesiumimplantaten der Legierung MgCa0.8 mit Magnesiumfluorid (MgF_2) zu einer langsameren und homogeneren Korrosion führte, verglichen mit reinen Magnesiumimplantaten. Auch in anderen Studien erwiesen sich Fluoridbeschichtungen als vielversprechend und verringerten die Degradationsrate von Magnesiumimplantaten (Chiu et al. 2007, Witte et al. 2010). Neben Fluoridbeschichtungen wurden außerdem Calciumphosphatbeschichtungen erforscht, die in einigen Studien neben der Degradationsgeschwindigkeit auch die Oberflächenbiokompatibilität von Magnesiumimplantaten verbessern konnten (Thomann et al. 2010, Dorozhkin 2014). Eine wichtige Anforderung an resorbierbare Knochenimplantate und deren Beschichtung ist die Förderung und Stimulation von Knochenbildung (Bondarenko et al. 2014). Xu et al. (2009) beschrieben in ihrer in vivo Studie mit Magnesiumimplantaten (Mg-Mn-Zn), die mit Calciumphosphat beschichtet wurden, eine bessere Bioaktivität und eine größere Menge an neugebildetem Osteoid im Vergleich zu unbeschichteten Implantaten. Calciumphosphat-Beschichtungen konnten somit die Knochenbildung

um Magnesiumimplantate durch Förderung der Osteoblastenproliferation beschleunigen (Xu et al. 2009).

3. Knochenersatzstoffe

Um große Knochendefekte zu heilen, sind synthetische Knochenersatzstoffe in den Vordergrund der Forschung gerückt. Sie sollten idealerweise biokompatibel, porös, dreidimensional und ausreichend stabil sein (Lalk et al. 2013, Augustin et al. 2020). Durch ihre poröse Architektur bilden die Knochenersatzstoffe die Form von Schwämmen (‚Scaffolds') (Julmi et al. 2019). Der Porendurchmesser der Scaffolds spielt hierbei eine wichtige Rolle, da die Scaffoldarchitektur dem spongiösen Knochen mit seinen feinen Knochentrabekeln ähneln und genug Raum für Vaskularisation bieten soll (Karageorgiou und Kaplan 2005, von Doernberg et al. 2006, Julmi et al. 2017). Für ein gutes Knochen- und Gefäßeinwachstum wurde in der Literatur eine optimale Porengröße von > 300 µm beschrieben (Karageorgiou und Kaplan 2005, Cheng et al. 2016, Julmi et al. 2017). Die Scaffolds sollten außerdem vielversprechende Eigenschaften für die Knochenregeneration aufweisen, wie z. B. osteokonduktive und osteoinduktive Eigenschaften für eine optimale Osseointegration sowie nützliche Eigenschaften für Zellanlagerung und Zellproliferation (Veronesi et al. 2015, Julmi et al. 2019). Knochenersatzstoffe können ebenfalls in nicht resorbierbare und resorbierbare Materialien unterteilt werden.

3.1 Nicht resorbierbare Knochenersatzstoffe

Nicht resorbierbare poröse Knochenersatzstoffe aus zum Beispiel Titan-Graphit-Legierungen wurden bereits in vitro getestet (Blackwood et al. 2000). Sie sollten eine gute Osseointegration gewährleisten, jedoch die Stabilität von Titan beibehalten. Das Graphit und die poröse Architektur erhöhten jedoch die Korrosionsrate der Titan Scaffolds und setzten somit die sonst vorteilhafte Festigkeit von Titan herab (Blackwood et al. 2000). Ein Nachteil von nicht resorbierbaren Knochenersatzstoffen ist der Verbleib im Körper und eventuelle Entzündungserscheinungen und allergische Reaktionen (Singh und Dahotre 2007).

3.2 Resorbierbare Knochenersatzstoffe

Resorbierbare Knochenersatzstoffe stellen eine fortschrittliche Alternative im Vergleich zu nicht resorbierbaren dar. Das Ziel ist, dass sie in einer geeigneten

Zeitspanne degradieren und im Laufe der Osseointegration mit neuem Knochengewebe ersetzt werden (Lalk et al. 2010, Pawelec und Planell 2018). Verschiedene resorbierbare Materialen wurden bereits untersucht. Vor allem Calciumphosphatverbindungen und Polymere, wie Polymer-Polycaprolacton (PCL)-, Polyethylenglycol (PEG)-, aber auch Polylactid (PLA)-Komposite wurden examiniert (Lalk et al. 2010, Shoichet 2010, Veronesi et al. 2015, Yang 2017). Polymere sind gut biokompatibel und gelten als gut verträglich und nicht toxisch (Shoichet 2010). Limitationen dieser Materialien sind ihre ungeeigneten mechanischen Eigenschaften und die lange Degradationszeit (Lalk et al. 2010, Feng et al. 2019). Keramische Biomaterialien wie Hydroxylapatit (HA) und Tricalciumphosphat (TCP) weisen eine hervorragende Osteokonduktivität, Biokompatibilität und Osseointegration auf (Grün et al. 2018). Keramik-Scaffolds werden bereits in der Humanmedizin eingesetzt, jedoch nur im unbelasteten Knochen, da sie als zu spröde und nicht stabil genug gelten (von Doernberg et al. 2006, Cao und Kuboyama 2010, Grün et al. 2018, Feng et al. 2019). Aufgrund der besseren mechanischen Eigenschaften und der guten Biokompatibilität wurde in letzter Zeit an resorbierbaren metallischen Knochenersatzstoffen geforscht, die auf Magnesiumlegierungen basieren (Witte et al. 2005, Staiger et al. 2006, Kleer et al. 2019). Die Degradation resorbierbarer Knochenersatzstoffe hängt von verschiedenen Faktoren ab. Unter anderem spielt die Porengröße der Scaffolds eine große Rolle. Scaffolds mit kleineren Poren degradieren schneller, da ein kleinerer Porendurchmesser eine größere Oberfläche bewirkt und dadurch die Korrosionsangriffsfläche der Scaffolds größer ist (Karageorgiou und Kaplan 2005, Augustin et al. 2020).

3.3 Einsatz von Magnesiumlegierungen als Knochenersatzstoff

Trotz schneller Degradation und Wasserstoffproduktion sind resorbierbare Schwämme aus Magnesiumlegierungen leicht, sehr stabil und fördern das Einwachsen von Knochen (Witte et al. 2007, Kirkland et al. 2009, Lalk et al. 2010). Magnesiumlegierungen wie AZ91 (9 wt.% Aluminium, 1 wt.% Zink), AX30 (3 wt.% Aluminium, ≤ 1 wt.% Calcium) und LAE442 (4 wt.% Lithium, 4 wt.% Aluminium, 2 wt.% Seltene Erden) wurden bereits in Form von offenporigen Schwämmen in vivo untersucht (Witte et al. 2006, Lalk et al. 2010, Lalk et al. 2013, Kleer et al. 2019). Im Hinblick auf eine langsame und gleichmäßige Degradation schien die Magnesiumlegierung LAE442 besonders vielversprechend zu sein

(Kleer et al. 2019, Augustin et al. 2020). Für die LAE442 Legierung wird die kommerziell erhältliche Legierung AE42 als Basismaterial verwendet, wobei Lithium hinzulegiert wird (Julmi et al. 2019). Das Hinzulegieren von Lithium erhöht die Duktilität, wobei Aluminium die Scaffoldfestigkeit sowohl in Druck- als auch in Zugrichtung erweitert (Julmi et al. 2019). Augustin et al. (2020) untersuchten LAE442 Scaffolds mit zwei unterschiedlichen Porengrößen (440 µm; 500 µm) in vivo. Sie beobachteten bei allen Scaffolds Osteoid-ähnliches Gewebe sowie Knochen-Scaffold-Kontakte. Dabei fiel auf, dass Scaffolds mit der größeren Porengröße signifikant mehr Knochenkontakte sowie eine langsamere Degradationsrate zeigten als Scaffolds der kleineren Porengröße.

3.4 Einsatz von Beschichtungen bei Knochenersatzstoffen aus Magnesium

Da Knochenersatzstoffe aufgrund ihrer porösen Struktur und daher größeren Oberfläche einer schnelleren Degradation ausgesetzt sind als Implantate, ist es wichtig geeignete Beschichtungen zu finden, die die Degradationsrate und die Gasproduktion verringern (Lalk et al. 2013, Julmi et al. 2019). Es wurde bereits an Beschichtungen aus Bioglas oder auch aus Calciumphosphaten wie z.B. Hydroxylapatit oder Magnesiumfluoriden geforscht (Lalk et al. 2010, Lalk et al. 2013, Augustin et al. 2020). Lalk et al. (2010) untersuchten zum Beispiel zylindrische, bioglasbeschichtete Magnesiumschwämme der Legierung AX30 in vivo, ermittelten jedoch keine zufriedenstellenden Ergebnisse hinsichtlich der Osseointegration. Nur wenige Knochentrabekel waren an die Scaffolds angewachsen (Lalk et al. 2010). Auch die Degradationsrate der bioglasbeschichteten Schwämme reduzierte sich nicht wie erwartet (Lalk et al. 2010). Fluoridbeschichtungen zeigten bei Knochenersatzstoffen auf Magnesiumbasis hingegen positive Resultate (Lalk et al. 2013, Augustin et al. 2020). In einer weiteren in vivo Studie mit Magnesiumscaffolds der Legierung AX30 untersuchten Lalk et al. (2013) Magnesiumfluorid (MgF_2)-beschichtete und Calciumphosphat-beschichtete Scaffolds. Sie fanden heraus, dass Fluorid-beschichtete Scaffolds eine dichtere Vaskularisation und eine bessere Integration in den Knochen mit mehr neuem mineralisiertem Knochengewebe aufwiesen als die mit Calciumphosphat beschichteten Scaffolds. Julmi et al. (2019) untersuchten Beschichtungskombinationen auf porösen Scaffolds der Magnesiumlegierung LAE442 in vitro und verglichen diese mit unbeschichteten Scaffolds. Dabei wurde MgF_2 als Basisschicht genutzt und eine zweite Schicht aus Polymilchsäure (PLA)

oder Calciumphosphat (CaP) darübergelegt (Julmi et al. 2019). MgF_2 fungierte dabei als erste Schutzschicht, um die anfänglich entstehende Wasserstofffreisetzung zu unterdrücken. PLA senkte in der Studie am stärksten die Degradationsrate, aber auch CaP erwies sich als eine geeignete Beschichtung für Scaffolds der Magnesiumlegierung LAE442 (Julmi et al. 2019).

4. Mikrocomputertomographie

4.1 Mikrocomputertomographische Analyse des trabekulären Knochens

In der Forschung der letzten Jahre hat der Einsatz und die Verwendung der Mikrocomputertomographie (µCT) stark zugenommen. Besonders für die Analyse der trabekulären und kortikalen Knochenmorphologie wird die hochauflösende µCT genutzt (Nägele 2005, Bouxsein et al. 2010, Lalk et al. 2013, Angrisani et al. 2016, Kleer et al. 2019). Die unterschiedlichen kommerziell erhältlichen µCT-Systeme bieten verschiedene Möglichkeiten zur Bilderfassung und Datenanalyse, was den Vergleich hinsichtlich einer mikrocomputertomographischen Terminologie schwierig macht (Bouxsein et al. 2010). In vergangenen Studien wurde die Mikroarchitektur von trabekulären Knochen anhand von 2D-Schnitten von Knochenbiopsien oder mithilfe der Histomorphometrie untersucht (Nägele 2005). Bei der Benutzung der µCT, die zu 2D- und zu 3D-Bildern führt, gibt es im Bereich der Knochenforschung viele Vorteile (Bouxsein et al. 2010). Im Vergleich zu 2D-Messungen bei histologischen Analysen ermöglicht die µCT eine umfangreichere und zudem auch genauere 3D-Messung der trabekulären Morphologie. Bei der µCT kann zudem auch ein größeres Volumen analysiert werden als in der Histologie (Bouxsein et al. 2010). Eine größere Menge an µCT-Messungen kann außerdem schneller durchgeführt werden als zum Beispiel bei histomorphometrischen Analysen von Knochenproben. Das µCT-Scanning ist außerdem zerstörungsfrei, sodass die Proben anschließend für weitere Untersuchungen verwendet werden können (Bouxsein et al. 2010). Die µCT hat noch mehr Vorteile im Vergleich zur herkömmlichen klinischen Computertomographie (CT). Bei der µCT liegt die maximale Ortsauflösung je nach Gerät in einem kleineren Bereich (5 – 50 µm) als bei der klinischen CT (0,3 – 1 mm). Außerdem wird bei der µCT nicht nur die Fächerstrahlgeometrie angewandt, welche für die klinische CT verwendet wird, sondern auch die Kegelstrahl- sowie die Parallelstrahlgeometrie genutzt. Dies führt insgesamt zu einem höher

aufgelösten µCT-3D-Scan, wobei vor allem auch kleinere Proben wie Nagetiere oder Körperteile gescannt werden können (Bouxsein et al. 2010). Schon 1990 verglichen Kuhn et al. (1990) die via µCT aufgenommenen Bilder von trabekulären Knochenwürfeln mit den optischen Bildern entsprechender histologischer Schnitte, um die Genauigkeit der Darstellung zu untersuchen. Dabei nahmen sie berechnete Messungen des Knochenvolumenanteils sowie der Trabekelplattendichte als Vergleichsparameter. Die Ergebnisse zeigten, dass sich die µCT-Messungen nicht signifikant von den histologischen Messungen unterschieden und daher als sehr akkurat angesehen werden konnten (Kuhn et al. 1990).

4.2 Technologie der Mikrocomputertomographie

Die µCT ist ein bildgebendes Verfahren, das isotrope 3D-Datensätze erzeugt und die Möglichkeit bietet Knochenstrukturen hochauflösend, quantitativ und nicht destruktiv zu messen (Feldkamp et al. 1989). Nachdem Elliot et al. (1984) die ersten µCT-Scanner mit Nadelstrahlgeometrie, einer Röntgenröhre (mit 15 µm Kollimator) und einem Szintillationszähler als Detektor entwickelten, arbeiteten Wissenschaftler wie Feldkamp et al. (1989) und Engelke et al. (1999) an der weiteren Entwicklung von unterschiedlichen Scannern. Rüegsegger stellte 1996 ein kommerziell verfügbares Gerät mit Mikrofokusröhre, Fächerstrahlgeometrie, CCD-Detektor und einer Auflösung von 20 µm her, dem heutige Geräte sehr ähneln (Kristin 2007). Die µCT kann heutzutage zwischen 5-50 µm Ortsauflösung erreichen (Engelke et al. 1999, Scherzer 2007). Das Objekt kann variabel zwischen Röntgenquelle und Detektor angeordnet werden und rotiert entweder selbst oder aber die Röntgenquelle rotiert um das Untersuchungsobjekt und durchstrahlt dasselbe (Kristin 2007). Die Strahlen werden von Detektoren aufgezeichnet und mit Hilfe von computergestützter Rekonstruktion in dreidimensionale Ansichten und Schnittbilder überführt (Kristin 2007). Für in vivo Analysen an kleinen Labortieren eignet sich dabei vor allem die monochromatische Synchrotronstrahlung (Engelke et al. 1999). Anhand der Mikrocomputertomographie können am Knochen folgende mikrostrukturelle Parameter quantitativ gemessen werden (Hildebrand et al. 1999, Kristin 2007):

- Bone Volume Fraction (BV/TV) in % (volumetrischer Anteil des Knochens am Gesamtvolumen der gemessenen Probe)
- Mean Trabecular Thickness (Tb.Th) in µm (direkte Bestimmung der Trabekeldicke; Tb.Th gibt den Durchschnitt der lokalen Dicken aller

Knochenvoxel wieder)

- Mean Trabecular Separation (Tb.Sp) in µm (Bestimmung des Raumes zwischen Knochentrabekeln/ der Voxel, welche nicht dem Knochen zugeordnet werden)
- Trabecular Number (Tb.N) in 1/cm (Bestimmung der Trabekelanzahl; wird definiert als Umkehrfunktion des mittleren Abstands zwischen den Achsen der Struktur, beziehungsweise zwischen den Achsen der Platten und Stäbe)
- Connectivity-Density (Conn. D) in 1/mm³ (Maß für die Vernetzung des trabekulären Geflechtes; das heißt die maximale Anzahl von Verbindungen, die innerhalb des Netzwerkes unterbrochen werden können, ohne das Netz in zwei Teile zu unterbrechen)
- Geometrischer Grad der Anisotropie (DA), dimensionslos (räumliche Orientierung der Trabekel innerhalb des Knochens; je mehr Trabekel in einer bestimmten Richtung innerhalb der Probe angeordnet sind, desto größer ist der DA)
- Structure Model Index (SMI), dimensionslos (Beschreibung der relativen Zusammensetzung des trabekulären Knochens aus Platten und Stäben, wobei die Tendenz der Knochenprobe zu vermehrt plattenförmigen oder vermehrt stabförmigen Trabekeln dargestellt wird; SMI = 0: ideale Platten; SMI = 3: ideale Stäbe)

4.3 Einsatz der Mikrocomputertomographie bei Magnesiumimplantaten

In den vergangenen Jahren wurden viele in vivo Studien im Bereich des ‚bone tissue engineering' mithilfe der µCT durchgeführt (Bouxsein et al. 2010). Vor allem für die Evaluierung der Biokompatibilität und Knochenneubildung sowie das Degradationsverhalten eines Knochenimplantates und die Wasserstoffbildung waren die genauen quantitativen Messungen der Mikrocomputertomographie von Vorteil (Lalk et al. 2010). Außerdem war es möglich in vivo Untersuchungen mit dem µCT durchzuführen, was bei Verfahren wie der Histomorphometrie nur ex vivo möglich war (Engelke et al. 1999). Lalk et al. (2010) untersuchten in ihrer in vivo Studie mit Kaninchen die Biokompatibilität und das Degradationsverhalten von bioglasbeschichteten Magnesiumschwämmen der Legierung AX30. Hierfür wurden zylinderförmige Implantate in die Kaninchenfemora implantiert. Anschließend wurden in vivo Parameter wie Implantatdegradation, Gas, periostale Zubildungen und Knochenstrukturen mit dem µCT gemessen und analysiert. Das

Ergebnis der Studie zeigte, dass die Bioglasbeschichtung nicht den gewünschten Effekt einer verlangsamten Implantatdegradation aufbrachte (Lalk et al. 2010). Thomann et al. (2010) untersuchten in ihrer in vivo Studie die Magnesiumlegierung LAE442 hinsichtlich ihrer Korrosionsbeständigkeit und mechanischen Stabilität. Dabei wurden Knochenimplantate intramedullär in die Tibia von Kaninchen implantiert und via µCT evaluiert. Durch die µCT-Scans konnte eine gleichmäßige Degradation und eine Knochenneubildung im Umkreis der Implantate festgestellt werden (Thomann et al. 2010). Auch Ullmann et al. (2011) analysierten in einer in vivo Studie mit Kaninchen das Degradationsverhalten von Magnesium Implantaten der Legierung LANd442 im Vergleich zu LAE442. Dabei setzten sie die Implantate in die Kaninchentibia ein und untersuchten das Implantat-Volumen, die Dichte und die Korrosionsrate via µCT. Festgestellt wurde, dass die Legierung LAE442 in Hinblick auf zukünftige Studien im krafttragenden Knochen stabiler und damit besser geeignet war als LANd442 (Ullmann et al. 2011).

5. Histologie

5.1 Histologische Untersuchungen von resorbierbaren Knochenersatzstoffen

Nicht nur die Computertomographie, auch die Histologie spielt eine wichtige Rolle in der Auswertung der Biokompatibilität von Knochenersatzstoffen im Knochengewebe. Die Biokompatibilität und Osseointegration hängen von der Grenzflächenreaktion zwischen Biomaterial und Knochengewebe ab (Jansen et al. 1994). Anhand von histologischen Dickschliffen oder Dünnschnitten kann die Gewebereaktion und Zellantwort auf ein Implantat beurteilt werden. Je nach Schnittdicke und Mikroskop-Objektiv können verschiedene Zelltypen und Gewebestrukturen beobachtet und ausgewertet werden (Donath und Breuner 1982). Proben können in verschiedene Medien, wie zum Beispiel Paraffin, Gelatine, Agar, Celloidin, Polyethylenglykol eingebettet werden, aber auch in Hartkunststoffe wie Technovit (Lang 2013). Die Toluidinblau-Färbung eignet sich sehr gut bei Dickschliffen, aber auch bei Dünnschnitten zum Nachweis von Osteozytenzellkernen, Osteoblasten und nicht-verkalkten osteoiden Bereichen, die aus Osteocalcin und Chondroitinsulfat bestehen (von Doernberg et al. 2006). Verkalkter Knochen erscheint in dieser Färbung dunkelblau (Willbold und Witte 2010). Aber auch andere Zellen, wie Makrophagen, Fremdkörperriesenzellen und

Fibrozyten können mit der Toluidinblaufärbung gut mikroskopisch erkannt werden (von Doernberg et al. 2006). Diese Färbung wird oft verwendet, um das Knocheneinwachsverhalten in das Implantat zu erforschen. Dabei kann eine Färbung mit Toluidinblau Auskunft über die Menge an Fremdkörperriesenzellen, Blutgefäßen und Knochen-Implantat-Kontakten geben (von Doernberg et al. 2006, Lalk et al. 2013).

5.2 Dünnschnitte

Dünnschnitte werden häufig in Paraffin, aber auch in Kunststoff eingebettet und mit einem Mikrotom unter Verwendung von Hartmetallmessern zugeschnitten (Lang 2013). Die Dünnschliffpräparat-Herstellung eignet sich aufgrund der sehr geringen Schnittdicke (0,5 – 10 µm) besonders für die Auswertung von Weichgewebe und zellulären Details (Schäfer 2011). Die histologische Präparation von Knochen gestaltet sich aufgrund der verkalkten Grundsubstanz jedoch schwieriger (Van der Lubbe et al. 1988). Eine vorherige Entkalkung des Knochens mit Säure kann zu einer Verzerrung und Denaturierung der Weichteile und des Knochenkollagens führen (Van der Lubbe et al. 1988). Entkalkt man den Knochen nicht, können bei Dünnschnitten die Kalziumsalze im Knochen das Schneiden mit dem Mikrotom stören und zu ausgefransten Schnitträndern führen (Van der Lubbe et al. 1988). Die Bearbeitung von Knochen-Implantat-Verbunden bereitet zusätzliche Schwierigkeiten (Van der Lubbe et al. 1988). Auch Willbold und Witte (2010) beschrieben in ihrer Studie, dass nicht resorbierbare Implantate aus Titan oder Stahl unmöglich zu schneiden waren, da sie beim Schneiden aus dem Gewebe herausbrachen und so der Implantat-Knochen-Kontakt nicht mehr beurteilt werden konnte. Heute kann durch spezielle Hartschnittmikrotome, Trenn-Dünnschliffverfahren und eine geeignete Einbettung mit Kunstharz der Erhalt von Zellen und Gewebe ermöglicht werden (Schäfer 2011). Dünnschnitte, die Knochen-Implantat-Verbunde enthalten, können unter anderem mit Toluidinblau, von Kossa/McNeal, TRAP, Masson-Goldner-Trichrom und Hämatoxylin-Eosin gefärbt werden (von Doernberg et al. 2006, Janning et al. 2010, Lang 2013, Willbold et al. 2015).

5.3 Dickschliffe

Besonders für mineralisierte nicht entkalkte Knochenproben und harte metallische Implantate sind Dickschliffe von Vorteil. Implantate brechen bei Dünnschnitten oft

aus dem Gewebe-Implantat-Verbund heraus, sodass die Grenzflächen nicht mehr ausreichend analysiert werden können (Willbold und Witte 2010). Dickschliffe haben den Vorteil, dass sie zunächst breiter zugeschnitten werden können und dann auf eine geringere Dicke geschliffen werden, ohne dabei das Gewebe direkt neben dem Implantat zu zerstören (Donath und Breuner 1982). Um Dickschliffe zu erzeugen, werden die Proben meist in Kunstharze wie Technovit eingebettet. Dieses Einbettsystem hat den Vorteil, dass es für mineralisiertes sowie für nicht mineralisiertes Gewebe verwendet werden kann (Willbold und Witte 2010, Lang 2013). Für die Herstellung von Dickschliffen werden die Probenblöcke auf Kunststoff-Objektträger geklebt und mit einem speziellen Diamantsägeblatt geschnitten. Anschließend werden die Schnitte geschliffen und poliert. Donath und Breuner (1982) entwickelten diese Säge-Schleif-Methode speziell zur histologischen Probenzubereitung von kalzifizierten Kieferknochen. Hierfür wurde der Knochen in Kunstharz eingebettet und auf Objektträger geklebt. Donath und Breuner nutzten Acryl-Harz. Heute wird oft Technovit 9100 verwendet (Lang 2013). Die Schnitte konnten laut Donath und Breuner (1982) mit einer Diamantsäge auf eine Dicke von 100-150 µm gesägt und anschließend auf eine Dicke von 5-10 µm geschliffen werden. Das maschinelle Schleifen hatte den Vorteil, dass die Schnitte gleichmäßig auf die gleiche Dicke geschliffen werden konnten (Donath und Breuner 1982). Dickschliffe, die Knochen-Implantat-Verbunde enthalten, können unter anderem mit Toluidinblau oder Hämatoxylin-Eosin gefärbt werden (Willbold und Witte 2010, Reifenrath et al. 2013). Mit beiden Färbungen kann man mikroskopisch unterschiedliche Gewebearten, wie Knochengewebe, Bindegewebe und verschiedene Zelltypen (u.a. Fibrozyten, Makrophagen, Fremdkörperriesenzellen, Erythrozyten) erkennen (Lang 2013).

5.4 Histomorphometrie

Um die Biokompatibilität von Biomaterialien auf histologischer Ebene zu beurteilen, kann man die Histomorphometrie zur Hilfe nehmen. Hierfür werden von gefärbten Dick- oder Dünnschnitten mittels Mikroskops digitale Bilder angefertigt, die an einen Computer weitergeleitet und mithilfe einer Analysesoftware ausgewertet werden (Bartels 2011). Dadurch ist es möglich aus zweidimensionalen Messungen Rückschlüsse auf dreidimensionale Strukturen wie zum Beispiel das Knochenvolumen zu ziehen (Carpenter 1979, Bartels 2011). Der genaue Anteil von Strukturen wie Knochenvolumen, Trabekelzahl oder Implantatmaterial kann

erkannt und in Prozent (%) quantitativ erfasst werden (Bartels 2011). In gefärbten Knochenpräparaten von Smith und Karagianes (1974) stellte sich Knochengewebe orange-rot dar. Mit Hilfe eines Histomorphometrie-Software-Programmes konnte aus diesem gefärbten Bild erstmals ein Binärbild erstellt werden, in dem Knochengewebe weiß und alles andere schwarz erschien (Bartels 2011). Für alle nachfolgenden Bearbeitungen galt nun das Binärbild als Grundlage (Bartels 2011) Heute werden erweiterte maschinelle Lernverfahren (‚machine learning') genutzt. Sie bilden eine Form der künstlichen Intelligenz (Rosy Manser 2018). Anhand einer intelligenten Software kann ein exakteres Erkennen von Gewebestrukturen erlernt und angewandt werden. So können Computerprogramme, die auf maschinellem Lernen basieren, mit Hilfe von Algorithmen selbständig Lösungen für neue und unbekannte Probleme finden (Rosy Manser 2018).

5.5 Vergleich Histomorphometrie – Mikrocomputertomographie

Aufgrund der zunehmenden Verbreitung der µCT-Technologie war es erforderlich, die neu entstandenen 3D-Daten der µCT mit den 2D-Daten der konventionellen Histomorphometrie zu vergleichen (Nägele 2005). Bereits 1998 führten Müller et al. (1998) eine Studie mit Beckenkammbiopsien durch und verglichen jeweils die Ergebnisse der µCT-Scans mit der Histomorphometrie-Auswertung (Müller et al. 1998). Die Bestimmung von Tb.Th und Tb.Sp via µCT erfolgte dabei unter Annahme eines Plattenmodelles, da dies in der histomorphometrischen Untersuchung verwendet wurde (Müller et al. 1998, Nägele 2005). Beim Vergleich der Ergebnisse der Histomorphometrie und der µCT wurden mehrere Korrelationen gefunden. Müller et al. (1998) schlussfolgerten, dass die µCT eine valide Methode für die Analyse des menschlichen trabekulären Knochens darstellte. Auch Kuhn et al. (1990) verglichen µCT-Bilder von trabekulären Knochenwürfeln mit den entsprechenden histomorphometrischen Bildern, um die Genauigkeit der Darstellung zu untersuchen. Dabei fungierten Messungen des Knochenvolumenanteils sowie der Trabekelplattendichte als Vergleichsparameter. Die Ergebnisse zeigten, dass sich die µCT-Messungen nicht signifikant von den histomorphometrischen Messungen unterschieden und dass die µCT als geeignetes Auswertungsmedium angesehen werden konnte (Kuhn et al. 1990). Eine etwas jüngere Vergleichsstudie lieferten Thomsen et al. (2005). Sie verglichen µCT-Datensätze von gewonnenen Knochenstrukturen aus humanen Tibia-Biopsien mit den entsprechenden konventionellen histologischen Schnitten. Dabei evaluierten

sie das trabekuläre Knochenvolumen (BV/TV), sowie die Konnektivitätsdichte (Conn. D) mit beiden Techniken. Es wurden ausgezeichnete Korrelationen zwischen der µCT und der Histologie gefunden. Thomsen et al. (2005) folgerten, dass µCT-Datensätze als Ersatz für konventionelle Histomorphometrie zur Untersuchung der spongiösen Knochenstruktur verwendet werden können.

III. PUBLIKATION I

‚Influence of coatings on degradation and osseointegration of open porous Mg scaffolds in vivo'

Journal: Materialia

Autoren: Laura Marie Witting, Anja-Christina Waselau, Franziska Feichtner, Lisa Wurm, Stefan Julmi, Christian Klose, Ann-Kathrin Gartzke, Hans Jürgen Maier, Peter Wriggers, Andrea Meyer-Lindenberg

Das Paper ‚Influence of coatings on degradation and osseointegration of open porous Mg scaffolds in vivo' wurde am 08.08.2020 zur Publikation im Journal ‚Materialia' eingereicht und am 04.11.2020 akzeptiert. Es wurde am 20.11.2020 publiziert.

https://doi.org/10.1016/j.mtla.2020.100949

Materialia 14 (2020) 100949

Contents lists available at ScienceDirect

Materialia

journal homepage: www.elsevier.com/locate/mtla

Full Length Article

Influence of coatings on degradation and osseointegration of open porous Mg scaffolds in vivo

L.M. Witting[a], A.-C. Waselau[a], F. Feichtner[a], L. Wurm[a], S. Julmi[b], C. Klose[b], A.-K. Gartzke[c], H.J. Maier[b], P. Wriggers[c], A. Meyer-Lindenberg[a,*]

[a] Clinic of Small Animal Surgery and Reproduction, Ludwig-Maximilians-University Munich, Veterinärstraße 13, 80539 Munich, Germany
[b] Institut für Werkstoffkunde (Materials Science), Leibniz Universität Hannover, Garbsen, Germany
[c] Institute of Continuum Mechanics, Leibniz Universität Hannover, Germany

ARTICLE INFO

Keywords:
Coating
PLA/CaP
Magnesium alloy
Open porous scaffolds
Osseointegration
Micro-tomography

ABSTRACT

Degradable bone substitutes like Mg-based alloys are promising due to their good osseointegration and biocompatibility. The objective of this study was to investigate the influence of additional coatings on the degradation behavior, osseointegration and gas release of 128 open porous scaffolds (Ø 4 mm, length 5 mm) of the magnesium alloy LAE442 (4 wt% Li, 4 wt% Al, 2 wt% rare earths). Along a base layer of MgF_2 polylactide acid (PLA) or calcium phosphate (CaP) were applied. While the resorbable PLA was supposed to delay the magnesium degradation, the CaP should form a nutrient depot for growing bone. The control group consisted of 32 β-tricalcium phosphate (TCP) scaffolds. The scaffolds were inserted into the greater trochanter of 80 adult female ZiKa rabbits. X-ray and in vivo μCT scans were performed postoperatively at regular intervals of 6, 12, 24, 36 weeks. Gas accumulation, scaffold degradation and osseointegration were evaluated. In comparison, PLA-coated scaffolds degraded slightly slower, but had a significantly greater amount of gas in the medullary canal at weeks 2 and 4 compared to CaP-coated scaffolds. CaP-coated scaffolds showed better values for drill hole closure and a significantly higher number of bone-scaffold contacts from week 12 to 36 compared to PLA. Furthermore, CaP-coated scaffolds showed higher bone volume and more new formed bone trabeculae than PLA-coated scaffolds. In total, an additional coating with CaP seemed to be promising in improving the degradation resistance and osseointegration, when using biodegradable bone substitutes.

1. Introduction

Large bone defects, so-called critical size defects, which are caused by severe trauma, infection or tumours, have to be treated with implants of any kind, be it autografts, allografts or synthetic materials. All of these types of implants are associated with different health risks or imply further surgical intervention [1,2]. For this reason, resorbable bone substitutes, such as polymers, ceramics and other metals, have been researched for several years [2,3]. Of this group, biodegradable magnesium alloys have been classified as especially promising bone substitutes in recent years [4–6], due to the fact that magnesium already occurs naturally in living organisms [7]. In bulk form, the mechanical properties of magnesium, such as the elastic modulus and the compressive strength, already resemble those of cancellous bone. That reduces the risk of stress shielding and offers more advantages than other implantable metals [8,9]. In addition to high mechanical stability, magnesium alloys exhibit good biocompatibility, inherent biodegradability and osteoconductive properties [10,11], which ceramics like ß-tricalcium phosphate (TCP) or polymers cannot achieve. The osteoconductivity of a material is closely linked with the potential for osseointegration of the surrounding bone. Osseointegration is the result of a bone healing process in which the bone cells grow directly onto the implant and achieve firm attachment to the implant surface [12]. New bone tissue can be created by the migration of osteoblasts or bone marrow cells into a scaffold that can intermediately be degraded, be absorbed by the body and be replaced by the surrounding tissue [11,37]. Thus, the scaffold provides the frame and dimensional space for cell ingrowth [11]. Principally, an ideal bone tissue engineering scaffold should have a pore size that is similar to cancellous bone to help bone cells growing into the pores [11,31].

However, implants made of pure magnesium (Mg) degrade too quickly for osseointegration to take place [2]. A fast degradation of Mg scaffolds is always related to the emergence of hydrogen gas, that can accumulate and spread out [10,13]. In order to reduce the degradation rate of Mg alloys, various material and manufacturing properties, such as the 'laser additive manufacturing process' have been investigated [11,14]. By adding other elements such as aluminium, lithium, or

* Corresponding author.
E-mail address: ameylin@lmu.de (A. Meyer-Lindenberg).

https://doi.org/10.1016/j.mtla.2020.100949
Received 8 August 2020; Accepted 4 November 2020
Available online 7 November 2020

even graphene oxide, the strength and corrosion resistance of Mg can be increased [15,16,17]. The addition of rare earths or their individual elements, such as lanthanum, cerium and neodymium, can also increase the stability and strength of Mg implants and cause corrosion to be reduced [17,18,19,20].

The magnesium alloy LAE442 (4 wt% Li, 4 wt% Al, 2 wt% rare earths) has been shown to be particularly advantageous. It has already been tested frequently as a solid implant [6,10] as well as a porous scaffold [22,30,31] in vivo and showed positive results with a relatively slow and uniform degradation behavior. Maier et al. summed up that samples from LAE442 scaffolds showed a dense homogeneous corrosion layer in vitro, which is obviously an effective barrier for further corrosion attack and the reason for the slow degradation of this alloy [23].

Pores with a size of >300 µm were found to be promising for bone ingrowth behavior [32]. To further slowdown the degradation rate and to improve the corrosion resistance of Mg implants, coatings, like magnesium fluoride ($MgF_{2)}$, are often used [21,22]. In several studies a singular MgF_2-coating already has shown a reduction in the degradation behavior of Mg implants [21,22,33,38]. However, even with the MgF_2-coating gas was produced to a significant degree during degradation [33,34], which displays still a too fast degradation [10,37,33,38]. Wang et al. investigated Mg-Sr alloy scaffolds with additional coatings, such as micro-arc oxidation coating (MAO), calcium phosphate- (CaP) and strontium phosphate- (SrP) coating [39]. They concluded that CaP-coated scaffolds showed the highest corrosion resistance in vitro and furthermore the least gas release in vivo, while SrP-coating lead to superior osteoinductive properties. In vivo and in vitro studies by Yang et al. and Dorozhkin described a significant decrease in the degradation rate of Mg implants with a CaP-coating and an associated improvement in surface biocompatibility [28,29]. Additionally to CaP, a coating with polylactide acid (PLA) seems encouraging. PLA, as coating on Mg implants already showed increased resistance to degradation compared to uncoated implants in previous in vitro studies [25,26,27]. However, until now PLA coatings have not been tested on porous LAE442 scaffolds in an in vivo setting.

To overcome the difficulties with an increased gas release and to fast degradation of LAE442, Julmi et al. and Maier et al. investigated in their in vitro study the combination of MgF_2 and PLA or CaP as specific coating layers [23,25]. They placed the implants in SBF and analyzed the loss of mass and volume over 12 weeks. Finally, they concluded that the degradation rate could be successfully decreased in vitro by using a second coating layer on top of MgF_2. Both additional coatings (PLA/CaP) improved the degradation resistance, while the combination of MgF_2 + PLA was the most effective one [25]. Jo et al. investigated a hydroxyapatite coating (HA) on Mg implants with MgF_2 interlayer in vivo. They found out that a double layer coating with MgF_2 an HA improved and elongated the corrosion resistance of the implants, compared to the ones only coated with MgF_2 [8].

In the present study 128 open porous LAE442 scaffolds with two distinct layers of coating, first the base layer of MgF_2 and furthermore an additional layer of either PLA or CaP were inserted into the greater trochanter of rabbits. All animals were closely inspected over a 36-week period, with periodical X-ray and µCT screenings. A special focus was directed to the degradation behavior, osseointegration and gas release of the Mg scaffolds. In particular, the influence of coating with PLA/CaP should be worked out and investigated. Based on in vitro experiments the resorbable PLA is supposed to delay the magnesium degradation, while CaP should form a nutrient depot for bone formation [21,25].

2. Material and methods

2.1. Scaffolds

For this study, cylindrical scaffolds (n = 128; Ø 4 mm, length 5 mm) made of the magnesium alloy LAE442 (4 wt% Li, 4 wt% Al, 2 wt% rare earths) were produced by investment casting [35]. The scaffolds were interspersed either with a maximum pore size of 400 µm (P1) or 500 µm (P2) (strut thickness P1: 0.4/0.3 mm; P2: 0.5/0.4 mm; porosity P1: 43.4%; P2: 41.4%; volume P1: 37.38 mm^3; P2: 38.37 mm^3; surface area P1: 303 mm^2; P2: 266 mm^2) [25].

Initially, the scaffolds were produced as wax models using a 3D printer (T612, Solidscape, Inc., Merrimack, USA). Those models were welded to a casting tree, which was then embedded in gypsum (Gilcast AM, BK Giulini GmbH, Ludwigshafen, Germany), from which the wax was later melted out. The investment casting was carried out with a benchtop casting furnace (MC50, Indutherm GmbH, Walzbachtal-Wössingen, Germany) at a nominal temperature of 310 °C. The liquid alloy was poured into the plaster mould, hardened and removed from the mould. The remaining plaster was removed with a plaster remover and an ultrasound bath. The scaffolds were coated with magnesium fluoride (MgF_2) using the conversion coating method [25]. Half of the scaffolds (n = 64) were additionally coated with polylactide acid (PLA), the other half (n = 64) with calcium phosphate (CaP). The PLA-coating was applied by deposition coating, with the scaffolds dipped in a PLA-Dichlormethane (DCM) solution. The CaP-coating was applied directly onto the scaffold surface using two solutions (phosphatic solution, pH 7.4 and calcium nitrate tetrahydrate). The immersion time of both solutions was 5 min with a pause of 10 s regardless of pore size. Subsequently, the scaffolds were immersed in distilled water. Both coatings on the implant surface have been distributed unevenly but without clogging the pores [25]. The PLA-coating was more homogeneous, while the CaP-coating had a lower viscosity so that the liquid could penetrate more easily into the pores. In total, both coatings were having a high adhesive force [25].

Altogether four different LAE442 scaffold groups (n = 32 per group, total n = 128) were produced for this study, which differed in pore sizes and the type of coating: PLA-P1, PLA-P2, CaP-P1, CaP-P2. The control group consisted of commercially available porous scaffolds (Ø 4 mm, length 5 mm, n = 32) of β-tricalcium phosphate (TCP) (multiporosity with meso- and macropores between 5 µm - 500 µm; total porosity: 65%; Cerasorb M, Curasan AG, Kleinostheim, Germany). TCP scaffolds are already clinically used and show very good degradation and osseointegration [47,48], however they are not mechanically stable enough for critical size defects, especially in weight bearing bone. All scaffolds were sterilized by gamma irradiation (> 25 kGy, BBF Sterilisationsservice GmbH, Kernen, Germany) prior to use.

2.2. Animal model and test procedure

The animal experiment was approved by the regional government of Upper Bavaria, paragraph 8 of the Animal Welfare Act (registration number: 55.2–1–54–2532–181–2015). For this study, 80 mature female Zimmermann rabbits (ZiKa, Asamhof, Kissing, Germany) were used. The rabbits were > 6 months old and weighed 4 kg (3.96 ± 0.27 kg). Water and hay were provided ad libitum combined with a fixed daily amount of pellets (Kanin Kombi, Rieder Asamhof GmbH, Kissing, Germany). The rabbits received enrofloxacin (10 mg/kg, Enrobactin®, CP-Pharma GmbH, Burgdorf, Germany) and meloxicam (0.3 mg/kg, Rheumocam®, Albrecht GmbH, Aulendorf, Germany) prior to surgery and for the following 5 days after. Ketamine (15 mg/kg, Anesketin®, Albrecht GmbH, Aulendorf, Germany) and medetomidine (0.25 mg/kg, Dorbene vet®, Zoetis Deutschland GmbH, Berlin, Germany) were given for anaesthetic induction. The rabbits were intubated, and anaesthesia was maintained with a mixture of oxygen and isoflurane. For intraoperative analgesia, the animals received intravenous administration of fentanyl as bolus (3 µg/kg, Fentadon®, Albrecht GmbH, Aulendorf, Germany) and buprenorphine (20 µg/kg, Bupresol®, CP-Pharma GmbH, Burgdorf, Germany). A continuous fentanyl drip infusion (5 µg/kg/h, Fentadon®, Albrecht GmbH, Aulendorf, Germany) was administered during surgery.

In advance, a randomization cross table has been established, in order to achieve an unbiased distribution of the animals and scaffolds per time group and material. One scaffold was inserted per greater

Fig. 1. Representative illustration of a rabbit femur, demonstrating the implantation position within the greater trochanter.

trochanter of each femur (Fig. 1). A lateral surgical approach was made with a 4 cm vertical skin incision. The fascia and the origin of the M. gluteus superficialis were split to expose the proximal part of the trochanter major. A 6 mm deep hole was drilled into the trochanter with a 4 mm drill. After insertion of the scaffold, the surgical incision closure was performed with resorbable and non-absorbable sutures (Monosyn 4/0 HR22 and Optilene 4/0 DS19, B.Braun Medical, Barcelona, Spain) in several standardized layers. The first µCT scan and a ventrodorsal X-ray image of the pelvis were made direct postoperatively. Antagonization of medetomidine was achieved after imaging by intramuscular administration of atipam (25 mg/kg, Atipam®, Albrecht GmbH, Aulendorf, Germany). The animals were clinically evaluated daily after surgery for signs of lameness and pain.

2.3. Imaging examinations (X-ray, µCT)

Radiographs and µCT scans of the region of interest (ROI) were performed directly post surgery, every two weeks until week 12 and then every four weeks until the end of the observation period (Fig. 2a,b). The animals were put under a short anaesthesia using medetomidine (0.25 mg/kg) and ketamine (15 mg/kg). The in vivo µCT examinations (XtremeCT II, Scanco Medical, Zurich, Switzerland) were performed with the following settings: 68 kV, 1000 projections, 200 ms integration time and an isotropic voxel size of 30.3 µm. The ROI for the µCT scans extended from the minor trochanter to just above the greater trochanter. The X-ray images were taken with the exposure settings of 54.9 kV and 4.5 mAs (Multix Select DR, Siemens Healthcare GmbH, Erlangen, Germany).

2.4. Semiquantitative evaluation

2.4.1. Semi-quantitative evaluation of X-ray images

The X-ray images were evaluated using the dicom PACS® software (version 8.3.20, dicom PACS, Oehm und Rehbein GmbH, Rostock, Germany). An adapted scoring system based on Lalk et al. and Augustin et al. was applied [34,36]. The gas accumulation in the surrounding musculature (descriptive), periosteal bone formation in the area of the drill hole (size in mm) and scaffold visibility (descriptive) were assessed. Scores between 0 (not present) and 2 (clearly changed) were assigned (Table 1).

2.4.2. Semi-quantitative evaluation of µCT scans

The evaluation of the µCT scans was performed with the software 'µCT Evaluation Software V6.6' (Scanco Medical, Zurich, Switzerland). A scoring system based on Lalk et al. and Augustin at al. [34,36] was applied. The following parameters were evaluated: scaffold position (descriptive), gas accumulation around the scaffold (descriptive), gas accumulation in the medullary canal (descriptive), periosteal bone formation in the area of the drillhole (size in mm) and the closure of the drillhole (descriptive) (Fig. 3a,b,c,d). These parameters were evaluated in the original µCT scans. Scores ranged from 0 (positive, physiological) to 2 (negative, clearly changed) (Table 1).

In order to achieve a comparable evaluation of the bone-scaffold contacts, all scaffolds were contoured on the original µCT scans and reoriented for a cross sectional view of the scaffolds. Six defined cross-sections were evaluated, with scores ranging from 0 (many bone-scaffold contacts) to 2 (no bone-scaffold contact).

2.5. Quantitative evaluation of µCT scans

For the quantitative evaluation of implant degradation and implant integration, scaffolds were analysed at the time of immediate post-op surgery, as well as at the respective observation end timepoints (6, 12, 24, 36 weeks).

2.5.1. Scaffold degradation

The reoriented µCT scans were also used in order to analyse the scaffold degradation. A cylindrical ROI (Ø 132 voxel = 3.99 mm; height: 50 slices = 1.52 mm (PLA-P1, CaP-P1); 60 slices = 1.82 mm (PLA-P2, CaP-P2, TCP) was defined (Fig. 4a–c), containing two strut- and two pore levels in the center of the scaffold cylinder. A threshold of 146 for LAE442 and 148 for TCP was determined and applied to evaluate the parameters scaffold volume (%) and scaffold density (mg HA/ccm) [33,34].

2.5.2. Scaffold integration

In order to assess scaffold integration in the surrounding cancellous bone an additional ROI was created by placing a second ring around the first ring. The space between these two rings was evaluated (Fig. 5a,b). The inner ring was 134 voxels (4.06 mm) in diameter to avoid including any implant material, while the outer ring was 160 voxels (4.82 mm) in diameter. A threshold of 120 was adopted for the cancellous bone from the study by Augustin et al. and applied for the evaluation of the double ring [34]. Bone density (mg HA/ccm), bone volume (%), number of trabeculae (1/mm) and trabecular thickness (mm) were evaluated.

2.6. Statistics

Statistical analyses were performed with 'Microsoft Excel 2016' (Microsoft Corporation, Redmond, WA 98052-6399, USA) and 'SPSS Statistics 25.0' (IBM, Armonk, NY 10,540, USA). All quantitative parameters (density and volume of scaffold and bone; trabecular number, trabecular thickness) were tested for normal distribution with a Kolmogorov-Smirnov-test. Due to the lack of normal distribution, all quantitative and semi-quantitative (gas accumulation, periosteal bone formation, bone-scaffold contacts) parameters were tested for statistical significance ($p < 0.05$) using the Kruskal-Wallis test. In case of significant differences an ANOVA was performed as a post hoc test with a Bonferroni correction. If only two samples had to be compared, a Mann–Withney-U test was used instead.

3. Results

Two implanted PLA-P1 scaffolds had to be excluded from evaluations after 2 or respectively 6 weeks post-surgery due to the separation of a bone piece at the greater trochanter, which was observed in X-rays and µCT scans. Therefore, the scaffolds were no longer completely embedded

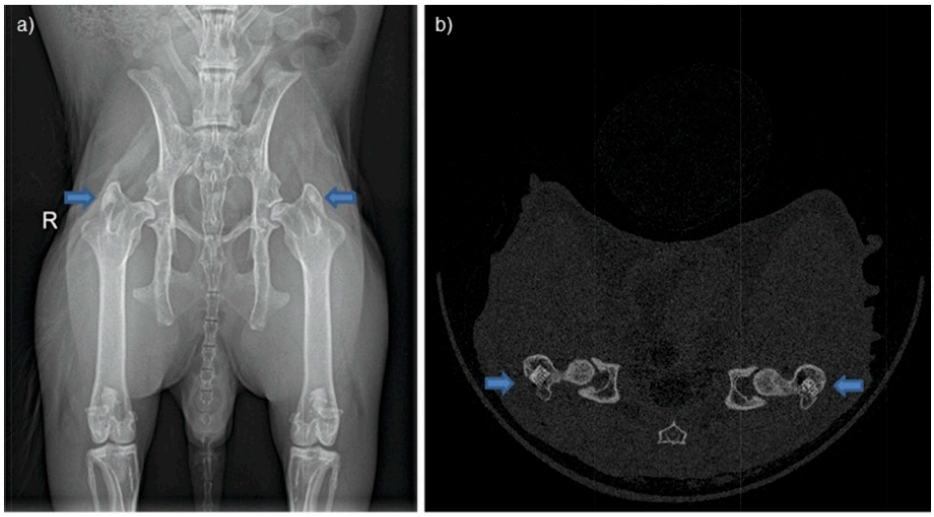

Fig. 2. In vivo imaging of the implants within the rabbit femora. (a) Radiograph of rabbit in ventro-dorsal position; (b) µCT scan, demonstrating the cross section of the scaffolds.

Table 1
Semi-quantitative scoring system to evaluate different parameters with the original µCT-scans (exemplary longitudinal section shown in Fig. 5a). The parameter 'bone-scaffold-contact' was evaluated by six cross sections through the scaffolds (exemplary cross section shown in Fig. 5b).

Parameter	Score 0	Score 1	Score 2
Gas[a]			
- around scaffold - in medullary canal	none	few or diffuse	clear and measurable bubbles
Periosteal bone formation[a]	none	≤ 7 mm in length and ≤ 2 mm wide	> 7 mm in length and > 2 mm wide
Drill hole closure	closed	partially closed	open
Bone-scaffold-contact	many direct contact points to trabecular bone, only isolated gaps in between	trabecular bone in surrounding but only few contacts points, clear gaps in between	no contact to trabecular bone, complete gap around the scaffold

*[a] The parameters 'gas' and 'periostal bone formation' also apply to the X-ray evaluations.

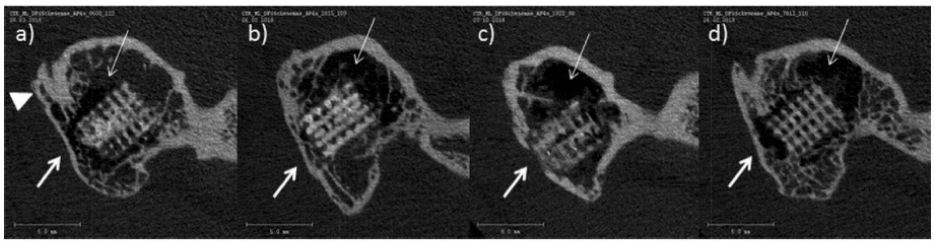

Fig. 3. In vivo µCT-scans of LAE442 scaffolds after 36 weeks of implantation. Longitudinal section; thin arrows: gas accumulation, thick arrows: drill hole closure; triangle: periosteal bone formation; (a) CaP-P1; (b) CaP-P2; (c) PLA-P1 (drill hole not closed); (d) PLA-P2.

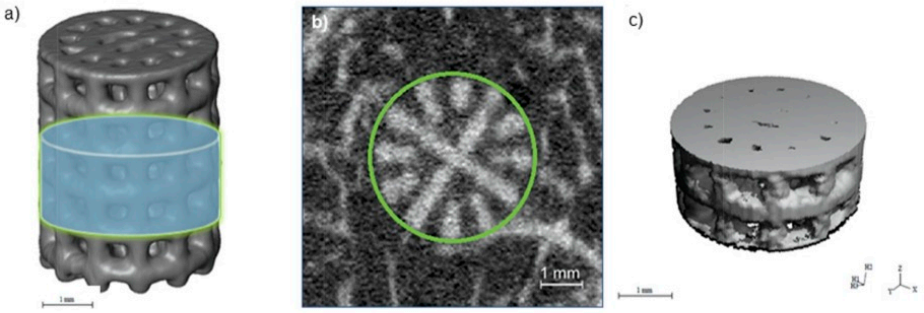

Fig. 4. Illustration of cylindrical region of interest used for quantitative measurement of the scaffold degradation. (a) The region contains 50 (P1) or 60 (P2) slices, including two struts and two pores in the middle of the scaffold with contact to cancellous bone; (b) ROI visible as a green ring around the scaffold, including scaffold material; cross section of scaffold; (c) 3D-view of the middle part of scaffold.

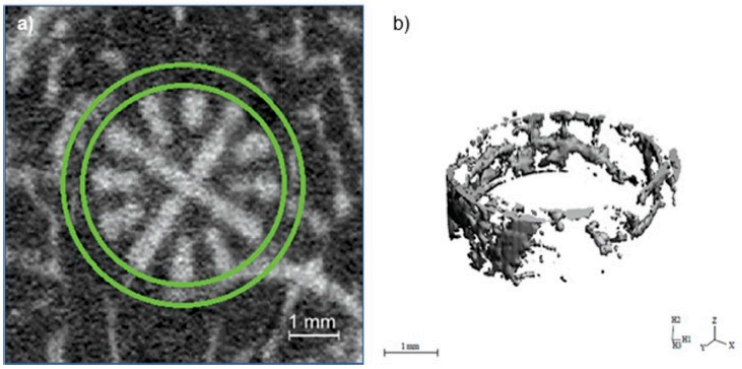

Fig. 5. Illustration of the ROI in form of a double ring around the scaffold used for quantitative evaluation of the scaffold integration. (a) ROI visible as a green double ring in the vicinity of the scaffold, including bone; cross section of scaffold; (b) 3D-view of the vicinity of scaffold.

in bone. Clinically, these two animals showed no signs of lameness or pain in the affected leg.

3.1. Clinic

Clinically, all scaffolds were well tolerated by the animals. Physiological redness and swelling were observed until day 3 after surgery. Surgical wounds healed without complications. No lameness or pain was observed in the hind limbs. A subcutaneous emphysema could not be palpated at the implantation site at any time.

3.2. Results of the semi-quantitative X-ray evaluation

All LAE442 scaffolds, regardless of pore size and coating, showed a steady increase in gas formation from the time of insertion up to the 36th week. In TCP scaffolds no gas was visible from week 2 on. Periosteal bone formation in the drill hole area was observed in all scaffold types and increased in size over time (Fig. 6). The LAE442 scaffolds were visible at all times. However, the TCP scaffolds were no longer clearly identifiable from week 10 onwards, with the visibility of LAE442 ($p < 0.05$) differing significantly from week 12.

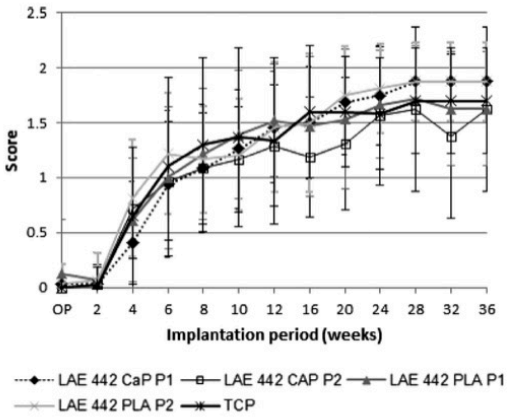

Fig. 6. Results of the semi-quantitative X-ray evaluation for the parameter: periosteal bone formation; score values from 0 (not existing) to 2 (> 7 mm long/ > 2 mm wide).

3.3. µCT results

3.3.1. Semi-quantitative evaluation results

The implants of all material groups were placed precisely in the cancellous part of the greater trochanter. Gas was visible in the radiographs as radiolucent volumes over the entire investigation period (Fig. 3a–d). The gas formation increased in close proximity to the implant until week 12 (CaP-P1), 16 (PLA-P2) and 20 (CaP-P2). A decrease in gas formation was only moderately noticeable at 36 weeks. PLA-P1, on the

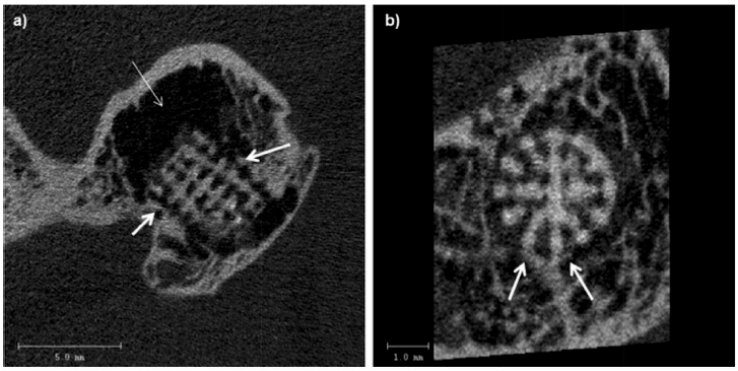

Fig. 7. In vivo μCT-scans of LAE442 scaffolds after 20 weeks of implantation. (a) Longitudinal section; thin arrows: gas accumulation, thick arrows: bone-scaffold-contacts; (b) Cross section; thick arrows: bone-scaffold-contacts (new bone trabeculae adhering to the scaffold surface).

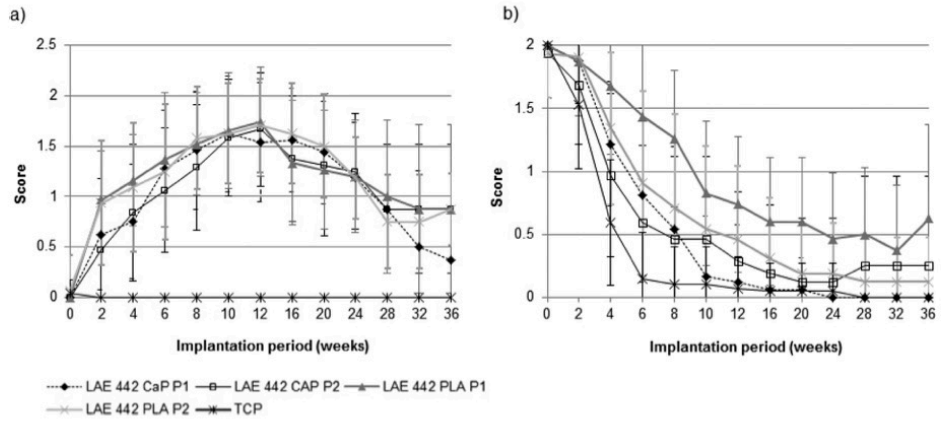

Fig. 8. Results of the semi-quantitative μCT evaluation for the parameters: (a) Gas accumulation in the medullary bone cavity, (b) Drill hole closure; score values from 0 (not existing) to 2 (clear alteration).

other hand, showed increasing gas formation up to week 28, with still higher gas volumes at the last investigation timepoints compared to the other LAE442 scaffolds. Gas accumulation could be also observed in the femoral medullary canal (Fig. 7a). The accumulated gas increased in all LAE442 scaffolds until week 12 and decreased significantly again until week 36 (Fig. 8a). It was noticeable that PLA-coated scaffolds had a significantly greater amount of gas in the medullary canal at weeks 2 and 4 compared to CaP-coated scaffolds (PLA-P1 vs. CaP scaffolds, $p \leq 0.042$). In TCP scaffolds, gas formation could only be detected around the implant directly post-surgery.

During the course of the examination periods, all scaffolds showed a significant increase in periosteal bone formation in the drill hole area with no significant differences between scaffold types ($p \geq 0.05$) (Fig. 3a).

With respect to drill hole closure, it was noted that the holes from the CaP-coated scaffolds closed faster than the PLA scaffolds (Fig. 8b) (Fig. 3a–d), with PLA-P1 differing significantly from all other implants from week 2 onwards ($p \leq 0.043$) . 8 of 32 PLA-P1 scaffolds still did not show a drill closure after 24 weeks, 4 of 32 holes were not closed after 36 weeks. By comparison, in CaP scaffolds all drill holes were closed at 24 weeks regardless of pore size. Overall, in TCP the drill holes closed significantly faster ($p < 0.05$) than in LAE442, with the majority (24 of 40) closed at week 6.

Looking at bone-scaffold contacts, CaP-coated implants showed a significantly higher number of bone-scaffold contacts from week 12 to 36 compared to PLA-coated implants regardless of pore size ($p \leq 0.017$) (Fig. 7a,b) (Fig. 9). From week 2 onwards, bone-scaffold contacts increased in CaP-P2. PLA-P2 and CaP-P1 showed an increase in bone-scaffold contacts from week 6. In contrast to these scaffolds, PLA-P1 exhibited a steady decrease in bone-scaffold contacts from the time of surgery until the end of the observation period, with the exception of week 20 to 28. Most contacts were seen in CaP-P2 scaffolds, with significantly more bone-scaffold contacts from week 12 to week 36 than in PLA-P1 ($p \leq 0.034$). It was noticeable that from week 28, a decrease in bone-scaffold contacts could be observed again in all LAE442 scaffolds regardless of the coating.

TCP scaffolds showed a decrease in the number of bone-scaffold contacts from week 2 to week 8, followed by an increase from week 8 to 36. From week 8 onwards, significantly more contacts could be observed with TCP than with the various LAE442 scaffolds ($p \leq 0.044$).

3.3.2. *Quantitative evaluation results*

Scaffold degradation: Scaffold degradation was measured with the parameters scaffold volume (%) and scaffold density (mg HA/ccm) of the implants. The data showed a significant difference for TCP in comparison to the LAE442 scaffolds ($p < 0.05$) with the largest volume loss of

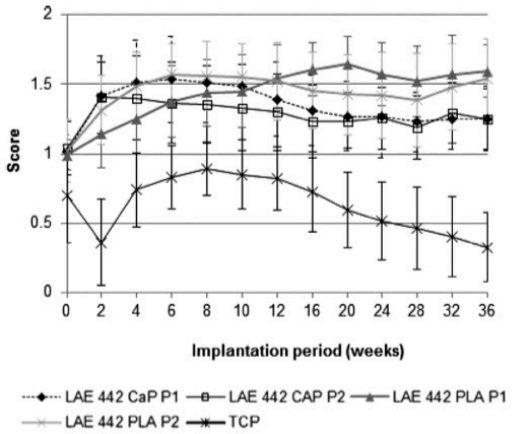

Fig. 9. Results of the semi-quantitative µCT evaluation for the parameter: bone-scaffold-contact; score values from 0 (not existing) to 2 (clear alteration).

74.7%, and a density loss of 6.4 mg HA/ccm in TCP. Volume and density of all LAE442 scaffolds decreased between surgery and week 36, regardless of coating and pore size. The volume and density loss at 36 weeks was 13.4%, 7.75 mg HA/ccm (CaP-P1), 10.0%, 5.76 mg HA/ccm (PLA-P1), 8.7%, 4.7 mg HA/ccm (CaP-P2), and 6.0%, 1.7 mg HA/ccm (PLA-P2) (Fig. 10a,b).

Scaffold integration: To evaluate the integration of the scaffold into the bone the following parameters were analysed: bone density (mg HA/ccm), bone volume (%), number of trabeculae (1/mm) and trabecular thickness (mm). Overall, bone density increased steadily over time in the surroundings of all LAE442 scaffolds, while higher density values were observed for scaffolds with larger pore sizes (CaP-P2, PLA-P2) compared to smaller pore sizes up to week 24 (Fig. 11a). TCP scaffolds also showed an increase in bone density in the surroundings. The bone volume of all LAE442 scaffolds decreased during the first 6 weeks of testing, increasing steadily from week 6 for CaP-P1 and week 12 for CaP-P2 and PLA-P2, respectively (Fig. 11b). PLA-P1 showed a visible increase in bone volume between week 6 and 12 with a steady decrease in bone volume from week 12, and the lowest values were reached at week 36. CaP-P2 constantly showed the highest bone volume values and differed significantly from PLA-P1 over the entire period ($p \leq 0.034$). LAE442 scaffolds showed a similar course with regard to the number of bone trabeculae with a decrease in the first weeks and an increase from week 12 (CaP-P1 and PLA-P2) and week 24 (CaP-P2), respectively (Fig. 11c). After 36 weeks, PLA-P1 showed the lowest number of trabeculae. The trabecular thickness of all LAE442 scaffolds remained approximately constant over time (Fig. 11d). TCP scaffolds also showed an increase in bone density in the surroundings. Bone volume and the number of trabeculae around the TCP scaffolds did not increase until week 24. The trabecular thickness of all LAE442 scaffolds remained approximately constant over time (Fig. 11d), while the trabecular thickness of TCP scaffolds increased from the day of implantation onwards. TCP showed a significant difference in trabecular thickness to all LAE442 scaffolds ($p < 0.05$) at all weeks.

4. Discussion

The objective of this study was to investigate osseointegration and degradation of open porousd Mg scaffolds with PLA-/CaP-coatings as bone substitutes in a rabbit model. Implants of the Mg alloy LAE442 have already been tested in vivo in previous studies in the form of non-porous [5,6,24] as well as porous structures [33,34] and showed a good biocompatibility. However, even with an MgF_2-coating, the disadvantage of these implants is their fast degradation and increased gas formation during degradation. To master this problem, this in vivo study attempted to regulate the degradation and gas formation in porous LAE442 scaffolds with an additional coating (PLA or CaP) on top of the regularly used MgF_2-coating.

Two implanted PLA-P1 scaffolds had to be excluded due to the detachment of a bone fragment on the greater trochanter, as no comparable evaluation could be performed. However, the cause of the detachment could not be completely clarified, other than both implants are PLA-P1. There are several possible options: a lesion could be provoked during surgery. However, this is unlikely as the detachments were only observed 2 or respectively 6 weeks after surgery. Furthermore, trauma could be possible, which might have happened during the daily physical activity time outside the cage of the rabbits. However, the clinical examination did not reveal any hematoma or lameness. Another cause could be gas that was produced during the degradation of the scaffold. In these two implants, however, there was no increased gas formation compared to other animals. Reifenrath et al. described a tibia fracture,

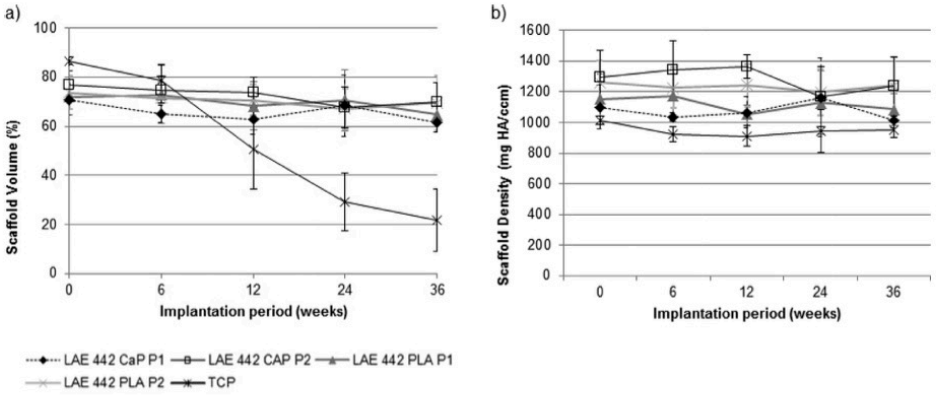

Fig. 10. Evaluation of scaffold degradation. Results of quantitative µCT measurements for (a) Scaffold volume and (b) Scaffold density (ROI corresponds to the middle area of the scaffolds).

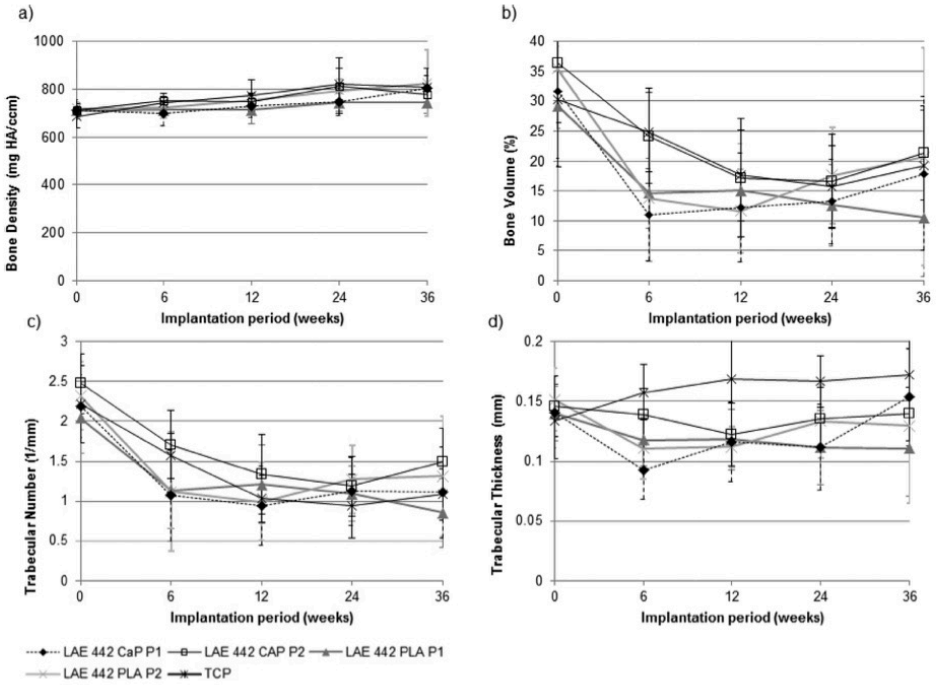

Fig. 11. Evaluation of scaffold integration. Results of quantitative µCT measurements for (a) Bone density; (b) Bone volume; (c) Trabecular number and (d) Trabecular thickness (ROI corresponds to the vicinity of the scaffolds).

as well as massive clinical problems due to increased gas formation and too rapid degradation of intramedullary pins of the Mg alloy LACer442 [40]. However, this was not the case in the present study, as all LAE442 scaffolds slowly degraded and were clinically well tolerated by the animals.

In the post-operative X-rays as well as in the µCT scans, radiolucent volumes could be observed in the LAE442 scaffolds in contrast to the TCP scaffolds. This is attributed to hydrogen gas formation, which is naturally produced during the corrosion of magnesium ($Mg + 2H_2O$ -> $Mg(OH)_2 + H_2$) [41]. The surrounding tissue is only able to absorb a certain amount of gas, if too much gas is formed it starts to accumulate [10]. Similar to previous studies these gas accumulations could be observed directly around the implants and in the medullary canal/shaft of the femur, though they had no clinical effect on the rabbits [33,34,36,42,44,45]. In the present study, less gas was observed in the CaP-coated scaffolds than in the PLA-coated ones from time of surgery to week 6, with PLA-P1 providing the worst values. The observation that PLA-coated scaffolds demonstrated higher gas formation than CaP-coated scaffolds might be explained by the nature of the different coatings. It is assumed that a PLA-coating binds the released gas onto the scaffold surface due to the different intermolecular bondings [43]. Consequently, the gas, emerged from the PLA-coated scaffolds, was possibly diffused slower into the surrounding tissue and led to an increased local gas accumulation. Furthermore, some authors described that degradation and gas formation are directly dependent, whereby slower corrosion should lead to lower gas production [38,50]. In this study the results are somewhat controversial, since the CaP scaffolds with a faster degradation formed less gas than scaffolds with a PLA-coating. Augustin et al. also described the production of hydrogen gas in their study with porous MgF_2-coated LAE442 scaffolds, with the same scaffold geometry and implantation site as in the present study [34]. The comparison of the results revealed that MgF_2-coated LAE442 scaffolds produced slightly more gas in weeks 2 and 4 compared to MgF_2-CaP coated scaffolds of the present study. It can therefore be assumed that the additional CaP-coating reduced the initial gas production and therefore positively influences the osseointegration.

From week 12 onwards less gas could be observed, indicating that from this point on more gas was absorbed by the surrounding tissue than was produced by the scaffolds.

Periosteal bone formation could be detected at the implant site similarly in X-rays and µCT scans in all scaffold types. Since the insertion of the scaffolds is always associated with periosteal trauma (exposure of the bone, drilling), the periosteal bone formation can possibly be traced back to manipulation of the bone surface. The in vivo study by von der Höh et al., with magnesium implants in rabbit femora, also describes periosteal growth that occurs independently of implant degradation and cites drilling as the cause [37]. Periosteal bone formation has also been observed in other studies in empty drill holes on the rabbit femur (trochanter major) [22].

In the semi-quantitative evaluation, the TCP scaffolds showed the most bone-scaffold contacts. It is known that TCP is biocompatible and osteoconductive and shows good osseointegration [46]. However, TCP is not mechanically stable enough to be used in more heavily loaded bone defects [47,48].

In this study, all LAE442 scaffolds, with the exception of PLA-P1, showed an increase in bone-scaffold contacts from week 6 at the latest. In the previous study of Augustin et al. LAE442 scaffolds with a single coating of MgF_2 showed an increase in bone-scaffold contacts from week

12 (smaller pore size, 400 μm) or week 16 (bigger pore size, 500 μm) onwards [34]. These results demonstrate that in the present study, an additional PLA- or CaP-coating compared to a single MgF_2-coating has a positive effect on osseointegration.

Osseointegration is described as second bone response after an implantation, which goes along with a direct bone-implant contact without a connective tissue layer [12]. This ensures a proper biomechanical fixation of the implant. New bone tissue, thus also new bone trabeculae that adhere to the implant, can be created by the migration of osteoblasts into the scaffold which can intermediately be degraded and replaced by the surrounding tissue [11,37].

It is known from the literature that the healing process of bone is influenced by physiological osteoconductive properties that can be enhanced by certain implant materials [39]. When comparing the PLA- and CAP-coating in the present study, more bone-scaffold contacts are generally found in CaP scaffolds from week 10 onwards. The reason for this could be an osteoconductive influence of calcium as Thomann et al., suggested based on their study with MgCa pins in rabbit femora [6]. Yang et al. also mentioned in his review about Mg bone implants, that calcium- and phosphorus- containing bioceramics are similar to natural bone and can promote the surface bioactivity and thus the growth of bone tissue [11]. Wang et al. investigated CaP-coated Mg scaffolds in their studies and wrote about better osteoconductive properties if the surface or coating of the scaffold possesses bioactive ions such as calcium [39]. The osteoconductive effect of calcium in the present study may also have resulted in the faster drill hole closure of the CaP scaffolds compared to the PLA scaffolds. The control group of TCP scaffolds generally showed the most bone-scaffold contacts as we expected based on previous findings [33,48].

In order to assess the degradation, density and volume of the scaffolds were determined. Witte et al. compared LAE442 with zinc containing Mg alloys (AZ31 and AZ91), as well as with the alloy WE43 and found that LAE442 provided a lower degradation rate in vivo [10]. In the present study, all types of LAE442 scaffolds showed a much slower degradation than TCP, which degraded strongly from week 6 due to its low degradation resistance [49]. When comparing double-coated P2 scaffolds of the present study with single MgF_2-coated LAE442 scaffolds of the same pore size, less volume loss was observed in the present study ($\leq$ 6.0% PLA P2, $\leq$ 8.7% CaP P2) than in the previous study by Augustin et al. ($\leq$ 11.1%) [34]. This observation may be due to the additional coatings with PLA or CaP, which led to a reduction of the scaffold degradation. Julmi et al. have already observed that porous MgF_2-coated LAE442 scaffolds degraded faster than MgF_2-CaP/PLA scaffolds when investigated in simulated body fluid [25]. Furthermore, it is noticeable that in the present study, the scaffolds with the larger pore size degraded slower than the scaffolds with the smaller pore size. This could have been caused by the fact that scaffolds with the smaller pore size (P1) demonstrated a smaller volume and a bigger surface area to be attacked by corrosion compared to the scaffolds with bigger pores [34].

When comparing the coatings, regardless of the pore size, the CaP-coated scaffolds showed a faster degradation until the study end after 36 weeks than the PLA scaffolds which is in correspondence with the previous in vitro study for these implants [25]. Julmi et al. have performed in-vitro corrosion experiments with scaffolds coated with MgF_2, MgF_2 + PLA or MgF_2 + CaP. Both additional coatings (PLA/CaP) improved the corrosion resistance, while the combination of MgF_2 + PLA was the most effective one [25]. After 12 weeks in SBF, PLA-coated scaffolds showed in vitro a more pronounced volume loss of 33% compared to <10% in the present study, while CaP-coated scaffolds showed a volume loss of 46% compared to <13.4%. This phenomenon of faster corrosion of Mg alloys in vitro compared to in vivo is well known. A possible reason for this could be explained due to different electrochemical conditions in the surrounding of the implant surfaces [50].

Bone volume and number of trabeculae in the vicinity of the coated scaffolds decreased in the first weeks. The cause for the decrease could be the resulting hydrogen gas, which accumulated and prevented bone ingrowth. This assertion is getting supported through the decrease in gas accumulation from week 12 onwards, while from week 12 or 24 at the latest, the bone volume and the number of trabeculae, with the exception of PLA-P1, increased again in the present study. These observations of emerge and disappearance of gas are consistent with those of other authors [10,51]. Witte et al. described gas bubbles appearing due to Mg implant degradation at week one and disappearing again after 2–3 weeks [10].

When comparing pore sizes, independent of the coatings, only small differences without any significance were found between them. However, the small difference in size (400 μm compared to 500 μm) could be the reason for this outcome. The LAE442 scaffolds with the larger pore size (CaP-P2 and PLA-P2) only showed slightly higher bone density values until week 24 and degraded slower. A slight difference could be observed in PLA-scaffolds, with PLA-P1 showing worse values than PLA-P2, regarding gas production, drill hole closing and trabecular contacts.

The effect of influence of pore sizes on the osseointegration of biomaterials is controversially discussed in the literature. Principally, a biodegradable scaffold should have a pore size that is similar to cancellous bone to help bone cells growing into the pores [11,31]. Cheng et al. described a beneficial effect with better bone ingrowth in implants with larger pore sizes (>250 μm) [31]. The authors found that open porousd Mg scaffolds with a pore size of 400 μm enhanced the formation of new bone tissue stronger compared to the smaller pore size of 250 μm [31]. At least pore sizes >300 μm are recommended in the literature [31,32]. The authors suspected that larger pores would facilitate vascularization. In contrast, other authors reported that different pore sizes have no influence on bone ingrowth and osseointegration [32]. In the present study there was also a slight positive effect in scaffolds with bigger pores, although it was not possible to find a cause for the differences in PLA scaffolds based on imaging and it will be reserved for further histological investigations.

5. Conclusion

LAE442 is handled as a future option for medical treatments of critical size defects due to its strong mechanical resistance. However, there are still some unsolved issues with this alloy, which the present study addressed in a rabbit model. In this novel setting a combination of MgF_2 as a base coating plus CaP or PLA were investigated. Both of the additional coatings were able to reduce the degradation rate and gas formation (only MgF_2–CaP coating) of Mg implants compared to Mg implants coated with only MgF_2 in previous studies. Hence, it was possible to confirm that additional surface coatings of LAE442 alloys strongly support their ability for osseointegration and positively influence the degradation behavior. Comparing the coating type, the CaP-coating proved to be even more promising in terms of osseointegration than the PLA-coating. Scaffolds with PLA-coating, however, degraded more slowly despite increased gas formation.

The CaP-coating proved to be a good candidate for the next step to be investigated in experiments in weight bearing bone defects.

Declaration of Competing Interest

The authors hereby declare that they do not have any conflict of interest with the content of the article.

Acknowledgments

This research is financially supported by the German Research Foundation (DFG) within the project “Interfacial effects and integration behaviour of magnesium-based sponges as bioresorbable bone substitute material” (Grant No. 271761343). The authors thankfully appreciate the financial support. Special thanks to Beatrix Limmer for outstanding help with laboratory activities and her support with the evaluations.

References

[1] S.K. Nandi, S. Roy, P. Mukherjee, et al., Orthopaedic applications of bone graft & graft substitutes: a review, Indian J. Med. Res. 132 (2010) 15–30.
[2] M.P. Staiger, A.M. Pietak, J. Huadmai, et al., Magnesium and its alloys as orthopedic biomaterials: a review, Biomaterials 27 (2006) 1728–1734.
[3] C. Hampp, N. Angrisani, J. Reifenrath, et al., Evaluation of the biocompatibility of two magnesium alloys as degradable implant materials in comparison to titanium as non-resorbable material in the rabbit, Mater. Sci. Eng. C Mater. Biol. Appl. 33 (2013) 317–326.
[4] N. Angrisani, J. Reifenrath, F. Zimmermann, et al., Biocompatibility and degradation of LAE442-based magnesium alloys after implantation of up to 3.5 years in a rabbit model, Acta Biomater. 44 (2016) 355–365.
[5] A. Krause, N. Von der Höh, D. Bormann, et al., Degradation behaviour and mechanical properties of magnesium implants in rabbit tibiae, J. Mater. Sci 45 (2010) 624–632.
[6] M. Thomann, C. Krause, D. Bormann, et al., Comparison of the resorbable magnesium. alloys LAE442 und MgCa0. 8 concerning their mechanical properties, their progress of degradation and the bone-implant-contact after 12 months implantation duration in a rabbit model, Materwiss. Werksttech. 40 (2009) 82–87.
[7] J. Vormann, Magnesium: nutrition and metabolism, Mol. Aspects Med. 24 (2003) 27–37.
[8] J.H. Jo, et al., Hydroxyapatite coating on magnesium with MgF(2) interlayer for enhanced corrosion resistance and biocompatibility, J. Mater. Sci. Mater. Med. 22 (11) (2011) 2437–2447.
[9] M.P. Sealy, Y Guo, Surface integrity and process mechanics of laser shock peening of novel biodegradable magnesium–calcium (Mg–Ca) alloy, J. Mech. Behav. Biomed. Mater. 3 (2010) 488–496.
[10] F. Witte, V. Kaese, H. Haferkamp, et al., In vivo corrosion of four magnesium alloys and the associated bone response, Biomaterials 26 (2005) 3557–3563.
[11] Y. Yang, C. He, E. Dianyu, et al., Mg bone implant: features, developments and perspectives, Mater. Des. 185 (2020) 108259 Jg., S.
[12] L. Le Guéhennec, A. Soueidan, P. Layrolle, et al., Surface treatments of titanium dental implants for rapid osseointegration, Dent. Mater. 23 (2007) 844–854 Jg., Nr. 7, S.
[13] C. Janning, E. Willbold, C. Vogt, et al., Magnesium hydroxide temporarily enhancing osteoblast activity and decreasing the osteoclast number in peri-implant bone remodelling, Acta Biomater. 6 (2010) 1861–1868.
[14] Y. Yang, et al., "Laser additive manufacturing of Mg-based composite with improved degradation behaviour, Virtual Phys. Prototyp. 15 (3) (2020) 278–293.
[15] C. Shuai, et al., TiO2-induced in situ reaction in graphene oxide-reinforced AZ61 biocomposites to enhance the interfacial bonding, ACS Appl. Mater. Interfaces 12 (20) (2020) 23464–23473.
[16] H. Haferkamp, M. Niemeyer, R. Boehm, et al., Development, processing and applications range of magnesium lithium alloys, Mater. Sci. Forum 350 (2000) 31–42.
[17] N. Angrisani, J.-.M. Seitz, A. Meyer-Lindenberg, et al., Rare earth metals as alloying components in magnesium implants for orthopaedic applications, New Featur. Magnes. Alloys 35 (2012) 81.
[18] N. Birbilis, M.A. Easton, A. Sudholz, et al., On the corrosion of binary magnesium-rare earth alloys, Corros. Sci. 51 (2009) 683–689.
[19] T.L. Chia, M.A. Easton, S.-.M. Zhu, et al., The effect of alloy composition on the microstructure and tensile properties of binary Mg-rare earth alloys, Intermetallics 17 (2009) 481–490.
[20] E. Willbold, X. Gu, D. Albert, et al., Effect of the addition of low rare earth elements (lanthanum, neodymium, cerium) on the biodegradation and biocompatibility of magnesium, Acta Biomater. 11 (2015) 554–562.
[21] M. Thomann, C. Krause, N. Angrisani, et al., Influence of a magnesium-fluoride coating of magnesium-based implants (MgCa0.8) on degradation in a rabbit model, J. Biomed. Mater. Res. A 93 (2010) 1609–1619.
[22] M. Lalk, J. Reifenrath, N. Angrisani, et al., Fluoride and calcium-phosphate coated sponges of the magnesium alloy AX30 as bone grafts: a comparative study in rabbits, J. Mater. Sci. Mater. Med. 24 (2013) 417–436.
[23] H.J. Maier, et al., "Magnesium Alloys for Open-Pored Bioresorbable Implants, JOM 72 (2020) 1–11.
[24] N. Hort, Y. Huang, D. Fechner, et al., Magnesium alloys as implant materials-s-principles of property design for Mg-RE alloys, Acta Biomater. 6 (2010) 1714–1725.
[25] S. Julmi, A.-.K. Krüger, A.-.C. Waselau, et al., Processing and coating of open–pored absorbable magnesium-based bone implants, Mater. Sci. Eng.: C 98 (2019) 1073–1086.
[26] A. Alabbasi, S. Liyanaarachchi, M.B Kannan, Polylactic acid coating on a biodegradable magnesium alloy: an in vitro degradation study by electrochemical impedance spectroscopy, Thin Solid Films 520 (2012) 6841–6844.
[27] Y. Chen, Y. Song, S. Zhang, et al., Interaction between a high purity magnesium surface and PCL and PLA coatings during dynamic degradation, Biomed. Mater. 6 (2011) 025005.
[28] J. Yang, F. Cui, I. Lee, et al., In vivo biocompatibility and degradation behavior of Mg alloy coated by calcium phosphate in a rabbit model, J. Biomater. Appl. 27 (2012) 153–164.
[29] S.V. Dorozhkin, Calcium orthophosphate coatings on magnesium and its biodegradable alloys, Acta Biomater. 10 (2014) 2919–2934.
[30] K. Bobe, E. Willbold, I. Morgenthal, et al., In vitro and in vivo evaluation of biodegradable, open-porous scaffolds made of sintered magnesium W4 short fibres, Acta Biomater. 9 (2013) 8611–8623.
[31] M.Q. Cheng, T. Wahafu, G.F. Jiang, et al., A novel open-porous magnesium scaffold with controllable microstructures and properties for bone regeneration, Sci. Rep. 6 (2016) 24134.
[32] V. Karageorgiou, D. Kaplan, Porosity of 3D biomaterial scaffolds and osteogenesis, Biomaterials 26 (2005) 5474–5491.
[33] N. Kleer, S. Julmi, A.-.K. Gartzke, et al., Comparison of degradation behaviour and osseointegration of the two magnesium scaffolds, LAE442 and La2, in vivo, Materialia 8 (2019) 100436.
[34] J. Augustin, F. Feichtner, A.-.C. Waselau, et al., Comparison of two pore sizes of LAE442 scaffolds and their effect on degradation and osseointegration behavior in the rabbit model, J. Biomed. Mater. Res. B (2020) 1–13, doi:10.1002/jbm.b.34607.
[35] S. Julmi, C. Klose, A.-.K. Krüger, et al., Development of sponge structure and casting conditions for absorbable magnesium bone implants., in: 146th Annual Meeting & Exhibition Supplemental Proceedings, TMS, Springer, Cham, 2017, pp. 307–317.
[36] M. Lalk, J. Reifenrath, D. Rittershaus, et al., Biocompatibility and degradation behaviour of degradable magnesium sponges coated with bioglass–method establishment within the framework of a pilot study, Materwiss. Werksttech. 41 (2010) 1025–1034.
[37] N. Von der Höh, D. Bormann, A. Lucas, et al., Influence of different surface machining treatments of magnesium-based resorbable implants on the degradation behavior in rabbits, Adv. Eng. Mater. 11 (2009) 47–54.
[38] F. Witte, J. Fischer, J. Nellesen, et al., In vivo corrosion and corrosion protection of magnesium alloy LAE442, Acta Biomater. 6 (2010) 1792–1799.
[39] W. Wang, K.C. Nune, L. Tan, et al. Bone regeneration of hollow tubular magnesium-strontium scaffolds in critical-size segmental defects: effect of surface coatings, Mater. Sci. Eng. C 100 (2019) 297–307 Jg., S.
[40] J. Reifenrath, A. Krause, D. Bormann, et al., Profound differences in the in–vivo-degradation and biocompatibility of two very similar rare-earth containing Mg-alloys in a rabbit model, Materwiss. Werksttech. 41 (2010) 1054–1061.
[41] M. Pourbaix, Atlas of Electrochemical Equilibria in Aqueous Solutions, NACE International, Houston, 1974.
[42] J. Reifenrath, N. Angrisani, N. Erdmann, et al., Degrading magnesium screws ZEK100: biomechanical testing, degradation analysis and soft-tissue biocompatibility in a rabbit model, Biomed. Mater. 8 (2013) 045012.
[43] P.W. Atkins, J de Paula, Kurzlehrbuch Physikalische Chemie, 4th ed., Wiley, Weinheim, 2006.
[44] N. Erdmann, A. Bondarenko, M. Hewicker-Trautwein, et al., Evaluation of the soft tissue biocompatibility of MgCa0.8 and surgical steel 316L in vivo: a comparative study in rabbits, Biomed. Eng. Online 9 (2010) 63.
[45] Y.-.K. Kim, K.-.B. Lee, S.-.Y. Kim, et al., Gas formation and biological effects of biodegradable magnesium in a preclinical and clinical observation, Sci. Technol. Adv. Mater 19 (2018) 324–335.
[46] M.C. Von Doernberg, B. von Rechenberg, M. Bohner, et al., In vivo behavior of calcium phosphate scaffolds with four different pore sizes, Biomaterials 27 (2006) 5186–5198.
[47] K.M. Nuss, B von Rechenberg, Biocompatibility issues with modern implants in bone - a review for clinical orthopedics, Open Orthop. J. 2 (2008) 66–78.
[48] H.E. Koepp, S. Schorlemmer, S. Kessler, et al., Biocompatibility and osseointegration of β-TCP: histomorphological and biomechanical studies in a weight-bearing sheep model, J. Biomed. Mater. Res. B 70 (2004) 209–217.
[49] H. Cao, N. Kuboyama, A biodegradable porous composite scaffold of PGA/β-TCP for bone tissue engineering, Bone 46 (2010) 386–395.
[50] F. Witte, J. Fischer, J. Nellesen, et al., In vitro and in vivo corrosion measurements of magnesium alloys, Biomaterials 27 (2006) 1013–1018.
[51] T. Kraus, S. Fischerauer, S. Treichler, et al., The influence of biodegradable magnesium implants on the growth plate, Acta Biomater. 66 (2018) 109–117.

IV. PUBLIKATION II

‚Histological evaluation of biocompatibility, osseointegration and degradation behaviour of open porous magnesium scaffolds with different coatings'

Journal: Materials Science and Engineering Technology

Autoren: Laura Marie Witting, Anja-Christina Waselau, Franziska Feichtner, Cristiane Meneghelli-Rudolph, Stefan Julmi, Christian Klose, Ann-Kathrin Gartzke, Hans Jürgen Maier, Peter Wriggers, Andrea Meyer-Lindenberg

Das Paper ‚Histological evaluation of biocompatibility, osseointegration and degradation behaviour of open porous magnesium scaffolds with different coatings' wurde am 08.07.2020 zur Publikation im Journal ‘Materials Science and Engineering Technology‘ eingereicht und am 10.09.2020 mit Anmerkungen an die Autoren zurückgesandt. Das Paper wurde überarbeitet und am 12.12.2020 erneut eingereicht. Nach einer zweiten Überarbeitung wurde das Paper am 13.07.2021 eingereicht.

Histological evaluation of biocompatibility, osseointegration and degradation behaviour of open porous magnesium scaffolds with different coatings

L.M. Witting[1], A.-C. Waselau[1], F. Feichtner[1], C. Meneghelli-Rudolph[1], S. Julmi[2], C. Klose[2], A.-K. Gartzke[3], H.J. Maier[2], P. Wriggers[3], A. Meyer-Lindenberg[1]

1 Clinic for Small Animal Surgery and Reproduction, Ludwig-Maximilians-University Munich, Germany

2 Institut für Werkstoffkunde (Materials Science), Leibniz University of Hannover, Garbsen, Germany

3 Institute of Continuum Mechanics, Leibniz University of Hannover, Germany

Corresponding author: Andrea Meyer-Lindenberg, Clinic for Small Animal Surgery and Reproduction, Ludwig-Maximilians-University Munich, Veterinärstraße 13, 80539 Munich, Germany. Tel.: +49 2180 2629; Fax: +49 89 395341; E-mail address: ameylin@lmu.de

Abstract

For the treatment of large bone defects, bioresorbable metallic bone substitutes, such as the magnesium alloy LAE442, are promising in previous studies. The objective of the present study was to investigate the biocompatibility, osseointegration and degradation behaviour of coated LAE442 scaffolds. For this purpose, open porous LAE442 scaffolds with different pore sizes were produced by an investment casting process. All scaffolds were coated with magnesium fluoride (MgF_2) and additionally with polylactic acid (PLA) or calcium phosphate (CaP). The scaffolds were inserted into the greater trochanter ossis femoris in rabbits for 6, 12, 24 or 36 weeks. Histological sections of the bone-implant-compound were produced and stained. A semiquantitative and quantitative evaluation was performed to assess implant degradation, cell ingrowth and new formed bone. All scaffolds degraded slowly and showed good biocompatibility. Calcium phosphate-coated scaffolds are considered most promising for future treatment of large bone defects since they showed more newly formed bone tissue and smaller gas accumulations than polylactic acid-coated ones. Scaffolds with the larger pore size (500 µm) showed better results compared to smaller pores (400 µm). Larger pores allowed a higher number of cells and blood vessels to form, which is essential for bone growth.

Keywords

biocompatibility, scaffold degradation, osseointegration, histological evaluation, magnesium scaffolds

1. Introduction

Large bone defects, so-called critical size defects, nowadays can be treated with bone substitutes [1, 2]. Bioresorbable metallic bone substitutes have attracted much interest in this context [3-6]. In addition to metallic materials, other artificial materials such as bioglass, ceramics, polymers and calcium phosphate can also replace the body's own transplants [7]. In contrast to autologous transplants, treatment with all of these bone substitutes involves fewer risks with regard to the donor site and predominantly promising results with regard to biocompatibility and osseointegration were reported [4, 8-10]. Biocompatibility refers to the tolerability between a technical and a biological system, i.e. between a bone substitute and the body [11]. Biocompatible materials are those that do not have a negative effect on the metabolism of living tissue when in direct contact with it [12]. Osseointegration is defined as a bone healing process which includes the bone cells growing directly onto the bone substitute and achieving firm attachment to the substitute’s surface [13]. Degradable materials, such as magnesium alloys, corrode and dissolve after a certain time [14]. Ideally, they degrade during the desired ingrowth of new bone tissue [21], which is making them an efficient implant material for bone tissue engineering. Magnesium alloys in particular have been classified as very promising bone replacement materials regarding biocompatibility, osseointegration and mechanical properties [3, 15-20]. Certain magnesium alloys are biocompatible and do not cause negative inflammatory effects at the cellular level [24, 25]. In addition, they are particularly suitable for load-bearing bone, since the Young's modulus is similar to that of natural bone [3, 26]. However, implants made of pure magnesium degrade quickly in the body [3, 21], which is why other elements such as lithium or aluminum are often added to reduce the rate of degradation [22, 23]. Rare earths are also often added in order to improve corrosion resistance, mechanical properties and strength [22, 26, 27]. This is how different corrosion rates occur in different

magnesium alloys [14]. The magnesium alloy LAE442 (4 wt % lithium, 4 wt % aluminium, 2 wt % rare earths) in particular, has been described in previous studies as a promising implant and bone replacement material in terms of biocompatibility and osseointegration in vitro and in vivo [4, 10, 28, 29]. The greatest limitations for the biomedical use of magnesium alloys are the rate of corrosion and the resulting hydrogen gas [15, 17]. In the literature, some authors describe a correlation between rapid degradation and gas formation [17, 30]. To counteract this, coatings have been developed in the past to slow down the rate of corrosion, reduce gas production and improve the osseointegration of magnesium alloys [31-33]. Magnesium fluoride (MgF_2)-, polymer- and calcium phosphate-coatings have proven to be promising [31, 32, 34]. In many studies [31, 35] a magnesium fluoride-coating of different magnesium alloys already has shown a reduction in the rate of degradation compared to uncoated implants and served as a base layer beneath another coating in this study. In an in vitro experiment with porous scaffolds (magnesium scaffolds with the alloy LAE442), a magnesium fluoride-coating served as a base layer and suppressed the initial bursting release of hydrogen gas [32]. The authors also described that an additional polylactic acid (PLA)- or calcium phosphate (CaP)-coating could further reduce the degradation rate of porous LAE442 scaffolds in vitro [32]. Other in vitro and in vivo studies also describe a slower rate of degradation of magnesium implants with polylactic acid- or calcium phosphate-coating compared to uncoated implants [36-39]. Not only the coating but also the porosity is important for good osseointegration. To mimic a trabecular bone structure, bone substitutes in the form of open porous sponges have been developed [40]. It has been observed that these porous structures improve the ingrowth of bone cells and blood vessels [24, 32, 34, 41], thus ensuring successful osseointegration [42]. It was also found that pores of different sizes yielded different results, whereby pores with a size of > 300 µm are generally promising for bone ingrowth behaviour [41]. In addition to imaging techniques such as X-rays and micro computer tomography [2, 4, 28, 29], histology plays a decisive role in the investigation of the biocompatibility of bone substitutes. Since the degradation requires the immigration of inflammatory cells such as macrophages, knowledge of the body's cell and tissue response is particularly important [26, 43, 44]. In order to assess more precisely the cell and tissue response, degradation and osseointegration of coated LAE442 scaffolds, the present study focuses on evaluation at the histological level. It is known that cell migration plays a major role in the foreign body reaction

of the body following implantation of bone substitutes [45-49]. A physiological foreign body reaction always causes an invasion of macrophages and fibroblasts [45]. Immigrating macrophages and the resulting connective tissue layer can be a sign of the beginning of implant integration [2, 24]. Sporadically occurring foreign body giant cells (FBGC), which are formed by aggregations of macrophages, may also indicate implant degradation, but may also signal a sign of a defense reaction [2, 24]. The amount and influence of immigrating cells on the biocompatibility of bone implants has already been controversially discussed in the literature. Some authors equate too many foreign body giant cells and a strong capsule formation with insufficient implant integration [45]. Others believe that cell migration is always a normal part of the wound healing process [45, 46, 48-51]. Cell migration and growth of new tissue and bone can be observed particularly well with histological staining such as toluidine blue staining [2, 4, 34]. Histomorphometry is also a suitable method for the quantitative measurement of ingrowing tissue [34, 52, 53]. The present study will evaluate for the first time scaffolds made of the magnesium alloy LAE442 with different pore sizes and additional calcium phosphate- or polylactic acid-coating. Special attention was paid to the influence of the coatings on the surrounding tissue and the cellular response to degradation over a period of 36 weeks. The objective was to obtain results on biocompatibility, osseointegration and degradation behaviour and to compare them scaffold-specific. In particular, the methodology and the results of the semiquantitative evaluation were compared with the quantitative results of histomorphometry.

2. Material and methods

2.1 Scaffolds

For the present study, a total of *128* cylindrical scaffolds (Ø 4 mm, length 5 mm) made of the magnesium alloy LAE442 (4 wt % Li, 4 wt % Al, 2 wt % rare earths) were used, which were produced by investment casting [32]. The scaffolds were produced with a maximum pore size of 400 µm (pore size 1 = P1) or 500 µm (pore size 2 = P2) (web thickness P1: 0.4/0.3 mm; P2: 0.5/0.4 mm; porosity P1: 43.4 %; P2: 41.4 %; volume P1: 37.38 mm^3; P2: 38.37 mm^3; surface P2: P1: 303.09 mm^2; 66.88 mm^2). All scaffolds were cast and coated by investment casting at the Institute of Materials Science, Hannover, Germany [29, 32, 40]. For the present study, a total of four different scaffold groups with two different pore sizes or two different

coatings were used: LAE442 scaffolds with polylactic acid-coating and pore size 1 (PLA-P1; *n = 32*), LAE442 scaffolds with polylactic acid-coating and pore size 2 (PLA-P2; *n* = 32), LAE442 scaffolds with calcium phosphate-coating and pore size 1 (CaP-P1; *n = 32*), LAE442 scaffolds with calcium phosphate and pore size 2 (CaP-P2; *n = 32*). Porous scaffolds (Ø 4 mm, length 5 mm) of ß-tricalcium phosphate (TCP) (*n = 32*) (multiporosity with meso- and macropores between 5 µm - 500 µm; total porosity: 65 %; Cerasorb®, Curasan AG, Kleinostheim, Germany) served as control group. The magnesium scaffolds were sterilised by gamma irradiation (> 25 kGy, BBF Sterilisationsservice GmbH, Kernen, Germany) prior to implantation into the bone.

2.2 Animal model and experimental procedure

According to §8 of the Animal Protection Act, the government of Upper Bavaria approved the animal experiment conducted (approval number: 55.2-1-54-2532-181-2015). Within the scope of the study 80 adult female Zimmermann rabbits (ZiKa, Asamhof, Kissing, Germany, weight 4 kg ± 0.2 kg) were kept. The rabbits were supplied with water, hay and pellets (Kanin Kombi 13,4 Rf and maize, Rieder Asamhof GmbH, Kissing, Germany). The LAE442 scaffolds with the two different pore sizes and coatings (PLA-P1, PLA-P2, CaP-P1, CaP-P2), as well as the ß-tricalcium phosphate scaffolds were randomised, as already described in a previous study [29], implanted into the greater trochanter of both femora and remained implanted for a period of 6, 12, 24 or 36 weeks (Fig.1 a,b). Post mortem both femora were removed for further examination. The greater trochanter was dissected and finally the bone-implant-compound was further processed.

Fig. 1

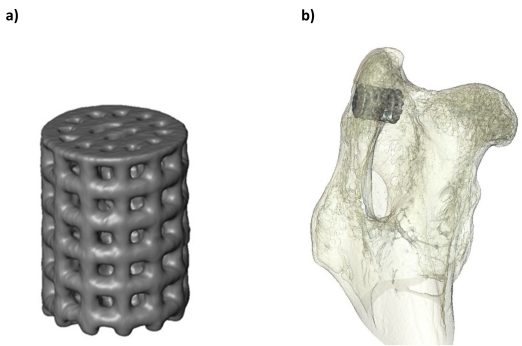

Fig. 1 Representative illustration of **a)** a LAE442-scaffold and **b)** a rabbit femur, demonstrating the implantation position within the greater trochanter

2.3 Sample preparation and histology

A diamond band saw (Cut Grinder Walter Messner, Oststeinbek, Germany) served to excise the bone-implant-compound. The samples were fixed in 4.0 % formalin (Roth, Karlsruhe, Germany), washed and dehydrated with series of ethanol (50 %, 70 %, 80 %, 90 %, 96 % and 100 %). Afterwards the samples were infiltrated with xylene and embedded in Technovit® 9100 (Heraeus Kulzer, Wehrheim, Germany).

2.4 Production of thick sections

After polymerisation the sample blocks were glued with a one component precision adhesive (Technovit® 7210 VLC, Heraeus Kulzer, Wehrheim, Germany) on plastic microscope slides (Maertin & Co AG, Freiburg, Germany) and cut into 150 - 500 µm thick sections using a diamond band saw (Cut Grinder, Walter Messner, Oststeinbek, Germany). Centrally located sections of the scaffolds were ground and polished (Lap Grinder, Walter Messner, Oststeinbek, Germany) to a thickness of approximately 70 -100 µm. The thick sections were surface stained with 0.1 % toluidine blue O (Waldeck, Münster, Germany) [49, 54]. Finally, the samples were evaluated with an optical microscope (Zeiss Axio Imager 2, Carl Zeiss Microscopy GmbH, Jena, Germany).

2.5 Production of thin sections

Thin sections (4 µm) ($n = 32$, 8 scaffolds of each time group) were made, using an automated rotary microtome (RM2255 Leica, Wetzlar, Germany). The thin sections were transferred into a water bath and from there onto microscopic glass slides (Glaswarenfabrik Karl Hecht, Sondheim, Germany) that were coated with Ponal-Poly-L-Lysine. All thin sections were stained with a von Kossa/McNeal stain to evaluate the tissue mineralisation.

2.6 Microscopy, histological evaluation and histomorphometry

The semiquantitative histological evaluation and the quantitative evaluation via histomorphometry was accomplished with a digital microscope (Zeiss Axio Imager 2, Carl Zeiss Microscopy GmbH, Jena, Germany). Photomicrographs of the samples were taken, using the Zeiss Axio Cam Mrc digital camera. All samples were analysed by Zeiss ZEN2 software (Carl Zeiss Microscopy, Jena, Germany) and Zen Intellesis software.

2.6.1 Thick sections

2.6.1.1 Semiquantitative evaluation of degradation behaviour, osseointegration and biocompatibility

Degradation behaviour

Material changes such as 'cracks', 'granulation', 'implant material' and 'implant black' were evaluated within the scaffolds, which could give an indication of the degradation behaviour of the scaffolds. ‘Cracks’ were defects that extended over the implant and the parameter 'granulation' described degraded granulated scaffold material. In particular, "cracks" gave an indication of degradation behavior and were found in the degradation layer of an implant whose material was corroded [55]. However, these two parameters were only related to the remaining scaffold material. The scoring point 'implant material' was used to evaluate how much scaffold material was not yet degraded in the histological section and was therefore visible. The parameter 'implant black' was defined as 'still original black implant material', as the material often only appeared dark grey due to degradation and granulation. Scores between 0 (0 %), 1 (1 - 25 %), 2 (26 - 50 %) and 3 (> 50 %) were assigned for the parameters 'cracks', 'granulation', 'implant material' and 'implant black'. Within the scaffolds and in their vicinity the parameters 'gas within” and “gas adjacent' were evaluated, which describes the accumulation of hydrogen gas. A score between 0 (0 %), 1 (1 - 25 %), 2 (26 - 50 %) and 3 (> 50 %) was assigned

Osseointegration

The toluidine blue stained thick sections were evaluated at magnifications from 2.5x/0.085 to 20x/0.5 (Zeiss Axio Imager 2, Carl Zeiss Microscopy GmbH, Jena, Germany). The semiquantitative evaluation was carried out in two areas (within scaffold/ scaffold periphery) (Fig. 2 a). The parameters assessing osseointegration were evaluated within the scaffold cross section (Table 1): 'bone', 'osteoid-like tissue' and 'granulation tissue'. The measurement of the 'bone-implant-contact' (BIC) was not performed in this study, as this value is more commonly used for evaluation in permanent solid implants to assess the direct implant boundary [56]. Instead, osseointegration was measured with the occurrence of the parameters bone and osteoid-like-tissue, since the scaffold degrades after a time and the direct

boundary of the scaffold was not consistently traceable. The term 'bone' was used to describe mineralised tissue shown in dark blue in the toluidine blue staining [2, 29]. The parameter 'osteoid-like tissue' included washed out pale blue tissue, which resembled osteoid in structure and colour [2]. As 'granulation tissue', tissue was assessed which was microscopically represented with a whitish-yellow colour and with many cells [2, 49, 57]. Granulation tissue is formed during the wound healing process by proliferating fibroblasts and newly sprouted capillaries [58, 59]. Scores between 0 (0 %), 1 (1 - 10 %), 2 (11 - 25 %) and 3 (> 25 %) were assigned for the parameters mentioned.

Biocompatibility

In the present study specifically the appearance of certain cells inside and outside the scaffolds were evaluated to assess biocompatibility, since cell types are an important marker for biocompatibility and inflammatory responses [45]. Biocompatible materials should not have a negative or toxic effect on living tissue in direct contact [12]. The field of view was divided into three ring zones inside the scaffolds and one ring zone outside the scaffolds (Fig. 2 b). The following parameters were evaluated at 20x/0.5 magnification (Table 2): 'fibrous cells', 'fibrous capsule', 'macrophages', 'blood vessels', 'foreign body giant cells' and 'osteoblasts' [2, 49]. The score values 0 (none), 1 (few), 2 (moderate) to 3 (many) were used. A 'fibrous capsule' is a one- to two-layered section of connective tissue that clearly forms around the scaffolds like a capsule [45]. In addition, the osteoid-like tissue was analysed in more detail. Osteoblast margins which physiologically surround osteoid tissue [59], were assessed around the osteoid-like tissue in the present study. Furthermore, osteocytes in the osteocyte lagoons within the osteoid-like tissue were evaluated. Since in toluidine blue staining only the nuclei of the osteocytes within the lacunae are stained and thus visible [58], they were evaluated. The following scores were assigned for the occurrence of osteoblasts and osteocytes: 2 (many), 1 (few), 0 (no cell nuclei) (Table 2).

Fig. 2

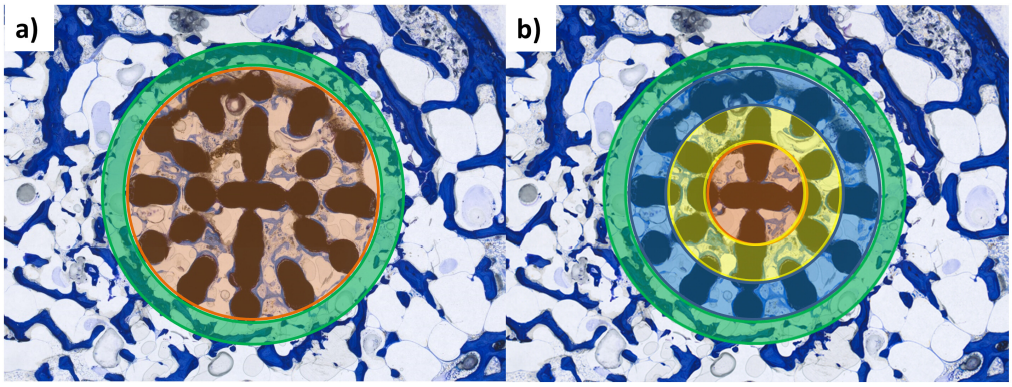

Fig. 2 Semi-quantitative histological evaluation of cross sections in different areas. **a)** The scaffold material was evaluated in two ring zones (orange ring: within scaffold, green ring: vicinity of scaffold). **b)** The tissue and cells were evaluated in 4 ring zones (orange ring: ring I within scaffold, yellow ring: ring II within scaffold, blue ring: ring III within scaffold, green ring: ring IV vicinity of scaffold)

Table 1 Semi-quantitative histological scoring system of 'scaffold material'

	Scaffold material			
Score	**0**	**1**	**2**	**3**
Implant material	0 %	1 - 25 %	26 - 50 %	> 50 %
Implant black	0 %	1 - 25 %	26 - 50 %	> 50 %
Implant granulation	0 %	1 - 25 %	26 - 50 %	> 50 %
Cracks	0 %	1 - 25 %	26 - 50 %	> 50 %
Bone	0 %	1 - 10 %	11 - 25 %	> 25 %
Osteoid-like tissue	0 %	1 - 10 %	11 - 25 %	> 25 %
Granulation tissue	0 %	1 - 10 %	11 - 25 %	> 25 %
Gas adjacent	0 %	1 - 25 %	26 - 50 %	> 50 %
Gas within scaffold	0 %	1 - 25 %	26 - 50 %	> 50 %

Table 2 Semi-quantitative histological scoring system of 'tissue and cells'

Tissue and Cells				
Score	**0**	**1**	**2**	**3**
Fibrous cells (tissue)	none	few	moderate	many
Fibrous capsule	none	mild	moderate	severe
Erythrocytes (blood vessels)	none	few	moderate	many
Macrophages	none	few	moderate	many
Foreign body giant cells	none	few	moderate	many
Osteoblasts	none	few	moderate	many
Osteocyte cell nuclei	none	few	many	-
Von Kossa	0 %	1 – 25 %	26 – 50 %	> 50 %

Mineralised bone tissue

2.6.1.2 Quantitative evaluation of degradation behaviour and osseointegration via histomorphometry

All thick sections stained with toluidine blue were also examined quantitatively via histomorphometry. For the image analysis, a suitable segmentation model was created with the help of the ZEN 'Intellesis' software through 'Machine Learning', with which all sectional images were segmented and evaluated equally. For image analysis, a ring of equal size (diameter: 3.9 mm) was placed around the edge of the scaffold, so that only tissue within the scaffold was evaluated (Fig. 3 a). This histomorphometric method was used to measure the degradation behaviour (parameters: gas, scaffold material) as well as osseointegration (parameters: bone, osteoid-like tissue, granulation tissue). The percentage area (%) of the visible scaffold material was evaluated, which was referred to as 'implant material' in analogy to the semiquantitative evaluation. In addition, the area (%) of 'gas' as well as ingrown tissue, such as 'bone' (Fig. 3 b), 'osteoid-like tissue' and 'granulation tissue'. All parameters were evaluated within the ring, in relation to the total ring (Fig.3 c).

Fig. 3

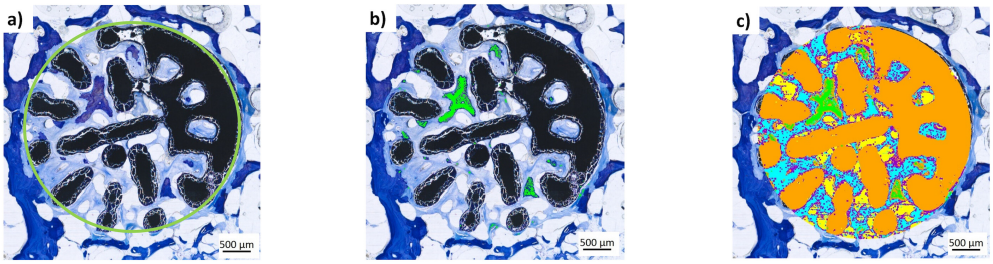

Fig. 3 Quantitative histomorphometrical evaluation of cross sections. **a)** The parameters were evaluated inside of the scaffold (green ring: ring that contains the whole scaffold); **b)** green colour field: new bone; **c)** orange: implant material; green: bone; turquoise: osteoid-like-tissue; yellow: gas; pink: granulation tissue

2.6.2 Thin sections

2.6.2.1 Semiquantitative evaluation of osseointegration (mineralised bone tissue in the vicinity of scaffolds, von Kossa/McNeal stain)

Thin sections stained with von Kossa/McNeal stain showed bone mineral deposition that appeared deep black. The amount of black tissue, which indicated osseointegration, in the direct vicinity of the scaffold was evaluated (in %). Score values of 0 (0 %), 1 (1 - 25 %), 2 (26 - 50 %) to 3 (> 50 %) were used. Since almost all of the hard material of the LAE442 scaffolds was extracted during the preparation of the thin sections with the microtome, only the peri-implant area with a thin residual hem of the scaffolds was evaluated.

2.7 Statistics

Analysis was performed with 'Microsoft Excel 2016' (Microsoft Corporation, Redmond, WA 98052-6399, USA) and 'SPSS Statistics 25.0' (IBM, Armonk, NY 10540, USA). Data from the semiquantitative evaluation of the histological evaluation (implant material, implant black, gas within implant, gas adjacent, bone, osteoid-like tissue, granulation tissue, bone resorption, implant granulation and implant cracks, fibrous cells, macrophages, blood vessels and foreign body giant cells) were tested for statistical significance using the Kruskal-Wallis test and the Chi-square test. In case of the Kruskal-Wallis test, all data were tested with ANOVA, adjusted by Bonferroni correction. Metric data from the quantitative

evaluation of the histomorphometry (implant material, bone, gas, osteoid-like tissue, and granulation tissue) were tested for normal distribution by means of the Kolmogorov-Smirnov test. In case of normal distribution, data were tested for statistical significance using ANOVA, adjusted by Bonferroni correction. In case of no normal distribution, quantitative data were tested with the Kruskal-Wallis test. To test for correlation between the non-normally distributed semiquantitative data and the quantitative histomorphometric data (parameters implant material, bone, gas, osteoid-like tissue, and granulation tissue), the Kendall's Tau correlation test was used. To calculate Kendall's correlation coefficients 'R statistical software' was required. Particularly, "Chart.Correlation" function from "PerformanceAnalytics" package was applied for it. The interpretation of the Kendall's Tau correlation coefficient was performed according to the literature [60]. The significance level in all statistical tests was defined as $p < 0.05$.

3. Results

3.1 Thick sections

3.1.1 Semiquantitative evaluation

3.1.1.1 Degradation behaviour

All LAE442 scaffolds degraded very slowly and homogeneously and showed low material loss at all end points without significant scaffold or coating-specific differences. Only ß-tricalcium phosphate showed a significantly higher material loss compared to all LAE442 scaffolds from week 6 on ($p < 0.05$) (Fig. 4 a-j). With regard to the parameters 'implant black', 'implant granulation' and 'implant cracks', there were only a few scaffold-specific differences between the differently coated LAE442 scaffolds. Even though the scaffold outline was still clearly visible after 36 weeks, less black and greyer scaffold material was visible at that time than after 6 weeks. Overall, 'cracks' increased significantly in all LAE442 scaffolds over time, with the majority of the scaffolds showing > 50 % 'implant cracks' in week 36 (Fig. 5). When comparing the coatings, it was noticeable that in week 12, the polylactic acid-coated scaffolds showed more cracked material in both the periphery and center of the scaffold than the calcium phosphate-coated scaffolds. Especially polylactic acid scaffolds with pore size 1 showed areas in week 6, which showed many cracks and a more significant loss of structure.

Fig. 4

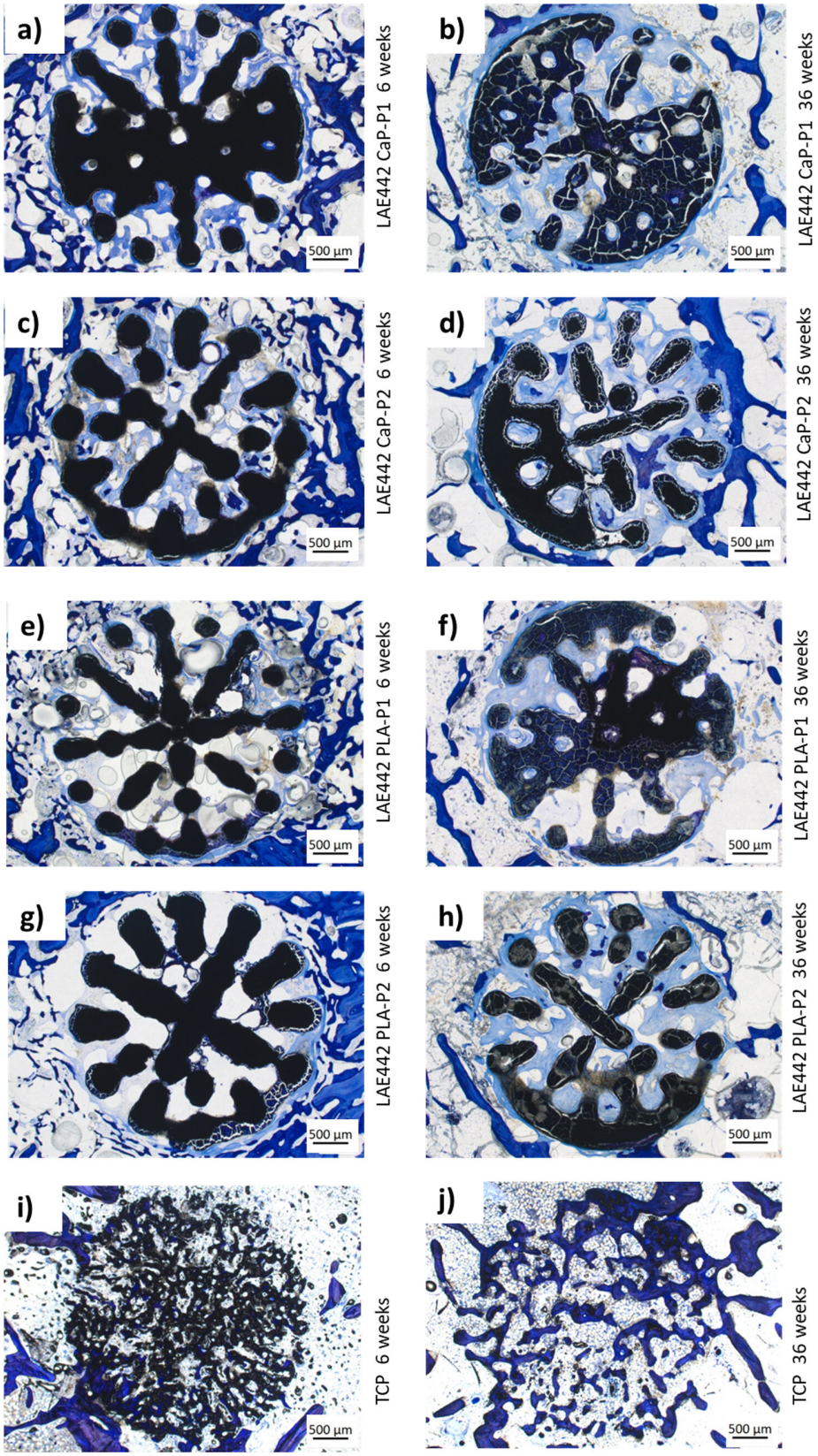

Fig. 4 Cross sections of different scaffolds, representing degradation and material loss after 6 weeks (left side), after 36 weeks (right side); **a)-b)** LAE442 CaP-P1; **c)-d)** LAE442 CaP-P2; **e)-f)** LAE442 PLA-P1; **g)-h)** LAE442 PLA-P2; **i)-j)** TCP

Fig. 5

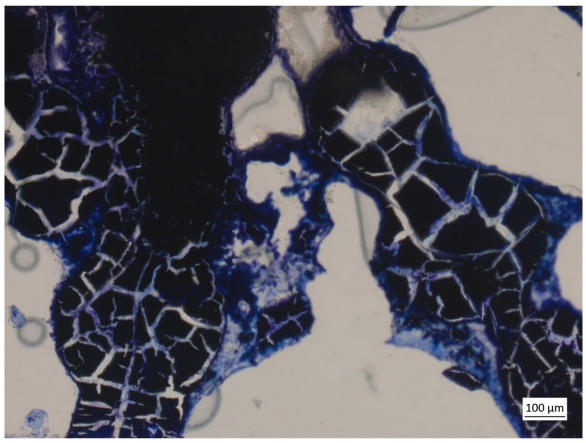

Fig. 5 Photograph of a LAE442-PLA scaffold with ‘cracks’ after an implantation period of 12 weeks

Fig. 6

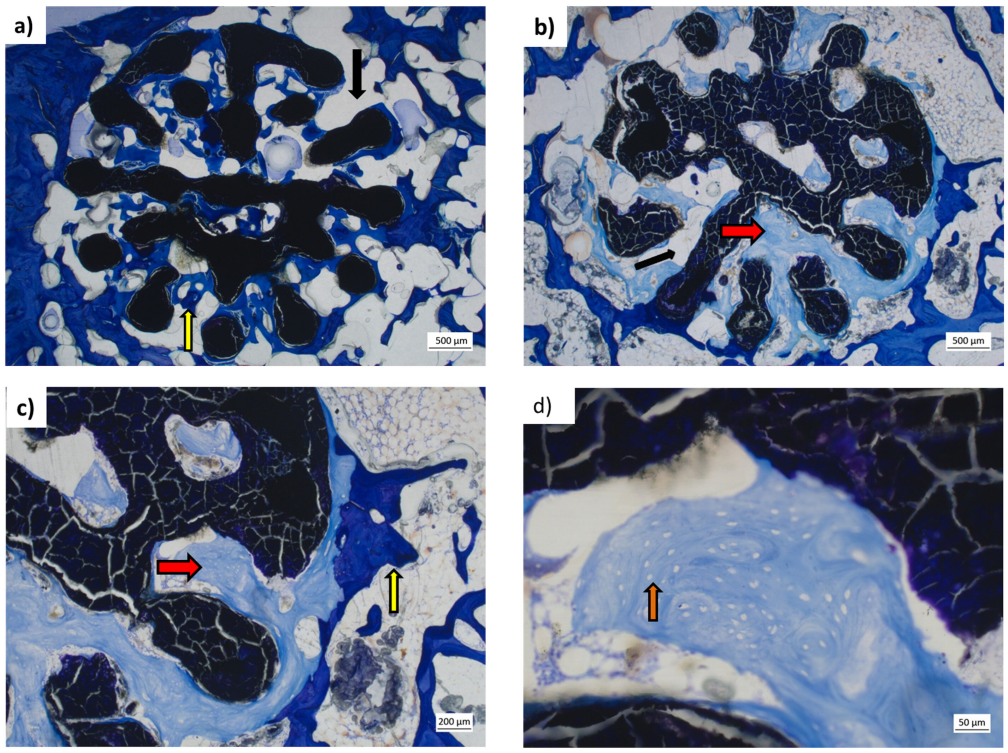

Fig. 6 Cross sections of scaffolds representing **a)** Bone tissue within LAE442-CaP scaffold (thin yellow arrow); gas accumulation within scaffold (thin black arrow)**; b)-c)** bone-like-tissue within LAE442-PLA scaffold (thick red arrow); bone tissue (thin yellow arrow) and gas accumulation within LAE442 scaffold (thin black arrow); **d)** bone-like tissue without osteocyte cell nuclei (orange arrow)

During degradation ‘gas’ accumulated inside the pores of all LAE442 scaffolds and outside near the scaffolds from week 6 to 36 (Fig. 6 a,b). The largest gas accumulations inside the scaffolds were observed in calcium phosphate scaffolds with pore size 1 and polylactic acid scaffolds with pore size 2 at week 6 and 12 (Fig.9). Polylactic acid scaffolds with pore size 1 initially formed less gas within the pores, but showed the most gas at week 36 compared to all other LAE442 scaffolds. Calcium phosphate scaffolds with pore size 2 showed the least gas accumulation at week 24 and 36. In terms of pore size, it was noticeable that LAE442 scaffolds with larger pore size (polylactic acid – pore size 2; calcium phosphate – pore size 2) showed a decrease in gas production within the scaffolds at week 36 compared to week 6. Scaffolds with the smaller pore size (polylactic acid – pore size 1; calcium phosphate – pore size 1) also showed a decrease in total gas production after 36 weeks compared to week 6. However, gas production increased again between week 24 and 36 compared to the larger pore size. With regard to gas accumulation in the vicinity of scaffold, polylactic acid scaffolds with pore size 1 were noticeable with generally more gas than all other LAE442 scaffolds at 36 weeks and significantly more gas than calcium phosphate scaffolds with pore size 2 ($p < 0.03$). In the circle of calcium phosphate scaffolds with pore size 2, the least gas could be observed at 36 weeks compared to the other LAE442 scaffolds. As expected, no gas was observed in ß-tricalcium phosphate scaffolds.

3.1.1.2 Osseointegration

All LAE442 scaffolds showed between 0 - 10 % newly formed ‘bone tissue’ within the pores at all times, which was dark blue in the toluidine blue staining (Fig. 6 a,c). When comparing the coatings, it was noticeable that calcium phosphate-coated scaffolds (calcium phosphate – pore size 1, calcium phosphate – pore size 2) showed more bone tissue between week 6 and 24 compared to polylactic acid-coated ones (polylactic acid – pore size 1 and polylactic acid – pore size 2) (Fig.7). In week 36, however, more new bone tissue was found in the pores of calcium phosphate scaffolds with pore size 2 compared to the other LAE442 scaffolds. Regardless of the time, new bone tissue was found in 17/64 (26.6 %) calcium phosphate-coated scaffolds, while only 5/64 (7.8 %) polylactic acid-coated scaffolds showed bone tissue. When comparing pore size, regardless of coating and time, more new bone was observed in larger pore size scaffolds (polylactic acid – pore size 2: 3/64; calcium phosphate – pore size 2: 11/64) than in smaller pore size

scaffolds (polylactic acid – pore size1: 2/64; calcium phosphate – pore size 1: 6/64). In contrast to LAE442 scaffolds, the control material ß-tricalcium phosphate formed significantly more new bone tissue from week 6 on ($p < 0.05$) (Fig. 7). From this time on, all ß-tricalcium phosphate scaffolds were traversed by bone trabeculae and the scaffold material was replaced by bone tissue over time.

In addition to bone tissue, which had a physiological structure and a typical blue colouration in toluidine blue stained sections, a large amount of ‘osteoid-like tissue’ was observed within the LAE442 scaffolds (Fig. 6 c-d). This showed a 'washed-out' pale blue structure with empty osteocyte lacunae (Fig. 6 d). The investigations showed that the scaffolds with the larger pore size (calcium phosphate – pore size 2 and polylactic acid – pore size 2) had the most 'osteoid-like tissue' between week 24 and 36 (Fig.8). In calcium phosphate scaffolds with pore size 2, a significantly larger amount of osteoid-like tissue was observed in week 6 and 12 compared to the remaining LAE442 scaffolds ($p < 0.05$). Polylactic acid scaffolds with pore size 1 produced the least osteoid-like tissue at all time endpoints. Calcium phosphate scaffolds with pore size 2 thus differed significantly from polylactic acid scaffolds at week 6 ($p < 0.02$) and week 36 ($p < 0.05$). Independent of the time endpoints, osteoid-like tissue was found in 61/64 (95.3 %) calcium phosphate-coated scaffolds (calcium phosphate – pore size 1: $n = 29$; calcium phosphate – pore size 2: $n = 32$) and in 52/64 (81.3 %) polylactic acid-coated scaffolds (polylactic acid – pore size 1: $n = 21$; polylactic acid – pore size 2: $n = 31$) within the scaffold pores.

Apart from osteoid-like tissue, moderate to large amounts of ‘granulation tissue’ were seen in all LAE442 scaffolds, regardless of pore size and coating. ß-tricalcium phosphate scaffolds showed significantly more granulation tissue than all LAE442 scaffolds ($p < 0.05$). It was noticeable that all LAE442 scaffolds showed less granulation tissue at the end of the study than in week 6. With regard to pore size, more granulation tissue was observed in the larger pore size scaffolds only in week 6.

Fig. 7

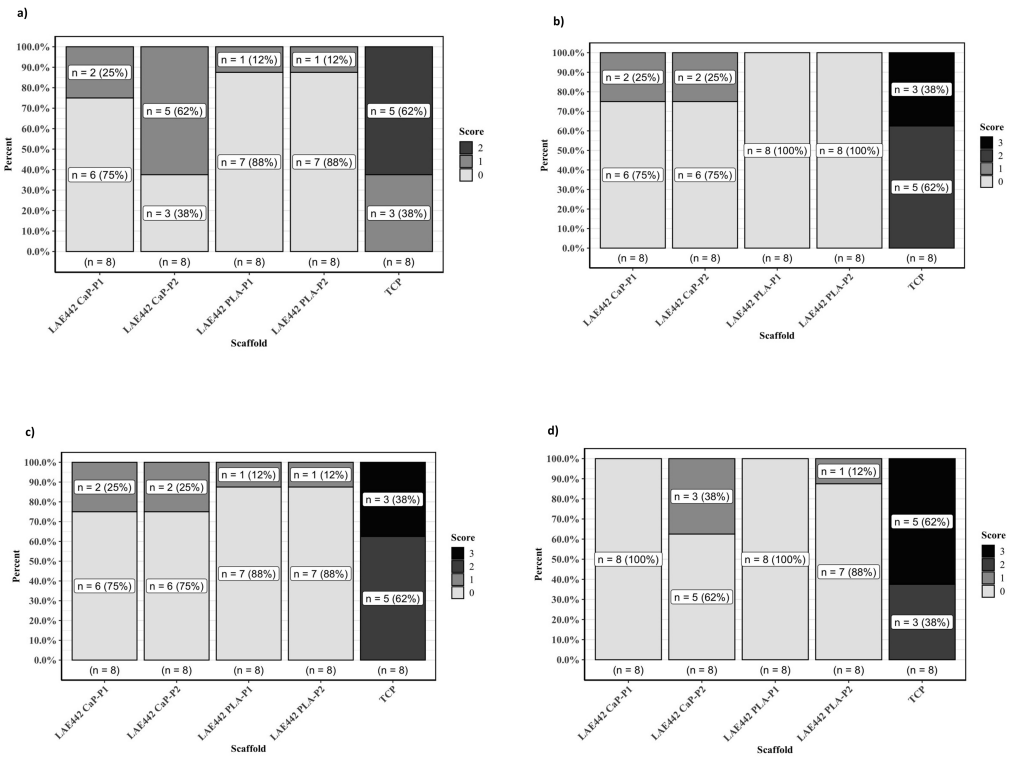

Fig. 7 Results of the semi-quantitative histological evaluation for the parameter bone tissue within scaffold for an implantation period of **a)** 6 weeks, **b)** 12 weeks, **c)** 24 weeks, **d)** 36 weeks

Fig. 8

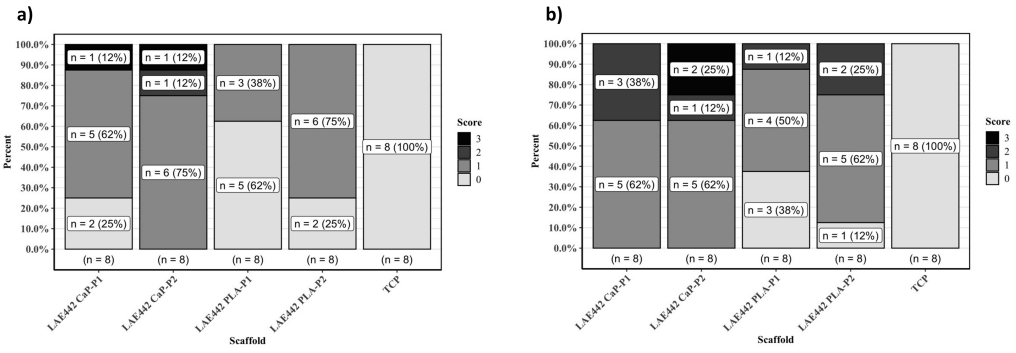

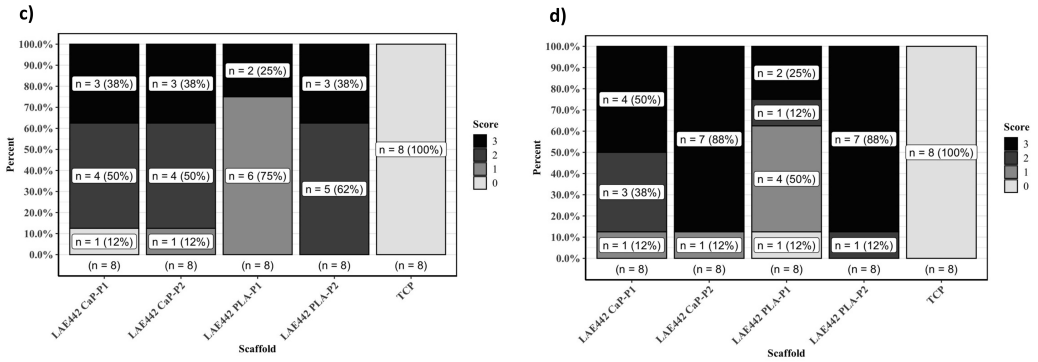

Fig. 8 Results of the semi-quantitative histological evaluation for the parameter bone-like-tissue within scaffold for an implantation period of **a)** 6 weeks, **b)** 12 weeks, **c)** 24 weeks, **d)** 36 weeks

Fig. 9

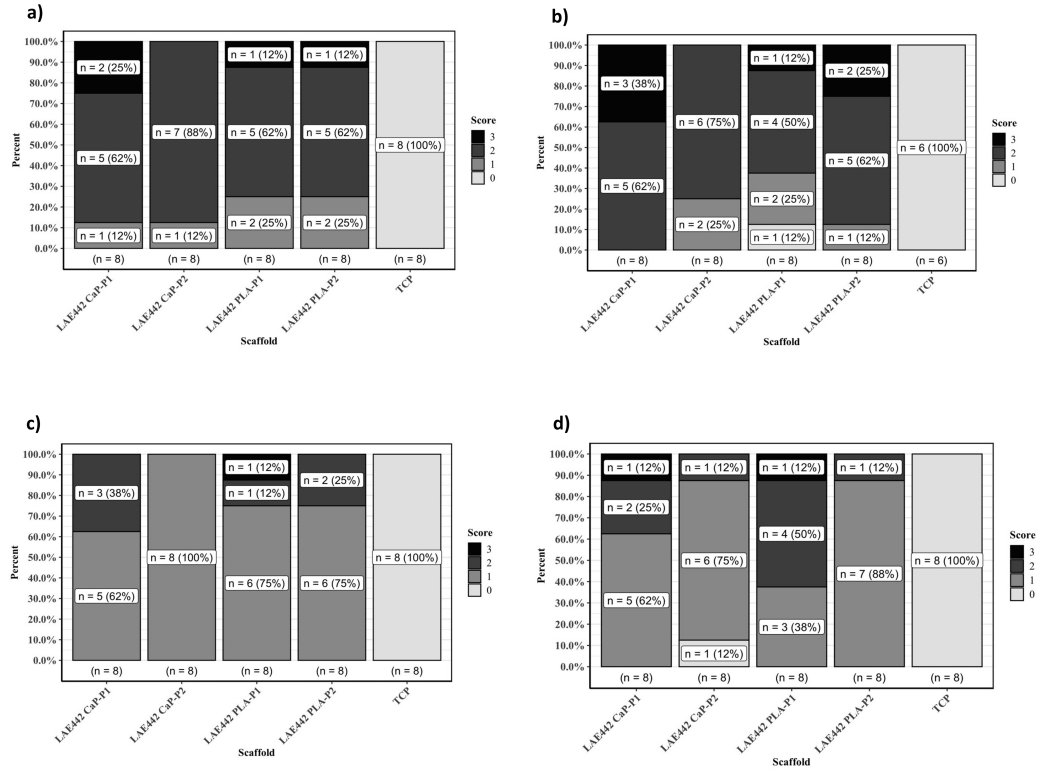

Fig. 9 Results of the semi-quantitative histological evaluation for the parameter gas accumulation within scaffold for an implantation period of **a)** 6 weeks, **b)** 12 weeks, **c)** 24 weeks, **d)** 36 weeks

3.1.1.3 Biocompatibility

In all LAE442 scaffolds a moderate to large amount (moderate - many) of macrophage accumulation was observed. In some cases, macrophage groups and individual foreign body giant cells were seen (Fig. 10 a,b). In all LAE442 scaffolds, except calcium phosphate scaffolds with pore size 2, more macrophages were seen in and around the scaffolds at 36 weeks than after 6 weeks. Foreign body giant cells were observed both in the pores and in the vicinity of the scaffolds. In the ß-tricalcium phosphate scaffolds, neither macrophages nor foreign body giant cells were seen.

Fibrocytes were observed in all LAE442 scaffolds and in ß-tricalcium phosphate (Fig.10 b). However, the number of fibrocytes decreased in all scaffolds over time until week 36. Compared to the other LAE442 scaffolds, polylactic acid scaffolds with pore size 1 had a larger number of fibrocytes around the scaffolds (adjacent). Isolated scaffolds (polylactic acid – pore size 1: $n = 5$, polylactic acid – pore size 2: $n = 3$, calcium phosphate – pore size 1: $n = 1$, calcium phosphate – pore size 2: $n = 1$) showed a connective tissue single- to multi-layered capsule (Fig. 10 c). This could be observed especially in week 12 around polylactic acid scaffolds with pore size 1. It was noticeable that the scaffolds that formed a capsule did not show any new bone tissue and only little osteoid-like tissue.

All LAE442 scaffolds also showed a moderate number of lymphocytes and some neutrophil granulocytes. In addition to inflammatory and macrophages, some blood vessels were observed growing into the pores (Fig. 10a). It was noticed that the number of blood vessels within the pores decreased over time in all LAE442 scaffolds and only increased in ß-tricalcium phosphate scaffolds (Fig. 11). From week 12, there were more blood vessels in the ß-tricalcium phosphate scaffolds than in LAE442 scaffolds. The amount of blood vessels in the ß-tricalcium phosphate scaffolds was significantly larger at week 24 and 36 compared to the amount of all LAE442 scaffolds. When comparing LAE442 scaffolds, the largest number of blood vessels was found in polylactic acid scaffolds with pore size 2 and calcium phosphate scaffolds with pore size 2 at week 6, 12 and 24. It was found that polylactic acid scaffolds with pore size 1 at week 12 had significantly fewer blood vessels than polylactic acid- and calcium phosphate scaffolds with pore size 2 ($p < 0.04$). Calcium phosphate scaffolds with pore size 1 also showed fewer blood

vessels at week 12 compared to polylactic acid scaffolds with pore size 2 and calcium phosphate scaffolds with pore size 2. The number of blood vessels of polylactic acid scaffolds with pore size 1 and calcium phosphate scaffolds with pore size 1 returned to the level of the other LAE442 scaffolds (polylactic acid – pore size 2 and calcium phosphate – pore size 2) at week 36.

On closer examination of the osteocyte lacunae within the osteoid-like tissue, many lacunae without nuclei were found in all LAE442 scaffolds with osteoid-like tissue (calcium phosphate: $n = 61$; polylactic acid: $n = 52$) (Fig.6 d). When comparing the calcium phosphate- and polylactic acid-coatings, more nuclei were found in the osteocyte lacunae of calcium phosphate-coated scaffolds. 7/61 (11.5 %) calcium phosphate-coated scaffolds with many nuclei, 27/61 (44.3 %) calcium phosphate-coated scaffolds with a few nuclei and 22/61 (36.1 %) calcium phosphate-coated scaffolds with no cell nuclei (calcium phosphate-coated scaffolds with osteoid-like tissue: $n = 61$) were observed. Polylactic acid-coated scaffolds included 4/52 (7.7 %) scaffolds with many nuclei, 15/52 (28.8 %) scaffolds with a few nuclei and 30/52 (57.7 %) scaffolds without no cell nuclei (polylactic acid-coated scaffolds with osteoid-like tissue; $n = 52$). In addition, osteoblasts were detected, which in some places formed a thin hem around the osteoid-like tissue. However, only very few osteoblasts were seen, with calcium phosphate-coated scaffolds showing more osteoblasts than polylactic acid scaffolds. Osteoblasts were found in 21 % of the calcium phosphate-coated scaffolds ($n = 61$) with osteoid-like tissue and in 13.4 % of the polylactic acid-coated scaffolds ($n = 52$). No osteoid-like tissue was observed in ß-tricalcium phosphate.

Fig. 10

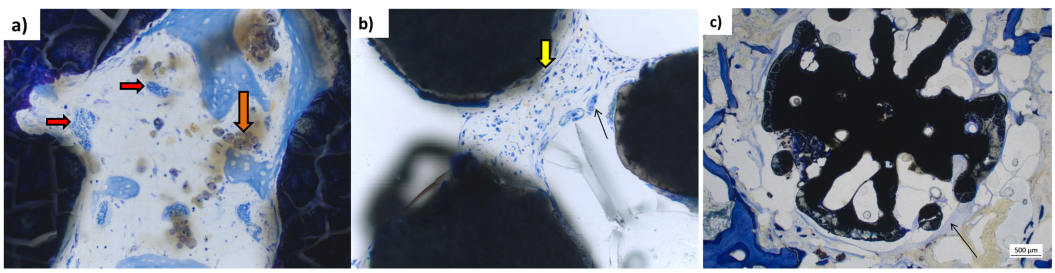

Fig. 10 Photograph of **a)** macrophages (thick orange arrow), blood vessels (small red arrows), **b)** fibrocytes (thick yellow arrow) and foreign body giant cells (thin black arrow)**; c)** capsule formation around PLA-P1 scaffold (thin black arrow)

Fig. 11

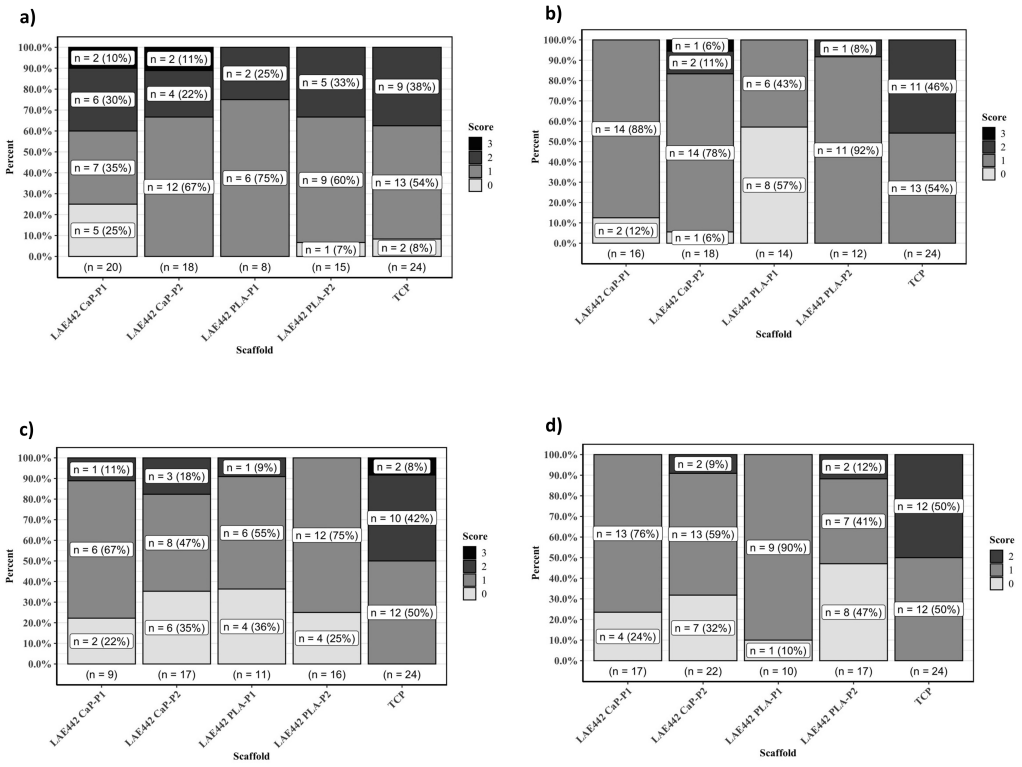

Fig. 11 Results of the semi-quantitative histological evaluation for the parameter blood vessels within scaffold for an implantation period of **a)** 6 weeks, **b)** 12 weeks, **c)** 24 weeks, **d)** 36 weeks

3.1.2 Quantitative evaluation of histomorphometry and correlation with semiquantitative evaluation

Regarding degradation, the surface area of 'implant material' on the overall ring was between 70 - 80 % in all LAE442 scaffolds after 6 weeks. After 36 weeks there were only between 60 - 70 % of ‘implant material’ (Table 3). There were no statistically significant differences between the scaffold groups. However, a stronger material loss was observed in polylactic acid-coated scaffolds than in calcium phosphate-coated scaffolds (material loss: polylactic acid – pore size 1: 13.6 %; polylactic acid – pore size 2: 12.4 %; calcium phosphate – pore size 1: 4.9 %; calcium phosphate – pore size 2: 3.1 %). In all LAE442 scaffolds, gas accumulations could be observed in the pores. Between week 6 and 36, the area of ‘gas’ decreased by 6 - 8 % in all LAE442 scaffolds except in polylactic acid scaffolds with pore size 1, so that after 36 weeks an area percentage of 7 - 15 % was

reached (Table 3). Polylactic acid scaffolds with pore size 1 measured more gas after 36 weeks than at the start of the study and significantly more ‘gas’ than calcium phosphate scaffolds with pore size 2 ($p < 0.05$). Calcium phosphate scaffolds with pore size 2 showed the least gas accumulation at 12, 24 and 36 weeks compared to all other scaffolds.

Regarding osseointegration, the area fraction of ‘granulation tissue’ in all LAE442 scaffolds except calcium phosphate scaffolds with pore size 2 increased between 1 - 4.7 % over time (Table 3). At all time endpoints, less 'granulation tissue' was measured in the smaller pore size scaffolds (calcium phosphate – pore size 1 and polylactic acid – pore size 1) than in the larger pore size scaffolds (calcium phosphate – pore size 2 and polylactic acid – pore size 2). At 6 weeks, the area of ‘granulation tissue’ in polylactic acid scaffolds with pore size 1 was significantly smaller compared to calcium phosphate scaffolds with pore size 2 ($p < 0.01$). The quantitatively measured proportion of ‘bone’ in all LAE442 scaffolds was between 0.4 - 0.5 % in week 6 and increased to 0.7 - 1.0 % in week 36 (Table 3). More bone tissue was measured in calcium phosphate scaffolds with pore size 2 at all time endpoints than in the other LAE442 scaffolds. Polylactic acid scaffolds with pore size 1 had the least bone tissue at 12 and 24 weeks. In addition to bone tissue, a higher proportion of ‘osteoid-like tissue’ was measured in all scaffolds. This proportion increased significantly over time in all LAE442 scaffolds and was between 4 - 12 % after 36 weeks (Table 3). It was noticeable that the scaffolds with the larger pores showed more ‘osteoid-like tissue’ at 24 and 36 weeks than the scaffolds with the smaller pores. Polylactic acid scaffolds with pore size 1 showed the least amount of ‘osteoid-like tissue’ throughout the entire period, with significantly less area than calcium phosphate scaffolds with pore size 2 at 6 weeks ($p < 0.01$), polylactic acid scaffolds with pore size 2 at 12 weeks ($p < 0.04$) and all LAE442 scaffolds at 36 weeks ($p < 0.05$).

When comparing the semiquantitative and quantitative histomorphometric data a moderate positive correlation was found for the parameter 'osteoid-like tissue' (correlation coefficient $\tau = 0.60$ ($p < 0.001$)). The parameters 'implant material' (correlation coefficient $\tau = 0.32$ ($p < 0.001$)), 'granulation tissue' (correlation coefficient $\tau = 0.18$ ($p < 0.02$)) and 'gas' (correlation coefficient $\tau = 0.44$ ($p < 0.001$)) showed a weak to moderate positive correlation. The parameter 'bone' (correlation coefficient $\tau = 0.11$ ($p > 0.05$)) showed a negligible correlation without

significance.

Table 3 Quantitative and semi-quantitative histological evaluation, in an examined circle area around the scaffold

		Implant material τ = 0.323***		Bone τ = 0.109		Osteoid-like-tissue τ = 0.597***		Gas τ = 0.435***		Granulation tissue τ = 0.181**	
Scaffold type	Weeks	Quanti-tative (%)	Semi-quantit.	Quanti-tative (%)	Semi-quantit.	Quanti-tative (%)	Semi-quantit.	Quanti-tative (%)	Semi-quantit.	Quanti-tative (%)	Semi-quantit.
CaP-P1	6	69.49	Sc. 2 - 3	0.49	Sc. 0 - 1	2.79	Sc. 0 - 3	18.92	Sc. 1 - 3	8.30	Sc. 1 - 2
	12	69.09	Sc. 2 - 3	1.50	Sc. 0 - 1	3.03	Sc. 1 - 2	17.38	Sc. 2 - 3	9.01	Sc. 1 - 2
	24	71.01	Sc. 2 - 3	1.07	Sc. 0 - 1	7.79	Sc. 0 - 3	11.83	Sc. 1 - 2	8.30	Sc. 1
	36	66.09	Sc. 2 - 3	0.77	Sc. 0	11.45	Sc. 1 - 3	10.92	Sc. 1 - 3	10.77	Sc. 1 - 2
CaP-P2	6	71.10	Sc. 2 - 3	0.57	Sc. 0 - 1	4.16	Sc. 1 - 3	13.11	Sc. 1 - 2	11.07	Sc. 1 - 3
	12	74.02	Sc. 2 - 3	3.84	Sc. 0 - 1	2.80	Sc. 1 - 3	11.74	Sc. 1 - 2	7.60	Sc. 1 - 3
	24	70.88	Sc. 2 - 3	1.38	Sc. 0 - 1	9.62	Sc. 1 - 3	8.72	Sc. 1	9.40	Sc. 1
	36	68.94	Sc. 2 - 3	1.08	Sc. 0 - 1	12.46	Sc. 1 - 3	7.47	Sc. 0 - 3	10.05	Sc. 1 - 2
PLA-P1	6	80.37	Sc. 2 - 3	0.41	Sc. 0 - 1	1.36	Sc. 0 - 1	12.53	Sc. 1 -3	5.34	Sc. 0 - 2
	12	73.59	Sc. 2 - 3	0.59	Sc. 0	1.39	Sc. 0 - 2	17.48	Sc. 0 - 3	6.95	Sc. 0 - 2
	24	74.82	Sc. 2 - 3	0.76	Sc. 0 - 1	5.01	Sc. 1 - 3	10.71	Sc. 1 - 3	8.70	Sc. 1 - 2
	36	69.43	Sc. 2 - 3	0.82	Sc. 0	4.74	Sc. 0 - 3	15.13	Sc. 1- 3	9.88	Sc. 1
PLA-P2	6	73.55	Sc. 3	0.40	Sc. 0 - 1	2.33	Sc. 0 - 1	15.04	Sc. 1 - 3	8.68	Sc. 1 - 2
	12	75.63	Sc. 2 - 3	1.62	Sc. 0	2.30	Sc. 0 - 2	12.88	Sc. 1 - 3	7.58	Sc. 1 - 2
	24	66.12	Sc. 2 - 3	1.01	Sc. 0 - 1	12.14	Sc. 2 - 3	10.42	Sc. 1 - 2	10.31	Sc. 1
	36	64.46	Sc. 2 - 3	1.00	Sc. 0 - 1	12.40	Sc. 2 - 3	8.80	Sc. 1 - 2	13.33	Sc. 1 - 2

Quantitative histomorphometrical evaluation, value given as mean in (%);
Semi-quantitative evaluation (Sc. = score) of the parameter 'implant material', 'gas', existing scores **0: 0%; 1: 1-25%; 2: 26-50%; 3: >50%** and the parameter 'bone', 'osteoid-like-tissue', 'granulation tissue', existing scores **0: 0%; 1: 1-10%; 2: 11-25%; 3: >25%;** τ = correlation coefficient

3.2 Thin sections

3.2.1 Osseointegration (mineralised bone tissue in the vicinity of scaffolds, von Kossa/McNeal stain)

Using the von Kossa/McNeal staining, mineralised bone tissue around the LAE442 scaffolds could be evaluated semiquantitatively in the thin sections. Overall, little black stained bone tissue was observed in the immediate vicinity of the scaffolds, with the amount of mineralised bone tissue decreasing between week 6 and 36 (Table 4). Overall, score 1 (between 1 - 25 % direct bone-scaffold-contact) was most frequently awarded (19/32 scaffolds). Score 0 (0 %, direct bone-scaffold-contact) was given for 9/32 scaffolds and score 2 (26 - 50 %) for 3/32 scaffolds. Only one single scaffold (calcium phosphate-P2 in week 6) was given score 3 (> 50 % direct bone-scaffold-contact).

Table 4 Semi-quantitative histological evaluation of immediate bone-scaffold-contact, von Kossa stain, thin sections

Scaffold type	Weeks	Number of scaffolds, Sc. 0 was given	Number of scaffolds, Sc. 1 was given	Number of scaffolds, Sc. 2 was given	Number of scaffolds, Sc. 3 was given
CaP-P1	6	2	0	0	0
(*n* = 8)	12	1	1	0	0
	24	0	2	0	0
	36	0	1	1	0
CaP-P2	6	0	1	0	1
(*n* = 8)	12	1	1	0	0
	24	0	2	0	0
	36	0	2	0	0
PLA-P1	6	1	1	0	0
(*n* = 8)	12	0	2	0	0
	24	2	0	0	0
	36	1	1	0	0
PLA-P2	6	0	2	0	0
(*n* = 8)	12	0	1	1	0
	24	0	1	1	0
	36	1	1	0	0

Semi-quantitative histological evaluation (value given as Score = Sc.) of LAE442 scaffolds (*n = 32*); (*n = 8* per scaffold type and *n = 2* per time group); Evaluation of the parameter: immediate 'bone-scaffold-contact'; existing Scores **0: 0%; 1: 1-25%; 2: 26-50%; 3: >50%**

4. Discussion

4.1 Thick sections

The main objective of this study was to investigate histologically the degradation behaviour, the osseointegration and the biocompatibility of open porous magnesium scaffolds with two different coatings. LAE442 implants have been tested in previous studies both as non-porous [4, 9, 10] and as porous structures [28, 29, 61]. Up to now, only a magnesium fluoride-coating has been demonstrated to

reduce the degradation rate of porous scaffolds made of the magnesium alloy LAE442 [29, 61]. In the present study additional coatings with polylactic acid and calcium phosphate (MgF_2/PLA or MgF_2/CaP), and two different pore sizes (pore size 1 = 400 µm; pore size 2 = 500 µm) were investigated. The different scaffold types should be compared in terms of degradation behaviour, osseointegration and biocompatibility. Another objective was to compare the results of the histological semiquantitative evaluation with the results of quantitative histomorphometry in order to validate the methods. Semiquantitative scoring is a common procedure of converting qualitative data on tissues and cells into numerical data, thus enabling reproducibility and targeted comparisons [62]. In contrast, quantitative histomorphometry allows more precise data and even smaller differences to be recorded using a computer system [63]. The accuracy of both methods should be compared.

The material loss gave an indication of the degradation behaviour of the LAE442 scaffolds. There occurred no statistically significant differences at the time points which were employed. The low loss of material, which became visible in histology in the form of cracks and scaffold granulation, pointed to a degradation of the scaffolds, which had already been observed more precisely using in vivo micro computer tomography examinations [29, 61]. In particular, "cracks" gave an indication of degradation behavior and were found in the degradation layer of implants whose material was corroded [55]. All LAE442 scaffolds degraded very slowly in both semiquantitative and quantitative histological evaluation. The detected significant positive correlation ($\tau = 0.32$; $p < 0.001$) of the two evaluation methods for this parameter indicated similar results.

The very slow degradation of LAE442 implants in the form of pins was already described histologically and in vivo [9]. However, although the scaffold framework and material of LAE442 scaffolds were still clearly visible after 36 weeks in the present study, all LAE442 scaffolds showed significant material changes in the form of granulation and cracks already at week 6. Especially polylactic acid scaffolds with pore size 1 showed a significant loss of structure with many cracks from week 6 on. In the histomorphometrically quantitative evaluation, a stronger material loss could also be observed in polylactic acid-coated scaffolds compared to the calcium phosphate-coated ones.

Using the histological thick sections, circular unstained areas without tissue or cells were observed within the LAE442 scaffolds or in the surrounding cancellous bone. These areas were evaluated as hydrogen gas. At 36 weeks, semiquantitatively and quantitatively less gas was observed in all LAE442 scaffolds than after 6 weeks, except in polylactic acid scaffolds with pore size 1. When magnesium degrades, hydrogen gas is produced, which spreads into the periphery, as degradation accelerates [25, 37, 64]. Gas production during magnesium degradation has been described in other studies [2, 4, 9, 20, 29, 65]. In the semiquantitative assessment of gas production in the present study, it was found that the amount of gas was greater in smaller pore size scaffolds (polylactic acid – pore size 1, calcium phosphate – pore size 1) at week 24 and 36 than in larger pore size scaffolds (polylactic acid – pore size 2; calcium phosphate – pore size 2). In the quantitative evaluation, a larger amount of gas could even be observed from week 12 onwards in the scaffolds with the smaller pore size (polylactic acid – pore size 1, calcium phosphate – pore size 1).

The earlier detection of gas increase of the scaffolds of the quantitative analysis compared to the semiquantitative analysis could argue for a higher accuracy of the quantitative histomorphometry, since with this method smallest gas amounts could already be detected in week 12. Nevertheless, both evaluation systems correlated significantly ($\tau = 0.44$; $p < 0.05$) and thus showed similar results overall.

The fact that smaller pore size scaffolds degraded more quickly due to their larger surface area and therefore formed more gas was already observed in previous studies on porous LAE442 scaffolds [29, 61]. The produced hydrogen gas is transported away through surrounding tissue [22]. In a study with various magnesium implants, gas removal in well-vascularized locations based on histological analyses was described [25]. Since in the present study, as in other studies [41] fewer vessels and granulation tissue were observed within the scaffolds with smaller pores, less gas may have been removed in scaffolds with the smaller pore size than in scaffolds with bigger ones. In other studies with magnesium implants, gas was also observed, but this had no clinical in vivo effect on the animals [2, 34, 66].

Regarding the osseointegration the semiquantitative evaluation showed that calcium phosphate-coated scaffolds formed more new bone tissue within the pores

than polylactic acid-coated scaffolds. However, even after 36 weeks, the proportion of bone tissue did not exceed 10 % in any of the scaffolds (corresponds to score 1; 1 - 10 % bone in the scaffold area). The quantitatively measured area percentage of bone in all LAE442 scaffolds, however, was only between 0.4 - 1.0 % and could be differentiated much more accurately with this method compared to the semiquantitative assessment. It was noticeable that calcium phosphate scaffolds with pore size 2 had more bone tissue than polylactic acid scaffolds with pore size 1 at all times. The reason for the difference in results, as well as a negligible correlation ($\tau = 0.11$; $p > 0.05$), between quantitative and semiquantitative evaluation could be the use of different analysis methods. In this case, the quantitative evaluation led to more precise results than the visual semiquantitative evaluation.

As a cause for the better osseointegration of calcium phosphate-coated scaffolds compared to polylactic acid-coated ones, an osteoconductive effect of calcium could be assumed. This effect was also determined in an in vivo experiment with magnesium-calcium implants using micro computer tomography data [10]. This study found increased bone-to-implant contacts around intramedullary implanted magnesium-calcium pins in comparison to the magnesium control group without calcium. However, since the quantitatively measured proportion of bone was very low in the present study, the data only provides an indication that calcium in magnesium alloys could be a source of mineralisation for new bone.

In addition to bone tissue, large amounts of osteoid-like tissue were found in almost all LAE442 scaffolds. The toluidine blue staining of the osteoid-like tissue was pale blue and resembled the colour of osteoid. Osteoblast margins adhering to osteoid-like tissue were observed in very few cases. In contrast to physiological osteoid, which can only be seen as a hem in new bone formation [67], the osteoid-like tissue in the present study was of faded and plain texture. Osteoid-like tissue within magnesium sponges was also found in another study with implants of the magnesium alloy AX30. Here it was suspected that this was hardly mineralised tissue [34]. In the present study it could not be clarified exactly whether the tissue was similar to the mentioned study. Using semiquantitative analysis and quantitative histomorphometry, a similar amount of osteoid-like tissue could be measured in all LAE442 scaffolds. The significantly positive correlation of the analysis methods indicated that the values of both evaluation methods were

corresponding ($\tau = 0.60$; $p < 0.001$). In week 24 and 36 a larger amount of osteoid-like tissue was measured in the larger pore size scaffolds (polylactic acid – pore size 2; calcium phosphate – pore size 2) than in the smaller pore size scaffolds (polylactic acid – pore size 1; calcium phosphate – pore size 1). This observation can be explained by excessive amounts of gas, which prevented the formation of osteoid-like tissue and which was observed both in the semiquantitative as well as in the quantitative evaluation at week 24 and 36 for scaffolds of the smaller pore size. In an in vivo study with two different magnesium alloys an impaired connectivity between osteocytes and implant surface due to large amounts of gas was observed [25].

Looking at the biocompatibility in the semiquantitative evaluation, different cells and tissues were found such as osteoid-like tissue. Regarding the osteocyte lacunae in the osteoid-like tissue, only a few nuclei were found in most LAE442 scaffolds. It was noticeable that already in week 6 empty osteocyte lacunae could be detected in the osteoid-like tissue. A reason for this observation could not be found. Active osteogenic cells inside the scaffolds need a sufficient supply of blood and oxygen to enable direct osteogenesis [34, 45, 68, 69]. The ingrowth of blood vessels into the scaffold pores was therefore essential for good osseointegration in the present experiment. Comparing the number of blood vessels, a moderate to large number of blood vessels were found within the ß-tricalcium phosphate scaffolds, which increased over time. In contrast, all LAE442 scaffolds showed a small to moderate number of blood vessels. It was striking that in the present study, more blood vessels were visible within the scaffolds with the larger pore size compared to the smaller pore size at the time of 12 weeks. It is known from the literature that increased vascularisation leads to better nutrient supply and thus to better osseointegration [41, 70]. In another study with open porous magnesium implants there were more blood vessels and new bone tissue observed in case of the larger pore size using histological and micro computer tomography data [41]. In connection with the present study another author reported a correlation between bone ingrowth and pore sizes [45], whereby more bone tissue was found in larger pores. For optimal cell migration not only the material but also the pore size is important [41, 28, 61]. Many studies recommend a minimum pore size of 300 - 400 µm, which is necessary for bone and capillary regeneration [34, 68].

In the present study the parameter granulation tissue was assessed and compared.

In comparison to larger pore size scaffolds, smaller pore size scaffolds featured quantitatively less granulation tissue at all times, along with a smaller number of blood vessels. In the semiquantitative evaluation, more granulation tissue was observed in the larger pore size scaffolds only in week 6. With the quantitative histomorphometric evaluation, a higher accuracy of the results could be achieved for the parameter 'granulation tissue' than with the semiquantitative scoring system. This was also shown by a significant but very weak correlation of the results (τ = 0.18; $p < 0.01$). The formation of granulation tissue is an important part of the physiological foreign body reaction in the degradation of resorbable bone substitutes [45]. Granulation tissue is formed by proliferating fibroblasts and by the ingrowth of blood capillaries and forms an important part of the healing process [58, 59].

During the semiquantitative evaluation of the cells, a moderate amount of macrophages and a small amount of foreign body giant cells were observed in the scaffold pores and in the vicinity of the scaffolds at all times. Since cell types are an important marker for biocompatibility and inflammatory responses [45], biocompatible materials should not have a negative or toxic effect on living tissue in direct contact [12]. Other authors who researched with magnesium implants also found macrophages and foreign body giant cells [34] and suggested a physiological healing process during wound healing and implant resorption [34, 45, 71]. The role of foreign body giant cells in bone implants was discussed in the literature [45]. Some authors described foreign body giant cells as a sign of good biodegradability [45]. However, in connection with large macrophage accumulations and large amounts of foreign body giant cells other authors demonstrated a negative influence on biomaterials and also on apoptosis [72]. In the present study, however, the amount of foreign body giant cells and macrophages was moderate and no negative influence on the biomaterials was seen.

Moreover, a moderate amount of fibrocytes and, in some scaffolds, a connective tissue capsule at the edge of the scaffold were also observed in the present study. A one to two-layer connective tissue capsule was most commonly found around polylactic acid scaffolds with pore size 1, suggesting a stronger foreign body response to this type of scaffold. In a previous study a stronger multi-layer capsule formation was described as a more intensive foreign body reaction and thus also as a foreign body isolation, which means that the implant material can no longer be

absorbed by macrophages and foreign body giant cells [45]. The same study mentioned that a stronger capsule formation also leads to a limited nutrient supply [45]. In the present study, however, no multilayer capsule formation could be demonstrated, so that an isolation of the scaffolds cannot be assumed.

In summary, the results of the semiquantitative scoring method and quantitative histomorphometry were in the present study in good agreement and showed good correlation. The parameters 'implant material', 'gas', 'granulation tissue', and 'osteoid-like tissue' correlated significantly. This suggests that both methods can be considered as equivalent and can be replaced by each other. In the literature, the comparison of semiquantitative and quantitative data revealed overall similar results between both methods [63, 73]. In the present study, the advantage of quantitative histomorphometry could be recognised with regard to the parameter 'bone'. The "computer eye" was able to quantify small quantities of new bone, by using classified colour pixels [74], which were lost in the semiquantitative analysis.

4.2 Thin sections

With the von Kossa/McNeal staining mineralised bone tissue can be assessed, which is stained black [50]. In this study, the quality of bone tissue in the immediate vicinity of the scaffold should be investigated with this staining. Unfortunately, it was not possible to produce uniformly evaluable thin sections, because the non-cuttable hard scaffold material led to artifacts and shearing of the histological material. This technical problem with magnesium implants was already observed in another study with $Mg(OH)_2$ implants as the implants came loose when preparing thin sections [75]. Despite this technical limitation, mineralised bone tissue was found in the direct vicinity of the scaffold in the present study. However, only little bone tissue was observed overall, which decreased over time. In total, it was noticeable that slightly more mineralised bone tissue was found in the vicinity of scaffolds with the larger pore size (polylactic acid – pore size 2; calcium phosphate – pore size 2).

5. Conclusion

Magnesium alloys, especially LAE442, represent a promising bone substitute material for critical size bone defects and a placeholder until new bone tissue grows in and replaces the scaffold. The LAE442 alloy characterised in the present study

demonstrated good biocompatibility, moderate osseointegration and slow degradation. At the cellular level all scaffolds were well tolerated. A moderate amount of macrophages and foreign body giant cells was found, which was evaluated as part of a physiological foreign body reaction. When comparing the coatings, both in the semiquantitative and quantitative results, better bone ingrowth and more osteoid-like tissue was observed in calcium phosphate-coated scaffolds (Magnesium fluoride coating/calcium phosphate) than in polylactic acid-coated ones (Magnesium fluoride/polylactic acid). With regard to pore size, scaffolds with larger pore size yielded better results with less gas formation at week 36, significantly more blood vessels at week 12 and more bone tissue around the scaffold. The results of histomorphometry correlated overall with the results of the semiquantitative evaluation method. Thus, it can be concluded that both methods are interchangeable. However, histomorphometry provided more accurate results and therefore offers many advantages for further studies.

6. Conflicts of interest

The authors hereby declare that they have no conflict of interest with the content of the article.

7. Acknowledgement

The research is sponsored by the German Research Foundation (DFG) within the project “Interfacial effects and integration behaviour of magnesium-based sponges as bioresorbable bone substitute material” (Grant No. 271761343). The authors gratefully appreciate the financial support. The authors would like to thank Beatrice Limmer for her outstanding work and support in laboratory techniques as well as Yuri Zablotski for his assistance in statistics.

8. References

[1] H. Liang, K. Wang, A.L. Shimer, X. Li, G. Balian, F.H. Shen, *Bone* **2010**, 47, 197-204.

[2] M. Lalk, J. Reifenrath, D. Rittershaus, D. Bormann, A. Meyer-Lindenberg, *Materialwiss. Werkstofftech.* **2010**, 41, 1025-1034.

[3] M.P. Staiger, A.M. Pietak, J. Huadmai, G. Dias, *Biomater.* **2006**, 27, 1728-1734.

[4] N. Angrisani, J. Reifenrath, F. Zimmermann, R. Eifler, A. Meyer-Lindenberg,

K. Vano-Herrera, C. Vogt, *Acta Biomater.* **2016**, 44, 355-365.

[5] J. Reifenrath, D. Bormann, A. Meyer-Lindenberg, *InTech.* **2011**

[6] F. Witte, *Acta Biomater.* **2015**, 23, 28-40.

[7] M. Navarro, A. Michiardi, O. Castano, J. Planell, *J. R. Soc., Interface* **2008**, 5, 1137-1158.

[8] S.K. Nandi, S. Roy, P. Mukherjee, B. Kundu, D.K. De, D. Basu, *Indian J. Med. Res.* **2010**, 132, 15-30.

[9] A. Krause, N. Von der Höh, D. Bormann, C. Krause, F.-W. Bach, H. Windhagen, A. Meyer-Lindenberg, *J. Mater. Sci.* **2010**, 45, 624.

[10] M. Thomann, C. Krause, D. Bormann, N. Von der Höh, H. Windhagen, A. Meyer-Lindenberg, *Materialwiss. Werkstofftech.* **2009**, 40, 82-87.

[11] E. Wintermantel, B. Shah-Derler, A. Bruinink, M. Petitmermet, J. Blum, *Medizintech.* **2009**, 67-104.

[12] L. Ghasemi-Mobarakeh, D. Kolahreez, S. Ramakrishna und D. Williams, *Curr. Opin. Biomed. Eng.* 10, **2019**, 45-50.

[13] L. Le Guéhennec, A. Soueidan, P. Layrolle, Y. Amouriq, *Dental mater.* **2007**, 23(7), 844-854.

[14] F. Witte, V. Kaese, H. Haferkamp, E. Switzer, A. Meyer-Lindenberg, C. J. Wirth, H. Windhagen, *Biomater.* **2005**, 26(17): 3557-3563.

[15] J. Gray, B. Luan, *J. Alloys Compd.* **2002**, 336, 88-113.

[16] F. Witte, J. Fischer, J. Nellesen, C. Vogt, J. Vogt, T. Donath, F. Beckmann, *Acta Biomater.* **2010**, 6, 1792-1799.

[17] F. Witte, J. Fischer, J. Nellesen, H.A. Crostack, V. Kaese, A. Pisch, F. Beckmann, H. Windhagen, *Biomater.* **2006**, 27, 1013-1018.

[18] J. Vormann, *Mol. Aspects Med.* **2003**, 24, 27-37.

[19] X.-N. Gu, Y.-F. Zheng, *Frontiers Mat. Sci.* **2010**, 4, 111-115.

[20] J. Walker, S. Shadanbaz, T.B. Woodfield, M.P. Staiger, G.J. Dias, *J Biomed. Mater. Res. B Appl. Biomater.* **2014**, 102, 1316-1331.

[21] Y.J. Liu, Z.Y. Yang, L.L. Tan, H. Li, Y.Z. Zhang, *Braz J. Med. Biol. Res.* **2014**, 47, 715-720.

[22] N. Angrisani, J.-M. Seitz, A. Meyer-Lindenberg, J. Reifenrath, *New Feat. Mg Alloys* **2012**

[23] H. Haferkamp, M. Niemeyer, R. Boehm, U. Holzkamp, C. Jaschik, V. Kaese, *Mater. Sci. For. Trans.* **2000**, 350, 31-42.

[24] F. Witte, H. Ulrich, M. Rudert, E. Willbold, *J. Biomed. Mater. Res.* **2007**, 81, 748-756.

[25] T. Kraus, S.F. Fischerauer, A.C. Hanzi, P.J. Uggowitzer, J.F. Loffler, A.M. Weinberg, *Acta Biomater.* **2012**, 8, 1230-1238.

[26] J. Reifenrath, N. Angrisani, N. Erdmann, A. Lucas, H. Waizy, J.M. Seitz, A. Bondarenko, A. Meyer-Lindenberg, *Biomed. Mater.* **2013**, 8, 045012.

[27] E. Willbold, X. Gu, D. Albert, K. Kalla, K. Bobe, M. Brauneis, C. Janning, J. Nellesen, W. Czayka, W. Tillmann, Y. Zheng, F. Witte, *Acta Biomater.* **2015**, 11, 554-562.

[28] L. Witting, A.-C. Waselau, F. Feichtner, L. Wurm, S. Julmi, C. Klose, A.-K. Gartzke, H. Maier, P. Wriggers, A. Meyer-Lindenberg, *Materialia* **2020**, 100949.

[29] N. Kleer, S. Julmi, A.-K. Gartzke, J. Augustin, F. Feichtner, A.-C. Waselau, C. Klose, H. Maier, P. Wriggers, A. Meyer-Lindenberg, *Materialia* **2019**, 100436.

[30] N.V.D. Höh, D. Bormann, A. Lucas, B. Denkena, C. Hackenbroich, A. Meyer-Lindenberg, *Adv. Eng. Mater.* **2009**, 11, B47-B54.

[31] F. Witte, J. Fischer, J. Nellesen, C. Vogt, J. Vogt, T. Donath, F. Beckmann, *Acta Biomater.* **2010**, 6, 1792-1799.

[32] S. Julmi, A.-K. Krüger, A.-C. Waselau, A. Meyer-Lindenberg, P. Wriggers, C. Klose, H.J. Maier, *Mater. Sci. Eng*. **2019**, 98, 1073-1086.

[33] M. Thomann, C. Krause, N. Angrisani, D. Bormann, T. Hassel, H. Windhagen, A. Meyer-Lindenberg, *J Biomed. Mater. Res. A* **2010**, 93, 1609-1619.

[34] M. Lalk, J. Reifenrath, N. Angrisani, A. Bondarenko, J.M. Seitz, P.P. Mueller, A. Meyer-Lindenberg, *J. Mater. Sci. Mater. Med*. **2013**, 24, 417-436.

[35] M. Thomann, C. Krause, N. Angrisani, D. Bormann, T. Hassel, H. Windhagen, A. Meyer-Lindenberg, *J. Biomed. Mater. Res. A* **2010**, 93, 1609-1619.

[36] A. Alabbasi, S. Liyanaarachchi, M.B. Kannan, *Thin Solid Films* **2012**, 520, 6841-6844.

[37] Y. Chen, Y. Song, S. Zhang, J. Li, C. Zhao, X. Zhang, *Biomed. Mater.* **2011**, 6, 025005.

[38] J. Yang, F. Cui, I. Lee, Y. Zhang, Q. Yin, H. Xia, S. Yang, *J. Biomater. Appl.* **2012**, 27, 153-164.

[39] S.V. Dorozhkin, *Acta Biomater.* **2014**, 10, 2919-2934.

[40] S. Julmi, C. Klose, A.-K. Krüger, P. Wriggers, H.J. Maier, *Annu. Meet. Exhib., Suppl. Proc., 146th*, **2017**, pp. 307-317.

[41] M.Q. Cheng, T. Wahafu, G.F. Jiang, W. Liu, Y.Q. Qiao, X.C. Peng, T. Cheng, X.L. Zhang, G. He, X.Y. Liu, *Sci. Rep.* **2016**, 6, 24134.

[42] M. Yazdimamaghani, M. Razavi, D. Vashaee, K. Moharamzadeh, A.R. Boccaccini, L. Tayebi, *Mater. Sci. Eng. C Mater. Biol. Appl.* **2017**, 71, 1253-1266.

[43] A. Clark, L. Hench, H. Paschall, *J. Biomed. Mater. Res.* **1976**, 10, 161-174.

[44] J.M. Anderson, M.S. Shive, *Adv. Drug Delivery Rev.* **2012**, 64, 72-82.

[45] K.M. Nuss, B. von Rechenberg, *Open Orthop. J.* **2008**, 2, 66-78.

[46] D. Williams, *Internat. Conf. Biomed. Polymers: Molec. Design Clinic. Appl.* **1991**

[47] A. Rosengren, L. Wallman, N. Danielsen, T. Laurell, L.M. Bjursten, *IEEE Trans. Biomed. Eng.* **2002**, 49, 392-399.

[48] J. Lassus, J. Salo, W.A. Jiranek, S. Santavirta, J. Nevalainen, M. Matucci-Cerinic, P. Horák, Y. Konttinen, *Clinic. Orthopaed. Rel. Res.* **1998**, 7-15.

[49] T.A. Huehnerschulte, J. Reifenrath, B. von Rechenberg, D. Dziuba, J.M. Seitz, D. Bormann, H. Windhagen, A. Meyer-Lindenberg, *Biomed. Eng. Onl.* **2012**, 11, 14.

[50] Y. Ikarashi, K. Toyoda, N. Ohsawa, T. Uchima, T. Tsuchiya, M.A. Kaniwa, M. Sato, M. Takahashi, A. Nakamura, *J. Biomed. Mat. Res.* **1992**, 26, 339-356.

[51] J.M. Anderson, *Biomater. Sci.* **2013**, pp. 503-512.

[52] F. Veronesi, G. Giavaresi, V. Guarino, M.G. Raucci, M. Sandri, A. Tampieri, L. Ambrosio, M. Fini, *J. Biomed. Mater. Res. A* **2015**, 103, 2932-2941.

[53] H.E. Koepp, S. Schorlemmer, S. Kessler, R.E. Brenner, L. Claes, K.P. Günther, A.A. Ignatius, *J. Biomed. Mater. Res. B, Appl. Biomater.* **2004**, 70, 209-217.

[54] E. Willbold, F. Witte, *Acta Biomater.* **2010**, 6, 4447-4455.

[55] N. Kleer-Reiter, S. Julmi, F. Feichtner, A. C. Waselau, C. Klose, P. Wriggers, H.J. Maier, A. Meyer-Lindenberg, *Biomed. Mater.* **2021**, *16*(3), 035037.

[56] I. S. Berglund, B. Y. Jacobs, K. D. Allen, S. E. Kim, A. Pozzi, J. B. Allen, M. V. Manuel, *Mater. Sci. and Eng. C*, **2016**, *62*, 79-85.

[57] X. Wang, F. Wei, F. Luo, K. Huang, Z. Xie, *J. Orthop. Surg. Res.* **2015**, 10, 147.

[58] R. Lüllmann-Rauch, *Histologie* **2015**

[59] A.L. Mescher, *Junqueira's Basic Histol. Mc Graw Hill Educ. Lange,* **2016**

[60] M. Mukaka, Malawi, *Med. J.* **2012**

[61] J. Augustin, F. Feichtner, A.C. Waselau, S. Julmi, C. Klose, P. Wriggers, H.J. Maier, A. Meyer-Lindenberg, *J. Biomed. Mater. Res. B: Appl. Biomater.* **2020**

[62] D.K. Meyerholz, A.P. Beck, *ILAR Journal* **2018**, 59, 13-17.

[63] E. McInnes, *Pathol. Toxicol.: Princip. Pract. Labor. Animal Pathol.* **2017**

[64] M. Pourbaix, *NACA* **1984**

[65] A. Angrisani, J. Reifenrath, J. Seitz, H. Waizy, A. Meyer-Lindenberg, *Bio. Nano. Mater*. **2012**, 13, 43.

[66] N. Erdmann, A. Bondarenko, M. Hewicker-Trautwein, N. Angrisani, J. Reifenrath, A. Lucas, A. Meyer-Lindenberg, *Biomed. Eng. Online* **2010**, 9, 63

[67] V. Raina, *J. Clinic. Pathol.* **1972**, 25, 229-232.

[68] V. Karageorgiou, D. Kaplan, *Biomater.* **2005**, 26, 5474-5491.

[69] P.R. Kuzyk, E.H. Schemitsch, *Indian J. Orthop.* 2011, 45, 108.

[70] K. Pawelec, J.A. Planell, *Bone Rep. Biomater., Regen. Clinic. Appl., Woodhead Publ.* **2018**

[71] T. Horbett, *Biomater. Sci., Introd. Mater. Med.* **2004**, 2, 237-246.

[72] W.G. Brodbeck, M.S. Shive, E. Colton, Y. Nakayama, T. Matsuda, J.M. Anderson, J. Biomed. *Mater. Res.* **2001**, 55, 661-668.

[73] C. Shackelford, G. Long, J. Wolf, C. Okerberg, R. Herbert, *Toxicol. Pathol.* **2002**, 30, 93-96.

[74] I. Arganda-Carreras, V. Kaynig, C. Rueden, K.W. Eliceiri, J. Schindelin, A. Cardona, H. Sebastian Seung, *Bioinf.* **2017**, 33, 2424-2426.

[75] C. Janning, E. Willbold, C. Vogt, J. Nellesen, A. Meyer-Lindenberg, H. Windhagen, F. Thorey, F. Witte, *Acta Biomater.* **2010,** 6, 1861-1868.

V. DISKUSSION

Ziel dieser Studie war es, die Osseointegration, die Degradation und die Biokompatibilität von offenporigen Knochenersatzstoffen (Scaffolds) der Magnesium Legierung LAE442 mit zwei unterschiedlichen Porengrößen (P1:400 µm; P2:500 µm) und mit einer Kombinationsbeschichtung (MgF_2/PLA; MgF_2/CaP) in einem Kaninchenmodell zu untersuchen. Die Magnesiumlegierung LAE442 wurde in früheren Studien bereits in vivo in Form von nicht porösen Implantaten (Thomann et al. 2009, Hort et al. 2010, Krause et al. 2010) sowie in Form von porösen Scaffolds (Kleer et al. 2019, Augustin et al. 2020) getestet und zeigte eine gute Biokompatibilität sowie eine gute Osseointegration. Magnesiumionen in Biomaterialien konnten in Studien einen osteoinduktiven Effekt bewirken und so die Knochenregeneration verbessern (Wang et al. 2019). Nachteile von Magnesium ließen sich dagegen in einer zu schnellen Degradation und daraus entstehender Gasbildung beobachten (Witte et al. 2006, Augustin et al. 2020). Um dieses Problem in den Griff zu bekommen, wurde in dieser in vivo Studie versucht, die Degradation mit Hilfe einer Kombinationsbeschichtung zu regulieren. Julmi et al. (2019) untersuchten die Kombinationsbeschichtungen (MgF_2/PLA; MgF_2/CaP) bereits in vitro und beobachteten gute Ergebnisse bezüglich der Senkung der Degradationsrate. Die Autoren beschrieben eine verbesserte Beschichtungshaftung, die zu einer verzögerten in vitro Korrosionsrate führte im Gegensatz zu einfach beschichteten MgF_2-Scaffolds (Julmi et al. 2019). MgF_2 fungierte dabei als Basisschicht mit dem Vorteil, dass die erste entstehende Menge an Wasserstoffgas, die bei der Degradation von Magnesium freigesetzt wird, unterdrückt wurde (Pourbaix 1984, Julmi et al. 2019).

Die beschichteten LAE442 Scaffolds (n = 128) (Scaffoldtypen: CaP-P1; CaP-P2; PLA-P1; PLA-P2) sowie die Kontrollgruppe mit Scaffolds aus ß-Tricalciumphosphat (TCP) (n = 32) wurden randomisiert in den spongiösen Teil des Trochanter major ossis femoris von Kaninchen eingesetzt. Als Implantationsort wurde ein spongiöser Knochenbereich gewählt, da das Gerüst der Scaffolds den spongiösen Knochentrabekeln ähnelte und somit die Osseointegration erleichterte (Lalk et al. 2010, Kleer et al. 2019, Augustin et al. 2020). Die Operation wurde entsprechend der Methodik von Lalk et al. (2010) ausgeführt, die in Vorstudien poröse Scaffolds der Legierung AX30 im Kaninchenmodell untersuchten. Die

Scaffolds wurden etwa 1 mm unter der Knochenoberfläche des Trochanter majors implantiert, sodass sie ringsum von Spongiosa umgeben waren (Lalk et al. 2010). Für die Auswertung der Scaffolds in der vorliegenden Studie wurden Röntgenbilder und µCT-Daten alle zwei Wochen (bis Woche 12), beziehungsweise alle vier Wochen (bis Woche 36) erhoben und analysiert. Die Daten wurden semiquantitativ und quantitativ nach einem Scoring-Schema nach Kleer et al. (2019) und Augustin et al. (2020) ausgewertet, welches nach Lalk et al. (2010) modifiziert wurde. Außerdem wurden in den Zeitintervallen von 6, 12, 24 und 36 Wochen histologische sowie histomorphometrische Daten erfasst und ebenfalls nach Kleer et al. (2019), Augustin et al. (2020) beziehungsweise Lalk et al. (2010) evaluiert.

Um die Degradation zu beurteilen, wurden Dichte und Volumen der Scaffolds mittels **Mikrocomputertomographie (µCT)** bestimmt. Die Kombinationsbeschichtung der vorliegenden Studie (MgF_2 + PLA/CaP) führte dazu, dass die Scaffolds langsam degradierten und das Grundgerüst der Scaffolds auch nach 36 Wochen noch sichtbar war. Julmi et al. (2019) untersuchten LAE442 Scaffolds mit der gleichen Beschichtungskombination bereits in vitro und stellten eine langsamere Degradation fest im Vergleich zu unbeschichteten LAE442 Scaffolds. Augustin et al. (2020) untersuchten in ihrer in vivo Studie LAE442 Scaffolds der gleichen Geometrie, ebenfalls mit zwei unterschiedlichen Porengrößen, jedoch nur einfach mit MgF_2 beschichtet. Beim Vergleich mit den Scaffolds von Augustin et al. (2020) fiel auf, dass die zweifach beschichteten Scaffolds der vorliegenden Studie deutlich langsamer degradierten als die einfach beschichteten. In der vorliegenden Studie konnte man außerdem beobachten, dass Scaffolds mit der größeren Porengröße (500 µm) langsamer degradierten als solche mit der kleineren Porengröße (400 µm). Dies fanden auch Augustin et al. (2020) mit Hilfe von Röntgen- sowie µCT-Daten heraus. Dieses Ergebnis könnte darauf zurückzuführen sein, dass Scaffolds mit kleinerem Porendurchmesser eine größere Oberfläche und auch eine größere Korrosionsangriffsfläche aufweisen, wodurch sie schneller degradierten (Karageorgiou und Kaplan 2005, Augustin et al. 2020). Beim Vergleich der Beschichtungen, unabhängig der Porengröße, zeigten die CaP-beschichteten Scaffolds eine schnellere Degradation als die PLA-beschichteten Scaffolds. Auf dieses Ergebnis kamen auch Julmi et al. (2019), die Scaffolds mit der gleichen Beschichtung in vitro untersuchten.

Bei allen LAE442 Scaffolds trat die Bildung von Wasserstoff auf, welcher

natürlicherweise bei der Degradation von Magnesium entsteht ($Mg + 2H_2O \rightarrow Mg(OH)_2 + H_2$) (Pourbaix 1984). Das Gas beeinträchtigte die Tiere klinisch nicht. In der vorliegenden Studie konnte das Gas in den Poren sowie im Umkreis der Scaffolds bis in den Markraum/Schaft beobachtet werden. Das umgebende Gewebe konnte dabei nur eine bestimmte Menge an Gas aufnehmen, sodass es akkumulierte. In anderen Studien wurden ebenfalls Gasansammlungen bei Magnesiumlegierungen beobachtet (Erdmann et al. 2010, Lalk et al. 2010, Reifenrath et al. 2013, Kim et al. 2018, Kleer et al. 2019). In der vorliegenden Studie wurde um die CaP-beschichteten Scaffolds bis Woche 6 weniger Gas beobachtet als um die PLA-beschichteten, wobei PLA-P1 Scaffolds die höchste Menge an Gas aufwiesen. Dieser Unterschied könnte auf die unterschiedlichen Beschichtungen zurückzuführen sein. Es wird vermutet, dass eine PLA-Beschichtung das freigesetzte Gas aufgrund der unterschiedlichen intermolekularen Bindungen stärker an die Scaffoldoberfläche bindet (Atkins 2006). Infolgedessen diffundierte das aus den PLA Scaffolds austretende Gas möglicherweise langsamer in das umgebende Gewebe und führte zu einer erhöhten lokalen Gasakkumulation. Des Weiteren beschrieben einige Autoren, dass Degradation und Gasbildung in direkter Abhängigkeit stehen, wobei eine langsamere Korrosion zu einer geringeren Gasproduktion führen soll (Witte et al. 2006, Witte et al. 2010). In der vorliegenden Studie waren die Ergebnisse zu Degradation und Gasbildung widersprüchlich, da die CaP Scaffolds trotz einer schnelleren Degradation weniger Gas bildeten als die PLA Scaffolds. Eine genaue Ursache für die Kontroversität zwischen Degradationsschnelligkeit und Gasbildung konnte in dieser Studie nicht ermittelt werden. Eine physikalische Erklärung hierfür wäre wiederum die stärkere intermolekulare Bindung von PLA (Atkins 2006). Augustin et al. (2020) beschrieben in ihrer Studie mit MgF_2-beschichteten LAE442 Scaffolds ebenfalls Gasansammlungen. Der Vergleich der Studien zeigte, dass die nur mit MgF_2-beschichteten Scaffolds von Augustin et al. (2020) in den Wochen 2 und 4 mehr Gas produzierten als die mit MgF_2/CaP-beschichteten Scaffolds aus der vorliegenden Studie. Es kann daher davon ausgegangen werden, dass die zusätzliche CaP-Beschichtung in der vorliegenden Studie die initiale Gasproduktion reduzierte und somit die Osseointegration positiv beeinflusste. Dass Kombinationsbeschichtungen nicht nur die Degradation verlangsamen, sondern auch die Gasenstehung verringern, stellten schon Julmi et al. (2019) in vitro fest. In ihrer Studie beschrieben sie eine Beschichtung aus MgF_2 als eine Art Schutzschicht,

die die anfängliche berstende Freisetzung von Wasserstoff unterdrückte (Julmi et al. 2019).

Im Bereich des Bohrloches entstanden bereits 2 Wochen post OP periostale Zubildungen, die auch andere Autoren in Studien mit Magnesium Scaffolds feststellten (Lalk et al. 2013, Kleer et al. 2019, Augustin et al. 2020). Periostale Knochenzubildungen konnte an der Implantationsstelle in Röntgenbildern und µCT-Scans bei allen Scaffold-Typen gleichermaßen nachgewiesen werden. Da das Einsetzen der Scaffolds immer mit einem Periosttrauma durch Freilegen des Knochens und Bohren verbunden ist, könnten die periostalen Knochenzubildungen möglicherweise auf eine Manipulation der Knochenoberfläche zurückzuführen sein. Diese Annahme bestätigten auch von der Höh et al. (2009) in ihrer in vivo Studie mit Magnesiumimplantaten. Sie verwiesen auf ein periostales Wachstum, das unabhängig vom Implantatabbau vermutlich durch das Bohren auftrat (Von Der Höh et al. 2009). Periostale Zubildungen konnten außerdem in anderen Studien an Leerbohrungen am Kaninchenfemur festgestellt werden (Lalk et al. 2013).

Osseointegration ist das Ergebnis eines Knochenheilungsprozesses, bei dem neue Knochenzellen wie Osteoblasten und Knochenmarkszellen direkt am Implantat oder am Knochenersatzstoff anwachsen (Le Guéhennec et al. 2007). Die Osseointegration selbst wird dann als direkte funktionelle und strukturelle Verbindung zwischen Scaffoldoberfläche und vitalem Knochen definiert (Le Guéhennec et al. 2007). In dieser Studie wurde die Osseointegration anhand der Knochen-Scaffold-Kontakte im µCT analysiert. Alle LAE442 Scaffolds, mit Ausnahme von PLA-P1, zeigten spätestens ab Woche 6 eine Zunahme der Knochen-Scaffold-Kontakte. Beim Vergleich der Beschichtungen PLA und CaP wurden in der vorliegenden Studie generell mehr Knochen-Scaffold-Kontakte bei CaP Scaffolds ab Woche 10 gefunden. Aus der Literatur ist bekannt, dass der Heilungsprozess des Knochens durch physiologische osteokonduktive Eigenschaften beeinflusst wird, die durch bestimmte Implantatmaterialien verstärkt werden können (Thomann et al. 2009, Wang et al. 2019). Der Grund für mehr Knochen-Scaffold-Kontakte im Umkreis der CaP Scaffolds könnte also ein osteokonduktiver Einfluss von Calcium gewesen sein, das Bestandteil der CaP-Beschichtung war. Auch Yang et al. (2020) erwähnten in ihrer Studie mit Magnesiumimplantaten, dass calcium- und phosphorhaltige Biokeramiken der Zusammensetzung des natürlichen Knochens ähneln und die

Oberflächenbioaktivität und damit das Wachstum von Knochengewebe fördern können. Wang et al. (2019) beschrieben ebenfalls bessere osteokonduktive Eigenschaften bei Magnesium Scaffolds, wenn die Oberfläche beziehungsweise die Beschichtung der Scaffolds bioaktive Ionen wie Calcium besaß.

Der Einfluss der Porengröße auf die Osseointegration von Biomaterialien wird in der Literatur kontrovers diskutiert. Grundsätzlich sollte ein resorbierbarer Knochenersatzstoff eine der Spongiosa ähnliche Porengröße haben, um das Einwachsen von Knochenzellen in die Poren zu fördern (Cheng et al. 2016, Yang et al. 2020). In der Literatur wurde ein besseres Knocheneinwachsverhalten bei Porengrößen > 300 µm beobachtet, da größere Poren die Vaskularisation begünstigen (Karageorgiou und Kaplan 2005, Cheng et al. 2016). Cheng et al. (2016) fanden in ihrer Studie heraus, dass Scaffolds mit einer Porengröße von 400 µm die Bildung von neuem Knochengewebe mehr förderten als eine Porengröße von 250 µm. In der vorliegenden Studie wurden deshalb zwei unterschiedliche Porengrößen > 300 µm untersucht. Beim Vergleich dieser Porengrößen (P1:400 µm; P2:500 µm) wurden keine signifikanten Unterschiede gefunden. Der Grund könnte der zu geringe Größenunterschied (400 µm im Vergleich zu 500 µm) sein. Die Scaffolds mit der größeren Porengröße zeigten bis Woche 24 nur geringfügig höhere Knochendichtewerte und degradierten etwas langsamer als Scaffolds mit der kleineren Porengröße. PLA-P1 Scaffolds wiesen insgesamt geringgradig schlechtere Werte als PLA-P2 auf, was die Gasproduktion, und die Knochen-Scaffold-Kontakte betraf. In der Studie von Augustin et al. (2020) wiesen die Scaffolds mit der größeren Porengröße (500 µm) in Woche 2 sogar signifikant bessere Werte bezüglich Knochen-Scaffold-Kontakte und Knochenvolumen auf, im Vergleich zur kleineren Porengröße (400 µm).

Für die **histologischen Untersuchungen** wurden Dickschliffpräparate hergestellt und mit Toluidinblau gefärbt. Dickschliffe haben den Vorteil, dass sie zunächst breiter zugeschnitten werden können und dann auf eine geringere Dicke geschliffen werden, ohne dabei das Gewebe direkt neben dem Implantat zu zerstören (Donath und Breuner 1982). Besonders für mineralisierte nicht entkalkte Knochenproben und harte metallische Implantate sind Dickschliffe von Vorteil (Willbold und Witte 2010).

Die Degradation der LAE442 Scaffolds wurde histologisch anhand des Materialverlustes in Form von Rissen (‚cracks') und Materialgranulation

(‚granulation') sichtbar. Der geringe Materialverlust wies auf eine langsame Degradation hin. Die langsame Degeneration der Scaffolds wurde bereits in vivo bei Augustin et al. (2020) anhand von einfach beschichteten LAE442 Saffolds via µCT-Untersuchungen genauer untersucht. Die sehr langsame Degradation von LAE442 wurde außerdem schon histologisch und in vivo in Form von Pins beschrieben (Krause et al. 2010, Angrisani et al. 2016). Wie bereits im µCT festgestellt, wurden in der vorliegenden Studie auch histologisch Wasserstoffakkumulationen um die Scaffolds, insbesondere um Scaffolds der kleineren Porengröße, beobachtet. Entstandenes Gas wird in vivo durch umgebendes Gewebe, vor allem durch gut vaskularisiertes Gewebe abtransportiert (Angrisani et al. 2012, Kraus et al. 2012). Da in der vorliegenden Studie weniger Blutgefäße in Scaffolds der kleineren Porengröße ab Woche 12 gefunden wurde, könnte dies mit einem geringeren Gasabtransport in Zusammenhang stehen (Erdmann et al. 2010, Lalk et al. 2010). Auch Cheng et al. (2016) beobachteten in einer in vivo Studie mit offenporigen Magnesium Scaffolds anhand von Histologie- und µCT-Daten mehr Blutgefäße und neues Knochengewebe bei der größeren Porengröße. Vaskularisation ist jedoch nicht nur für den Transport von entstandenem Gas und anderen Korrosionsprodukten wichtig. Blutgefäße sind essentiell für die Versorgung von Zellen und spielen eine große Rolle bei der Knochenheilung und somit bei der Osseointegration von Knochenersatzstoffen (Pawelec und Planell 2018). Ist die Vaskularisation gestört, ist nur noch eine Nährstoffversorgung über Diffusion möglich, was sehr ineffizient ist (Pawelec und Planell 2018). In der Histologie wurde außerdem beobachtet, dass Scaffolds der größeren Porengröße insgesamt mehr neues Knochengewebe ausbildeten als Scaffolds der kleineren Porengröße. Auch andere Autoren fanden heraus, dass durch größere Poren mehr Raum für Vaskularisation und damit verstärktes Knocheneinwachstum ermöglicht wurde (Nuss und von Rechenberg 2008, Cheng et al. 2016, Augustin et al. 2020).

Vergleicht man in der vorliegenden Studie die Beschichtungen unabhängig der Porengröße, wurde bei CaP Scaffolds mehr neues Knochengewebe in den Poren beobachtet als bei PLA-Scaffolds. Als Ursache für die bessere Osseointegration von CaP Scaffolds könnte, wie schon in der µCT-Auswertung beschrieben, ein osteokonduktiver Effekt von Calcium vermutet werden (Thomann et al. 2009).

Neben Knochengewebe wurden in nahezu allen LAE442 Scaffolds große Mengen

an Osteoid ähnlichem Gewebe (‚Osteoid-like-tissue') gefunden, welches sich in der Toluidinblau-Färbung blassblau darstellte und der Farbe von Osteoid ähnelte. Aktive Osteoblastensäume, die am ‚Osteoid-like-tissue' anhafteten, konnten hingegen nur sehr wenige beobachtet werden. Im Gegensatz zu physiologischem Osteoid, welches nur als schmaler Saum bei einer Knochenneubildung zu sehen ist (Raina 1972), stellte sich das ‚Osteoid-like-tissue' in der vorliegenden Studie flächig und verwaschen dar. Auch Lalk et al. (2013) beobachteten ein ähnliches Gewebe in ihrer Studie mit Magnesium Scaffolds der Legierung AX30. Sie vermuteten, dass es sich hierbei um kaum mineralisiertes Gewebe handelte. Auch Witte et al. (2007) beobachteten Osteoid-Gewebe um Magnesium Scaffolds der Legierung AZ91D. Sie maßen die Breite des Osteoid-Saums und stellten fest, dass dieser um die Magnesium Scaffolds fast dreimal so breit war wie bei der Kontrollgruppe mit autologen Knochenimplantaten (Witte et al. 2007). In der vorliegenden Studie konnte nicht geklärt werden, um welches Gewebe es sich genau handelte. Im ‚Osteoid-like-tissue' wurden zudem nur wenige sichtbar angefärbte Zellkerne gefunden, was dafür sprechen könnte, dass das Gewebe nicht ausreichend versorgt wurde. Denn aktive osteogene Zellen im Inneren der Scaffolds benötigen eine ausreichende Versorgung mit Blut und Sauerstoff, um eine direkte Osteogenese zu ermöglichen (Karageorgiou und Kaplan 2005, Nuss und von Rechenberg 2008, Kuzyk und Schemitsch 2011, Lalk et al. 2013).

In Hinblick auf die Anzahl der Blutgefäße wurde bei allen LAE442 Scaffolds nur eine kleine bis mittlere Anzahl von Blutgefäßen beobachtet. In der vorliegenden Studie wurde außerdem eine moderate Menge an Makrophagen sowie eine geringe Menge an Fremdkörperriesenzellen (FBGC) in den Scaffoldporen und in der Umgebung der Scaffolds gefunden. Die Zuwanderung von Makrophagen ließ einen physiologischen Heilungsprozess im Zuge der Knochenheilung und der Scaffoldresorption vermuten (Horbett 2004, Nuss und von Rechenberg 2008, Lalk et al. 2013). Die Rolle von Fremdkörperriesenzellen bei Knochenimplantaten wurde in der Literatur kontrovers diskutiert (Brodbeck et al. 2001, Nuss und von Rechenberg 2008). Einige Autoren beschrieben Fremdkörperriesenzellen als ein Zeichen für eine gute biologische Abbaubarkeit (Nuss und von Rechenberg 2008). In Verbindung mit großen Ansammlungen von Makrophagen und Fremdkörperriesenzellen beschrieben andere Autoren jedoch einen negativen Einfluss auf Biomaterialien, auch durch Apoptose (Brodbeck et al. 2001). In der

vorliegenden Studie war die Menge an Fremdkörperriesenzellen und Makrophagen moderat und es konnte kein negativer Einfluss auf die Scaffolds beobachtet werden. Darüber hinaus wurde in der vorliegenden Studie eine moderate Menge an Fibrozyten und bei einigen Scaffolds eine Bindegewebskapsel am Rand beobachtet. Eine ein- bis zweischichtige Bindegewebskapsel wurde am häufigsten um PLA-P1 Scaffolds gefunden, was eine stärkere Fremdkörperreaktion auf diesen insgesamt schlechter abschneidenden Scaffold-Typ vermuten lässt. Eine stärkere mehrschichtige Kapselbildung könnte eine intensivere Fremdkörperreaktion und damit auch eine Fremdkörperisolation auslösen (Nuss und von Rechenberg 2008). In der vorliegenden Studie wurde jedoch keine mehrschichtige Kapselbildung beobachtet, so dass von einer Isolierung der Scaffolds nicht ausgegangen werden konnte.

VI. ZUSAMMENFASSUNG

Resorbierbare Magnesiumlegierungen haben in einigen Studien bereits gute Ergebnisse bezüglich Biokompatibilität, Osseointegration und Degradationsverhalten gezeigt. Als Nachteile von Magnesium wurden eine zu schnelle Degradation und die Wasserstoffentstehung beschrieben. Dabei wurde ein bedeutender Einfluss von Legierungsbestandteilen sowie Beschichtungen auf Degradation und Osseointegration beobachtet. Ziel dieser in vivo Studie war es resorbierbare doppelt beschichtete Magnesium Scaffolds der Legierung LAE442 als offenporige Schwammstruktur im unbelasteten spongiösen Knochen zu untersuchen. Dabei sollte vor allem der Einfluss der Beschichtungen beobachtet werden. Die wesentliche Neuheit der Studie war die Verwendung einer Kombinationsbeschichtung (MgF_2/PLA; MgF_2/CaP). Die Beschichtungen sollten die Korrosionsbeständigkeit der Scaffolds erhöhen, die Gasbildung verringern sowie das Knocheneinwachstum stimulieren. Die Scaffolds hatten zudem zwei unterschiedliche Porengrößen (P1: 400 µm; P2: 500 µm), um den Einfluss von Poren zu untersuchen. Alle Scaffolds (PLA-P1, PLA-P2, CaP-P1, CaP-P2; (n = 32)) wurden beidseits in den Trochanter major femoris von insgesamt 80 adulten Kaninchen eingesetzt. Als Kontrollgruppe dienten ß-TCP Scaffolds (n = 32). Postoperativ wurden Röntgenaufnahmen, in vivo µCT-Scans und histologische Analysen in regelmäßigen Abständen von 6, 12, 24 und 36 Wochen durchgeführt. PLA-Scaffolds degradierten etwas langsamer, wiesen aber in den Wochen 2 und 4 eine signifikant größere Menge an Gas auf als CaP-Scaffolds. Dagegen zeigten CaP-Scaffolds bessere Werte für den Bohrlochschluss und eine signifikant höhere Anzahl von Knochen-Scaffold-Kontakten von Woche 12 bis 36. Bei der Messung des Knocheneinwachsverhaltens wurde bei CaP-Scaffolds außerdem ein höheres Knochenvolumen beobachtet. Insgesamt schien eine Kombinationsbeschichtung aus MgF_2/CaP vielversprechend in Bezug auf Degradation, Osseointegration und Biokompatibilität zu sein. In Hinblick auf die Porengröße schienen größere Poren besser geeignet zu sein, um das Einwachsen von Blutgefäßen und die damit ausreichende Nährstoffversorgung von neuem Knochengewebe zu gewährleisten. Neben mineralisiertem Knochen wurde in dieser Studie eine große Menge an Osteoid-ähnlichem Gewebe im Scaffoldinneren beobachtet. In zukünftigen Studien sollen Scaffolds im krafttragenden belasteten Knochen eingesetzt werden.

VII. SUMMARY

In many studies, resorbable magnesium alloys have already provided good results in the literature in terms of biocompatibility, osseointegration and degradation behavior. Rapid degradation and resulting hydrogen evolution have been described as disadvantages of magnesium. Thus, components of magnesium alloys as well as coatings have shown a high influence on degradation and osseointegration. The aim of this in vivo study was to investigate degradable coated magnesium scaffolds of the alloy LAE442 as an open porous sponge structure in unloaded cancellous bone. Its main purpose was to observe the influence of the coatings. The novelty of the study was the use of a double combination coating with MgF_2/PLA or MgF_2/CaP. The coatings were intended to increase the corrosion resistance of the scaffolds as well as to stimulate bone ingrowth and to decrease gas production. Moreover, the scaffolds had two different pore sizes (P1: 400 µm; P2: 500 µm) to investigate the influence of pores. All scaffolds (PLA-P1 (n = 32), PLA-P2 (n = 32), CaP-P1 (n = 32), CaP-P2 (n = 32)) were inserted bilaterally into the greater trochanter femoris of 80 adult rabbits. Scaffolds of ß-tricalcium phosphate (n = 32) served as control group. X-rays, in vivo µCT-scans, and histologic analyses were performed postoperatively at regular intervals of 6, 12, 24, and 36 weeks. PLA-scaffolds degraded slightly more slowly but had a significantly greater amount of gas than CaP-scaffolds at weeks 2 and 4. In contrast, CaP-scaffolds showed better values for borehole closure and a significantly higher number of bone-scaffold-contacts from weeks 12 to 36. In the measurement of bone ingrowth behavior, CaP-scaffolds exhibited a higher bone volume. Overall, a combination coating of MgF_2/CaP appeared most promising with regard to degradation, osseointegration and biocompatibility. In terms of pore size, larger pores seemed to be more suitable to ensure ingrowth of blood vessels and thus sufficient nutrient supply to new bone tissue. Beside mineralized bone, a large amount of ‘osteoid-like-tissue’ was observed in the scaffold interior in this study. In future studies, scaffolds should be investigated in load-bearing bone.

VIII. LITERATURVERZEICHNIS

Anderson, J. M. (1988). "Inflammatory response to implants." ASAIO transactions 34(2): 101-107.

Anderson, J. M. (2015). "Exploiting the inflammatory response on biomaterials research and development." Journal of Materials Science: Materials in Medicine 26(3): 121.

Angrisani, A., J. Reifenrath, J. Seitz, H. Waizy und A. Meyer-Lindenberg (2012). "Gasbildung und deren Analysemöglichkeiten im Verlauf der in vivo Degradation von Magnesiumlegierungen." Bio Nano Materials 13: 43.

Angrisani, N., J. Reifenrath, F. Zimmermann, R. Eifler, A. Meyer-Lindenberg, K. Vano-Herrera und C. Vogt (2016). "Biocompatibility and degradation of LAE442-based magnesium alloys after implantation of up to 3.5 years in a rabbit model." Acta Biomaterialia 44: 355-365.

Angrisani, N., J.-M. Seitz, A. Meyer-Lindenberg und J. Reifenrath (2012). "Rare earth metals as alloying components in magnesium implants for orthopaedic applications." New Features on Magnesium Alloys (Kapitel 4).

Atkins, P. W. (2006). Kurzlehrbuch Physikalische Chemie (Vol. 27), John Wiley & Sons.

Augustin, J., F. Feichtner, A. C. Waselau, S. Julmi, C. Klose, P. Wriggers, H. J. Maier und A. Meyer-Lindenberg (2020). "Comparison of two pore sizes of LAE442 scaffolds and their effect on degradation and osseointegration behavior in the rabbit model." Journal of Biomedical Materials Research Part B: Applied Biomaterials.

Bartels, F. (2011). "Histomorphometrische Untersuchungen der Knochenstruktur am ovarektomierten Göttinger Minischwein zur Etablierung eines Großtiermodells zur Simulation der postmenopausalen Osteoporose.", Universität Göttingen

Blackwood, D., A. Chua, K. Seah, R. Thampuran und S. Teoh (2000). "Corrosion behaviour of porous titanium–graphite composites designed for surgical implants." Corrosion Science 42(3): 481-503.

Bobe, K., E. Willbold, I. Morgenthal, O. Andersen, T. Studnitzky, J. Nellesen, W. Tillmann, C. Vogt, K. Vano und F. Witte (2013). "In vitro and in vivo evaluation of biodegradable, open-porous scaffolds made of sintered magnesium W4 short fibres." Acta Biomaterialia 9(10): 8611-8623.

Bondarenko, A., N. Angrisani, A. Meyer-Lindenberg, J. Seitz, H. Waizy und J. Reifenrath (2014). "Magnesium-based bone implants: Immunohistochemical analysis of peri-implant osteogenesis by evaluation of osteopontin and osteocalcin expression." Journal of biomedical materials research Part A 102(5): 1449-1457.

Bouxsein, M. L., S. K. Boyd, B. A. Christiansen, R. E. Guldberg, K. J. Jepsen und R. Müller (2010). "Guidelines for assessment of bone microstructure in rodents using micro–computed tomography." Journal of bone and mineral research 25(7): 1468-1486.

Brodbeck, W. G., M. S. Shive, E. Colton, Y. Nakayama, T. Matsuda und J. M. Anderson (2001). "Influence of biomaterial surface chemistry on the apoptosis of adherent cells." Journal of biomedical materials research 55(4): 661-668.

Cao, H. und N. Kuboyama (2010). "A biodegradable porous composite scaffold of PGA/β-TCP for bone tissue engineering." Bone 46(2): 386-395.

Carpenter, A.-M. (1979). "Stereology. Definition and historic background." Journal of Histochemistry & Cytochemistry 27(11): 1535-1535.

Cheng, M. Q., T. Wahafu, G. F. Jiang, W. Liu, Y. Q. Qiao, X. C. Peng, T. Cheng, X. L. Zhang, G. He und X. Y. Liu (2016). "A novel open-porous magnesium scaffold with controllable microstructures and properties for bone regeneration." Scientific Reports 6: 24134.

Chia, T. L., M. A. Easton, S.-M. Zhu, M. A. Gibson, N. Birbilis und J. F. Nie (2009). "The effect of alloy composition on the microstructure and tensile properties of binary Mg-rare earth alloys." Intermetallics 17(7): 481-490.

Chiu, K., M. Wong, F. Cheng und H. Man (2007). "Characterization and corrosion studies of fluoride conversion coating on degradable Mg implants." Surface and Coatings Technology 202(3): 590-598.

Dahme, E. und M. Reinacher (1988). "Stütz und Bewegungsapparat." Grundriss der speziellen Anatomie der Haustiere. Stuttgart, Enke Verlag: 314-351.

Donath, K. und G. Breuner (1982). "A method for the study of undecalcified bones and teeth with attached soft tissues* The Säge-Schliff (sawing and grinding) Technique." Journal of Oral Pathology & Medicine 11(4): 318-326.

Dorozhkin, S. V. (2014). "Calcium orthophosphate coatings on magnesium and its biodegradable alloys." Acta Biomaterialia 10(7): 2919-2934.

Elliott, J. und S. Dover (1984). "Three-dimensional distribution of mineral in bone at a resolution of 15 μm determined by x-ray microtomography." Metabolic Bone Disease and Related Research 5(5): 219-221.

Engelke, K., M. Karolczak, A. Lutz, U. Seibert, S. Schaller und W. Kalender (1999). "Mikro-ct technologie und applikationen zur erfassung von knochenarchitektur." Der Radiologe 39(3): 203-212.

Erdmann, N., A. Bondarenko, M. Hewicker-Trautwein, N. Angrisani, J. Reifenrath, A. Lucas und A. Meyer-Lindenberg (2010). "Evaluation of the soft tissue biocompatibility of MgCa0.8 and surgical steel 316L in vivo: a comparative study in rabbits." Biomedical Engineering Online 9: 63.

Feldkamp, L. A., S. A. Goldstein, M. A. Parfitt, G. Jesion und M. Kleerekoper (1989). "The direct examination of three-dimensional bone architecture in vitro by computed tomography." Journal of bone and mineral research 4(1): 3-11.

Feng, P., J. He, S. Peng, C. Gao, Z. Zhao, S. Xiong und C. Shuai (2019). "Characterizations and interfacial reinforcement mechanisms of multicomponent biopolymer based scaffold." Materials Science and Engineering: C 100: 809-825

Gray, J. und B. Luan (2002). "Protective coatings on magnesium and its alloys—a critical review." Journal of alloys and compounds 336(1-2): 88-113.

Grün, N. G., N. Donohue, P. Holweg und A.-M. Weinberg (2018). "Resorbierbare Implantate in der Unfallchirurgie." Journal für Mineralstoffwechsel & Muskuloskelettale Erkrankungen 25(3): 82-89.

Haferkamp, H., M. Niemeyer, R. Boehm, U. Holzkamp, C. Jaschik und V. Kaese (2000). Development, processing and applications range of magnesium lithium alloys. Materials Science Forum, Trans Tech Publications, Vol. 350

Hampp, C., N. Angrisani, J. Reifenrath, D. Bormann, J. M. Seitz und A. Meyer-Lindenberg (2013). "Evaluation of the biocompatibility of two magnesium alloys as degradable implant materials in comparison to titanium as non-resorbable material in the rabbit." Mater Science Engineering C 33(1): 317-326.

Hildebrand, T., A. Laib, R. Müller, J. Dequeker und P. Rüegsegger (1999). "Direct three-dimensional morphometric analysis of human cancellous bone: microstructural data from spine, femur, iliac crest, and calcaneus." Journal of bone and mineral research 14(7): 1167-1174.

Horbett, T. (2004). "The role of adsorbed proteins in tissue response to biomaterials." Biomaterials science: an introduction to materials in medicine 2: 237-246.

Hort, N., Y. Huang, D. Fechner, M. Stormer, C. Blawert, F. Witte, C. Vogt, H. Drucker, R. Willumeit, K. U. Kainer und F. Feyerabend (2010). "Magnesium alloys as implant materials--principles of property design for Mg-RE alloys." Acta Biomaterialia 6(5): 1714-1725.

Janning, C., E. Willbold, C. Vogt, J. Nellesen, A. Meyer-Lindenberg, H. Windhagen, F. Thorey und F. Witte (2010). "Magnesium hydroxide temporarily enhancing osteoblast activity and decreasing the osteoclast number in peri-implant bone remodelling." Acta Biomaterialia 6(5): 1861-1868.

Jansen, J. A., W. J. Dhert, J. P. van der Waerden und A. F. von Recum (1994). "Semi-quantitative and qualitative histologic analysis method for the evaluation of implant biocompatibility." Journal of Investigative Surgery 7(2): 123-134.

Joeris, A., S. Goldhahn, E. Rometsch und D. Höntzsch (2017). "Titan oder Stahl als Osteosynthesematerial." Der Unfallchirurg 120(2): 96-102.

Julmi, S., C. Klose, A.-K. Krüger, P. Wriggers und H. J. Maier (2017). Development of Sponge Structure and Casting Conditions for Absorbable Magnesium Bone Implants. TMS 2017 146th Annual Meeting & Exhibition Supplemental Proceedings, Springer.

Julmi, S., A.-K. Krüger, A.-C. Waselau, A. Meyer-Lindenberg, P. Wriggers, C. Klose und H. J. Maier (2019). "Processing and coating of open-pored absorbable magnesium-based bone implants." Materials Science and Engineering: C 98: 1073-1086.

Karageorgiou, V. und D. Kaplan (2005). "Porosity of 3D biomaterial scaffolds and osteogenesis." Biomaterials 26(27): 5474-5491.

Kim, Y.-K., K.-B. Lee, S.-Y. Kim, K. Bode, Y.-S. Jang, T.-Y. Kwon, M. H. Jeon und M.-H. Lee (2018). "Gas formation and biological effects of biodegradable magnesium in a preclinical and clinical observation." Science and Technology of advanced Materials 19(1): 324-335.

Kirkland, N. T., I. Kolbeinsson, T. Woodfield, G. Dias und M. P. Staiger (2009). "Processing-property relationships of as-cast magnesium foams with controllable architecture." International Journal of Modern Physics B 23(06n07): 1002-1008.

Kleer, N., S. Julmi, A.-K. Gartzke, J. Augustin, F. Feichtner, A.-C. Waselau, C. Klose, H. Maier, P. Wriggers und A. Meyer-Lindenberg (2019). "Comparison of degradation behaviour and osseointegration of the two magnesium scaffolds, LAE442 and La2, in vivo." Materialia: 100436.

König, H. und H. G. Liebich (2012). Anatomie der Haustiere, Thieme.

Kraus, T., S. F. Fischerauer, A. C. Hanzi, P. J. Uggowitzer, J. F. Loffler und A. M. Weinberg (2012). "Magnesium alloys for temporary implants in osteosynthesis: in vivo studies of their degradation and interaction with bone." Acta Biomaterialia 8(3): 1230-1238.

Krause, A., N. Von der Höh, D. Bormann, C. Krause, F.-W. Bach, H. Windhagen und A. Meyer-Lindenberg (2010). "Degradation behaviour and mechanical properties of magnesium implants in rabbit tibiae." Journal of materials science 45(3): 624.

Kristin, J. (2007). Vorhersagekraft der Versagenslast des distalen Radius mit Mikro-Computertomographie und Zweienergie-Röntgen-Absorptiometrie, Ludwig-Maximilians-Universität München.

Kuhn, J., S. Goldstein, L. Feldkamp, R. Goulet und G. Jesion (1990). "Evaluation of a microcomputed tomography system to study trabecular bone structure." Journal of orthopaedic research 8(6): 833-842.

Kuzyk, P. R. und E. H. Schemitsch (2011). "The basic science of peri-implant bone healing." Indian journal of orthopaedics 45(2): 108.

Lalk, M., J. Reifenrath, N. Angrisani, A. Bondarenko, J. M. Seitz, P. P. Mueller und A. Meyer-Lindenberg (2013). "Fluoride and calcium-phosphate coated sponges of the magnesium alloy AX30 as bone grafts: a comparative study in rabbits." Journal of Materials Science: Materials in Medicine 24(2): 417-436.

Lalk, M., J. Reifenrath, D. Rittershaus, D. Bormann und A. Meyer-Lindenberg (2010). "Biocompatibility and degradation behaviour of degradable magnesium sponges coated with bioglass–method establishment within the framework of a pilot study." Materialwissenschaft und Werkstofftechnik 41(12): 1025-1034.

Lang, G. (2013). Histotechnik: Praxislehrbuch für die Biomedizinische Analytik, Springer.

Le Guéhennec, L., A. Soueidan, P. Layrolle und Y. Amouriq (2007). "Surface treatments of titanium dental implants for rapid osseointegration." Dental materials 23(7): 844-854.

Liu, Y. J., Z. Y. Yang, L. L. Tan, H. Li und Y. Z. Zhang (2014). "An animal experimental study of porous magnesium scaffold degradation and osteogenesis." Braz Journal of Medical and Biological Research 47(8): 715-720.

Lüllmann-Rauch, R. (2015). Histologie, Thieme.

Maier, H. J., S. Julmi, S. Behrens, C. Klose, A.-K. Gartzke, P. Wriggers, A.-C. Waselau und A. Meyer-Lindenberg (2020). "Magnesium Alloys for Open-Pored Bioresorbable Implants." JOM: 1-11.

McCarthy, E. F. und F. J. Frassica (2014). Pathology of bone and joint disorders print and online bundle, Cambridge University Press.

Meyer-Lindenberg, A., M. Thomann, A. Krause, D. Bormann, B. von Rechenberg und H. Windhagen (2010). "Untersuchungen zum Einsatz einer Magnesiumbasislegierung als neues resorbierbares Implantatmaterial für die Osteosynthese." Kleintierpraxis 55: 349-363.

Müller, R., H. Van Campenhout, B. Van Damme, G. Van der Perre, J. Dequeker, T. Hildebrand und P. Rüegsegger (1998). "Morphometric analysis of human bone biopsies: a quantitative structural comparison of histological sections and micro-computed tomography." Bone 23(1): 59-66.

Nägele, E. (2005). Mikrocomputertomographische Analyse der trabekulären Architektur des menschlichen Femurs, Ludwig-Maximilians-Universität München.

Nagels, J., M. Stokdijk und P. M. Rozing (2003). "Stress shielding and bone resorption in shoulder arthroplasty." Journal of shoulder and elbow surgery 12(1): 35-39.

Nandi, S. K., S. Roy, P. Mukherjee, B. Kundu, D. K. De und D. Basu (2010). "Orthopaedic applications of bone graft & graft substitutes: a review." Indian Journal of Medical Research 132: 15-30.

Nickel, R., A. Schummer und E. Seiferle (1992). Lehrbuch der Anatomie der Haustiere. J. Frewein, K. H. Wille and H. Wilkens, Parey.

Nuss, K. M. und B. von Rechenberg (2008). "Biocompatibility issues with modern implants in bone - a review for clinical orthopedics." Open Orthopaedics journal 2: 66-78.

Pawelec, K. und J. A. Planell (2018). Bone Repair Biomaterials: Regeneration and Clinical Applications, Woodhead Publishing.

Platzer, W. (2009). Taschenatlas anatomie, Georg Thieme Verlag.

Pohler, O. E. (2000). "Unalloyed titanium for implants in bone surgery." Injury 31: D7-D13.

Pourbaix, M. (1984). "Atlas of electrochemical equilibria in aqueous solutions." NACA.

Raina, V. (1972). "Normal osteoid tissue." Journal of clinical pathology 25(3): 229-232.

Rammelt, S., C. Heck, R. Bernhardt, S. Bierbaum, D. Scharnweber, J. Goebbels, J. Ziegler, A. Biewener und H. Zwipp (2007). "In vivo effects of coating loaded and unloaded Ti implants with collagen, chondroitin sulfate, and hydroxyapatite in the sheep tibia." Journal of orthopaedic research 25(8): 1052-

1061.

Reifenrath, J., N. Angrisani, N. Erdmann, A. Lucas, H. Waizy, J. M. Seitz, A. Bondarenko und A. Meyer-Lindenberg (2013). "Degrading magnesium screws ZEK100: biomechanical testing, degradation analysis and soft-tissue biocompatibility in a rabbit model." Biomedical Materials 8(4): 045012.

Reifenrath, J., M. Badar, D. Dziuba, P. P. Muller, T. Heidenblut, A. Bondarenko und A. Meyer-Lindenberg (2013). "Assessment of cellular reactions to magnesium as implant material in comparison to titanium and to glyconate using the mouse tail model." Journal of applied biomaterials & functional materials 11(2): e89-94.

Reifenrath, J., D. Bormann und A. Meyer-Lindenberg (2011). Magnesium alloys as promising degradable implant materials in orthopaedic research. Magnesium Alloys-Corrosion and Surface Treatments, InTech.

Rosy Manser, R. E., Volker Döring, Carl Zeiss Microscopy GmbH (2018). "Machine Learning Approaches for Easy and Precise Image Segmentation." Zeiss

Schäfer, M. (2011). "Vergleichende histologische Untersuchungen von intramedullären Implantaten auf Magnesiumbasis im Kaninchenmodell." Tierärztliche Hochschule Hannover

Scherzer, C. (2007). "Untersuchung der trabekulären Architektur des caninen Femurkopfes am Beispiel des Morbus Legg-Calvé-Perthes." Tierärztliche Hochschule Hannover.

Shahrezaee, M., M. Salehi, S. Keshtkari, A. Oryan, A. Kamali und B. Shekarchi (2018). "In vitro and in vivo investigation of PLA/PCL scaffold coated with metformin-loaded gelatin nanocarriers in regeneration of critical-sized bone defects." Nanomedicine: Nanotechnology, Biology and Medicine 14(7): 2061-2073.

Shoichet, M. S. (2010). "Polymer scaffolds for biomaterials applications." Macromolecules 43(2): 581-591.

Singh, R. und N. B. Dahotre (2007). "Corrosion degradation and prevention by surface modification of biometallic materials." Journal of Materials Science: Materials in Medicine 18(5): 725-751.

Song, G. (2007). "Control of biodegradation of biocompatable magnesium alloys." Corrosion Science 49(4): 1696-1701.

Staiger, M. P., A. M. Pietak, J. Huadmai und G. Dias (2006). "Magnesium and its alloys as orthopedic biomaterials: a review." Biomaterials 27(9): 1728-1734.

Sutherland, D. und M. Bostrom (2005). Grafts and bone graft substitutes. Book Bone Regeneration and Repair, Springer: 133-156.

Thomann, M., C. Krause, N. Angrisani, D. Bormann, T. Hassel, H. Windhagen und A. Meyer-Lindenberg (2010). "Influence of a magnesium-fluoride coating of magnesium-based implants (MgCa0.8) on degradation in a rabbit model." Journal of Biomedical Materials Research A 93(4): 1609-1619.

Thomann, M., C. Krause, D. Bormann, N. Von der Höh, H. Windhagen und A. Meyer-Lindenberg (2009). "Comparison of the resorbable magnesium. alloys LAE442 und MgCa0. 8 concerning their mechanical properties, their progress of degradation and the bone-implant-contact after 12 months implantation duration in a rabbit model." Materialwissenschaft und Werkstofftechnik 40(1-2): 82-87.

Thomsen, J. S., A. Laib, B. Koller, S. Prohaska, L. Mosekilde und W. Gowin (2005). "Stereological measures of trabecular bone structure: comparison of 3D micro computed tomography with 2D histological sections in human proximal tibial bone biopsies." Journal of Microscopy 218(2): 171-179.

Ullmann, B., J. Reifenrath, D. Dziuba, J. M. Seitz, D. Bormann und A. Meyer-Lindenberg (2011). "In Vivo Degradation Behavior of the Magnesium Alloy LANd442 in Rabbit Tibiae." Materials (Basel) 4(12): 2197-2218.

Van der Lubbe, H., C. Klein und K. De Groot (1988). "A simple method for preparing thin (10 μm) histological sections of undecalcified plastic embedded bone with implants." Stain Technology 63(3): 171-176.

Veronesi, F., G. Giavaresi, V. Guarino, M. G. Raucci, M. Sandri, A. Tampieri, L. Ambrosio und M. Fini (2015). "Bioactivity and bone healing properties of biomimetic porous composite scaffold: in vitro and in vivo studies." Journal of Biomedical Materials Research A 103(9): 2932-2941.

Von Der Höh, N., A. Krause, C. Hackenbroich, D. Bormann, A. Lucas und A.

Meyer-Lindenberg (2009). "Influence of different surface machining treatments of resorbable implants made from different magnesium-calcium alloys on their degradation--a pilot study in rabbit models." DTW. Deutsche tierarztliche Wochenschrift 113(12): 439.

von Doernberg, M. C., B. von Rechenberg, M. Bohner, S. Grunenfelder, G. H. van Lenthe, R. Muller, B. Gasser, R. Mathys, G. Baroud und J. Auer (2006). "In vivo behavior of calcium phosphate scaffolds with four different pore sizes." Biomaterials 27(30): 5186-5198.

Waizy, H., J.-M. Seitz, J. Reifenrath, A. Weizbauer, F.-W. Bach, A. Meyer-Lindenberg, B. Denkena und H. Windhagen (2013). "Biodegradable magnesium implants for orthopedic applications." Journal of materials science 48(1): 39-50.

Walker, J., S. Shadanbaz, T. B. Woodfield, M. P. Staiger und G. J. Dias (2014). "Magnesium biomaterials for orthopedic application: a review from a biological perspective." Journal of Biomedical Materials Research B: Applied Biomaterials 102(6): 1316-1331.

Wang, W., K. Nune, L. Tan, N. Zhang, J. Dong, J. Yan, R. Misra und K. Yang (2019). "Bone regeneration of hollow tubular magnesium-strontium scaffolds in critical-size segmental defects: Effect of surface coatings." Materials Science and Engineering: C 100: 297-307.

Weizbauer, A., J. M. Seitz, P. Werle, J. Hegermann, E. Willbold, R. Eifler, H. Windhagen, J. Reifenrath und H. Waizy (2014). "Novel magnesium alloy Mg-2La caused no cytotoxic effects on cells in physiological conditions." Materials Science and Engineering: C 41: 267-273.

Willbold, E., X. Gu, D. Albert, K. Kalla, K. Bobe, M. Brauneis, C. Janning, J. Nellesen, W. Czayka, W. Tillmann, Y. Zheng und F. Witte (2015). "Effect of the addition of low rare earth elements (lanthanum, neodymium, cerium) on the biodegradation and biocompatibility of magnesium." Acta Biomaterialia 11: 554-562.

Willbold, E. und F. Witte (2010). "Histology and research at the hard tissue-implant interface using Technovit 9100 New embedding technique." Acta Biomaterialia 6(11): 4447-4455.

Witte, F., J. Fischer, J. Nellesen, H. A. Crostack, V. Kaese, A. Pisch, F. Beckmann und H. Windhagen (2006). "In vitro and in vivo corrosion measurements of magnesium alloys." Biomaterials 27(7): 1013-1018.

Witte, F., J. Fischer, J. Nellesen, C. Vogt, J. Vogt, T. Donath und F. Beckmann (2010). "In vivo corrosion and corrosion protection of magnesium alloy LAE442." Acta Biomaterialia 6(5): 1792-1799.

Witte, F., V. Kaese, H. Haferkamp, E. Switzer, A. Meyer-Lindenberg, C. J. Wirth und H. Windhagen (2005). "In vivo corrosion of four magnesium alloys and the associated bone response." Biomaterials 26(17): 3557-3563.

Witte, F., J. Reifenrath, P. Müller, H. A. Crostack, J. Nellesen, F. Bach, D. Bormann und M. Rudert (2006). "Cartilage repair on magnesium scaffolds used as a subchondral bone replacement." Materialwissenschaft und Werkstofftechnik: Entwicklung, Fertigung, Prüfung, Eigenschaften und Anwendungen technischer Werkstoffe 37(6): 504-508.

Witte, F., H. Ulrich, C. Palm und E. Willbold (2007). "Biodegradable magnesium scaffolds: Part II: Peri-implant bone remodeling." Journal of biomedical materials research Part A 81(3): 757-765.

Wolters, L., S. Besdo, N. Angrisani, P. Wriggers, B. Hering, J. M. Seitz und J. Reifenrath (2015). "Degradation behaviour of LAE442-based plate-screw-systems in an in vitro bone model." Materials Science and Engineering: C 49: 305-315.

Xu, L., F. Pan, G. Yu, L. Yang, E. Zhang und K. Yang (2009). "In vitro and in vivo evaluation of the surface bioactivity of a calcium phosphate coated magnesium alloy." Biomaterials 30(8): 1512-1523.

Xu, Y., H. Meng, H. Yin, Z. Sun, J. Peng, X. Xu, Q. Guo, W. Xu, X. Yu, Z. Yuan, B. Xiao, C. Wang, Y. Wang, S. Liu, S. Lu, Z. Wang und A. Wang (2018). "Quantifying the degradation of degradable implants and bone formation in the femoral condyle using micro-CT 3D reconstruction." Experimental and therapeutic medicine 15(1): 93-102.

Yang, J., F. Cui und I. S. Lee (2011). "Surface modifications of magnesium alloys for biomedical applications." Annals of biomedical engineering 39(7): 1857-1871.

Yang, Y. (2017). "Surface Modification of Biodegradable Metallic Materials with Focus on Magnesium and Iron." Friedrich-Alexander-Universität Erlangen-Nürnberg

Yang, Y., C. He, E. Dianyu, W. Yang, F. Qi, D. Xie, L. Shen, S. Peng und C. Shuai (2020). "Mg bone implant: Features, developments and perspectives." Materials & Design 185: 108259.

Zeng, R.-C., W.-C. Qi, Y.-W. Song, Q.-K. He, H.-Z. Cui und E.-H. Han (2014). "In vitro degradation of MAO/PLA coating on Mg-1.21Li-1.12Ca-1.0Y alloy." Frontiers of Materials Science 8(4): 343-353.

IX. DANKSAGUNG

Ich möchte mich von Herzen bei allen bedanken, die zum Gelingen dieser Arbeit beigetragen haben.

Meiner Doktormutter Frau Prof. Dr. Andrea Meyer-Lindenberg gilt mein ganz besonderer Dank für die Überlassung dieses spannenden Themas, für die sehr nette Betreuung, sowie die konstruktive Kritik bei der Durchsicht dieser Arbeit.

Ein weiteres riesiges Dankeschön geht an Dr. Anja-Christina Waselau, Franziska Feichtner, PhD. und Lisa Wurm für unzählige Vorschläge, Korrekturen, Diskussionen und aufbauende Worte. Ohne euch hätte ich es nicht geschafft!

Vielen lieben Dank an Bea und Cris, die mir in einem tollen Team tatkräftig zur Seite standen, mich immer wieder zum Lachen gebracht und motiviert haben. Ohne eure zusätzliche Hilfe und zuverlässige Arbeit im Labor wäre es nicht gegangen.

Herrn Yury Zablotski, PhD. möchte ich für seine kompetente und engagierte Unterstützung bei der statistischen Auswertung danken.

Ganz besonders danke ich allen beteiligten Mitarbeitern der Leibniz Universität Hannover für die Herstellung der Scaffolds; vor allem jedoch Stefan Julmi, Ann-Kathrin Gartzke, Dr. Christian Klose, Prof. Dr. Hans Jürgen Maier und Prof. Dr. Peter Wriggers.

Mein allergrößter Dank gebührt meiner Familie, insbesondere meiner Mutter Petra, meinem Vater Wolfgang und meinem Bruder Janis. Ich danke euch von ganzem Herzen, dass ihr jederzeit für mich da wart und mich finanziell und seelisch unterstützt habt. Ihr habt mir das Gefühl gegeben eine wahnsinnig tolle Familie zu haben, auf die ich mich verlassen kann! Ohne eure immerwährende Unterstützung und Liebe wäre ich niemals so weit gekommen. Meiner Oma Marion danke ich für ihre ausdauernden Fragen und Freude über diese Arbeit.

Außerdem danke ich meinen Freunden und Patentanten, die mich immer wieder aufgemuntert und motiviert haben und mir in diesem Lebensabschnitt bedingungslos zur Seite standen.

Am meisten danke ich meinem Hund Oskar, der mein treuester Begleiter in dieser Zeit war. Ich vermisse Dich!